SIGNAL DESIGN AND PROCESSING TECHNIQUES FOR WSR-88D AMBIGUITY RESOLUTION

PART 2

National Severe Storms Laboratory Report

prepared by: M. Sachidananda
with contributions by: D.S. Zrnic, R.J. Doviak, and S.Torres

June 1998

NOAA, National Severe Storms Laboratory
1313 Halley Circle, Norman, Oklahoma 73069

SIGNAL DESIGN AND PROCESSING TECHNIQUES FOR WSR-88D AMBIGUITY RESOLUTION
Part 2

Contents

LIST OF SYMBOLS:

c	-	speed of light
C_k	-	modulation code [$C_k = \exp(j\phi_k)$]
e_1, e_2	-	complex time series of 1st and 2nd trips
E_1	-	complex time series with 1st trip coherent and 2nd trip coded
E_2	-	complex time series with 2nd trip coherent and 1st trip coded
E_i	-	complex time series samples
$err()$	-	error in the parameter in brackets
i,k,n,m	-	used as indices
j	-	$(-1)^{1/2}$
M	-	number of samples
n_w	-	normalized notch filter width (normalized to $2v_a$)
p_1, p_2	-	mean powers of the 1st and 2nd trip signals
p_n	-	noise power
p_c	-	clutter power
P_k	-	power spectral coefficients
p_{coh}	-	coherent part of the power
p_{inc}	-	incoherent part of the power
r_a	-	unambiguous range
$r(k)$	-	random number array of length k
$R(n)$	-	autocorrelation for n pulse lag
R_c	-	clutter rejection ratio
R_p	-	residual power ratio (ratio of the power, p_1, to the residual $(p_1)_r$ after notch filtering)
R_{pe}	-	effective residual power ratio with random phase error in the phase shifter
R_{pt}	-	residual power ratio (ratio of the power (p_1+p_c), to the residual power of (p_1+p_c) after notch filtering)
R_o	-	overlapped power to total power ratio
s_k	-	k^{th} complex spectral coefficient
$sd()$	-	standard deviation of the parameter in brackets
S_1, S_2	-	spectrum of E_1 and E_2 [$S_1 = \mathrm{DFT}(E_1)$]
T	-	pulse repetition time
v_a	-	unambiguous velocity
v_m	-	mean velocity
v_1, v_2	-	mean velocities of the 1st and 2nd trip signals
w_1, w_2	-	spectrum widths of the 1st and 2nd trip signals
w_c	-	clutter spectrum width
w_{cf}	-	clutter filter width
z	-	$\exp(j2\pi/M)$
^	-	estimate

$\mathcal{P}$	-	probability
$\mathcal{E}$	-	expected value
τ	-	range time
ψ_k	-	switching phase code sequence
ϕ_k	-	modulation phase code sequence
μ	-	ratio of residual powers before and after subtraction

ABBREVIATIONS:

CD	-	Contiguous Doppler
CNR	-	Clutter-to-Noise Ratio
CS	-	Contiguous Surveillance
DFT	-	Discrete Fourier Transform
FFT	-	Fast Fourier Transform
GCF	-	Ground Clutter Filter
IDFT	-	Inverse Discrete Fourier Transform
PNF	-	Process Notch Filter (notch filter in the SZ decoding algorithm)
PRT	-	Pulse Repetition Time
SCR_1	-	Signal-to-Clutter ratio (1st trip signal)
SCR_2	-	Signal-to-Clutter ratio (2nd trip signal)
SNR	-	Signal-to-Noise Ratio
SNR_1	-	SNR of the 1st trip signal ($=p_1/p_n$)
SNR_2	-	SNR of the 2nd trip signal ($=p_2/p_n$)
$\pi/4$ code	-	{ 0, $\pi/4$, 0, $\pi/4$, ... }
$\pi/2$ code	-	{ 0, 0, $\pi/2$, $\pi/2$, ... }

SIGNAL DESIGN AND PROCESSING TECHNIQUES FOR WSR-88D AMBIGUITY RESOLUTION

PART 2

1. INTRODUCTION

The Operational Support Facility (OSF) of the National Weather Service (NWS) has funded the National Severe Storms Laboratory (NSSL), the National Center for Atmospheric Research (NCAR), and the Forecast Systems Laboratory (FSL) to address the mitigation of the range and velocity ambiguities in the WSR-88D system. This is Part 2 of the report on the ambiguity resolution. It documents the work done at the NSSL which was completed in the second year of the project.

In the first part of this report, several ambiguity resolution algorithms were studied theoretically, and extensive simulations were carried out to evaluate their performance. A comparison of the capabilities of each of these algorithms led to the selection of a systematic phase coding technique (the SZ code) as the best among the methods considered. In this second part of the report, we examine the properties of the SZ code in more detail, especially related to the processing steps used in the decoding algorithm. Several important practical aspects which were not included in the earlier simulation, and some aspects of implementation of the algorithm on the WSR-88D, are also included.

Some of the effects present in a practical radar signal are the window effect, ground clutter, and receiver noise. These are addressed here, and their contribution to the degradation in the performance of the systematic phase coding scheme is evaluated. A new and important consideration that needs scrutiny is the accuracy of the phase shifts that has to be maintained for the effective operation of the phase coding scheme. An analysis of the effect of random errors in the phase shifter on the performance of the algorithm, especially the velocity recovery, is carried out, and the results are presented. These practical aspects of the radar signal affect the performance of the different algorithms with respect to the recovery of the weaker signal velocity. Therefore, although the SZ(8/64) code was selected to be the best code in the first part of this report, we also study SZ codes with alternative values of (n/M), and with appropriately modified decoding algorithms, in an effort to evolve a phase coding scheme which performs best with all the practical constraints in place.

Another important practical consideration is the compatibility of the phase coding scheme with the present scan strategy of the WSR-88D. There are several parameters, such as the scan rate, the PRT, the number of samples, etc., that are pre-set in the WSR-88D, depending on the operating mode. The points to be addressed are: (a) how many of these parameters need to be changed in order to implement the phase coding scheme, and (b) how to integrate the phase coding scheme in the WSR-88D so that the meteorological performance of the radar is not

compromised. Ideally, one would like to make the least amount of changes. However, if a change leads to a significant advantage without compromising existing capabilities, it should be made. All these, and many finer points of practical implementation of the algorithm, are discussed in this report.

With the implementation of the coding scheme to recover velocities of the first two trip echoes, we would have a range coverage of about 230 km for v_a= 32 m s^{-1} with a transmitting frequency of 3 GHz. The requirement of the reflectivity data over a range of 460 km at low elevation angles makes it imperative that we retain the present long PRT scan (Contiguous Surveillance mode of the WSR-88D). Some of the information obtained from this long PRT scan can be used in the short PRT Doppler scan (Contiguous Doppler mode) data processing to improve, speed up, and channel the computations along different paths in the algorithm.

At the intermediate elevation angles (2.5° to 6.5°), the batch mode of data acquisition is used, in which alternate radials have long and short PRT transmissions. Here also, the information obtained from the long PRT data can be used in the processing of the short PRT data. However, a change in the scanning mode of the WSR-88D is possible for these elevation angles because the lower edge of the beam at 2.5° elevation is above 11 km at ranges beyond 230 km. Thus, practically all of the storms detected at elevation angles 2.5° and above will be within 230 km, the range to which Doppler velocity processing is required. But we show that the SZ phase coding scheme can recover all the three parameters (i.e., if p_1/p_2<40dB) over twice the unambiguous range interval without the need for long PRT data. Thus, above 2.5° elevation, we can increase the data acquisition rate which can be used to decrease the scan time. Because of this possibility, we have developed the decoding algorithm in two different forms (SZ-1 and SZ-2). The first one works in a stand alone mode to recover all three spectral parameters of both trips, and the second algorithm recovers only the velocities of both trips and uses the long PRT scan data for the recovery of the reflectivity and the spectrum width. (The long PRT data in the present WSR-88D is used to estimate reflectivity only.) The second algorithm can be used if the long PRT data is available, and the first algorithm can be used if the batch mode is replaced by a phase coded Doppler scan.

Throughout this report, we use the following assumptions and notations for convenience: it is assumed that only the 1st and 2nd trip echoes are present in the radar signal, and the first trip is always stronger. The signal parameters, viz., the mean power, the mean velocity, and the spectrum width, are represented by p_i, v_i, and w_i, respectively, with the subscript i=1,2 representing 1st or the 2nd trip. Generally, the stronger signal parameters are easily recovered with the phase coding scheme; the limitation is in the recovery of the velocity of the weaker signal. Therefore, most of the discussions will be about the recovery of the velocity, v_2, of the weaker signal. When the spectral parameters are estimates, obtained from the time series (or spectrum), the symbol ^ is used to represent estimates. However, for convenience, this symbol has been omitted in many places. But it is clear from the context whether the parameter is an estimate or not.

In the lowest two elevation scans there is a possibility of multiple trip echoes. However, the SZ algorithm is developed for recovery of the first two trip signal parameters in the absence of the 3rd and 4th trip echoes. The multiple trip overlay case is discussed in some detail in section 5.6.

In Part 1 of this report, the error in the spectral parameters, estimated using the SZ decoding algorithm, were computed with respect to the autocovariance estimates of the same parameters obtained from the individual time series before they are combined to form the overlaid signal time series. This was done specifically to present the performance of the algorithms relative to the autocovariance processor, so that the comparison among the algorithms is made easier. This can give a false impression that the estimation error is zero in some cases (e.g., $err(\hat{v}_1)$ is zero for large p_1/p_2). Results presented in this report use errors computed with respect to the nominal parameters of the simulation, so that they represent realistic errors.

In Section 2, a comprehensive discussion on the SZ phase code, vis-a-vis the processing steps in the decoding algorithm, is presented. Section 3 is a detailed study of the various effects which are normally present in weather signals. Specifically, we address the effects of various window functions, white noise, and ground clutter filtering. Several practical aspects, which are specific to the phase coding scheme and the WSR-88D, such as the errors in the phase shifter and its effect on the performance of the phase coding scheme, the sample length selection, the code synchronization, etc., are discussed in Section 4. The two versions of the SZ decoding algorithms are given in Section 5 along with some results on the overall performance of the SZ phase coding schemes. Specifically, the performance of three SZ codes, viz., the SZ(8/64), SZ(12/64), and the SZ(16/64), is discussed and compared to arrive at an optimum code with all the practical effects included. A proposed schematic of the algorithm for implementation on the radar is also discussed in this section.

Whereas the simulated time series is a very good tool in the design stage of the phase coding scheme, it cannot represent all the variations in the actual radar derived time series. Due to the diversity in the weather phenomenon, there are situations which produce a non-Gaussian shaped spectra. Therefore, the actual performance of the phase coding scheme has to be obtained by testing it on real weather signals. This will be investigated in Part 3 of the report, which will be devoted to the study of the WSR-88D data. Here, simulated data fields are generated with overlaid echoes to demonstrate the performance of the algorithm. These results are discussed in Section 6 of this report. The conclusions drawn from this study are in the last section.

2. SZ PHASE CODING SCHEME

In a phase coded radar, the transmitter pulses are phase shifted by a pre-determined phase sequence, ψ_k, and the received echo samples are phase corrected (multiplied by $\exp\{-j\psi_k\}$) so that the 1st trip signal is coherent. However, the 2nd trip echo would not be cohered but will be modulated by a phase sequence $\phi_k = (\psi_{k-1} - \psi_k)$. If the second trip is cohered, then the 1st trip echo is modulated by a phase sequence $-\phi_k$. Here, ψ_k is the **SZ switching code** (phase shifter switching sequence), and ϕ_k is the **SZ modulation code**. In autocovariance processing, the mean velocity is estimated from the phase of the autocorrelation for lag 1, $R(1)$. The modulation code, ϕ_k ($-\phi_k$), modifies the spectrum of the 2nd (1st) trip echo so that its $R(1)$ is made zero; thus, the bias error in the velocity estimate of the cohered 1st (2nd) trip signal, due to the overlaid 2nd (1st) trip signal, is removed. For a given spectrum width, the variance of the velocity estimate increases directly with the increase in the overlaid power, and the estimated velocity is usable when the modulated overlaid power is less than the coherent power (i.e., equivalent to 0 dB SNR, considering the modulated power as noise). Therefore, further processing is needed to remove as much of the overlaid power as possible from the spectrum so that the ratio of the coherent signal power to the residual overlaid modulated signal power is greater than unity. This is accomplished by the notch filtering and cohering steps in the decoding algorithm. There is a certain amount of self-noise (Zrnic and Mahapatra, 1985) generated in the process of notch filtering and cohering which results in a decreased SNR. The self-noise power is a function of the code, the notch filter width, and the spectrum width. The SZ code is designed to allow the removal of the maximum amount of overlaid power, and at the same time minimize the self-noise, to improve the recovery of the velocity of the weaker signal.

2.1. Properties of the SZ phase code.

The modulation phase sequence is given by $\phi_k = n\pi k^2/M$, where M and n are integers (modulation code is $\exp\{j\phi_k\}$). If M is not divisible by n, this code has a property of zero autocorrelation for all lags except zero or multiples of M. This code was reported in a correspondence by Chu (1972). To modulate the 2nd trip signal with this code, if the 1st trip is made coherent, the transmitted phases have to be

$$\psi_k = -\sum_{p=0}^{k}\{n\pi p^2/M + \text{const.}\} \; ; \; k=0,1,2,... \qquad (2.1).$$

The constant is arbitrary and is set to zero. Another important property of the SZ modulation code is that its autocorrelation (as explained earlier) and power spectrum are independent of a shift in the code (i.e., in Eq. 2.1, k values can be from m to $m+M-1$, with arbitrary m). We refer to this code as SZ(n/M) code. Note that the symbol M is also used for representing the number of samples in the time series, and we consider values of n less than $M/2$ only. The reason for considering $1 \le n \le M/2$ is that the modulation phase code repeats after $n=M/2$, except for a shift and/or conjugation. For a given M and $n=x$, $n=iM-x$, and $n=iM+x$, the modulation codes are

essentially the same for any integer i except for a conjugation and/or shift by integer multiples of $\pi/2$. The reason for choosing the parameter M to be the same as the number of samples is that M/n is the basic periodicity of the modulation code (if M/n is an integer), and for effective operation of the phase coding scheme, it is required to limit the periodicity to M or less. The indicated choice automatically limits the periodicity of the modulation code to sub-multiples of the number of samples. The number of samples available in the WSR-88D is between 44 and 66; hence, M=64 is selected as a convenient number for most of the computations in this report.

In general, for M=64 and any n, the periodicity of the modulation code can be obtained by expressing $M/n = P/q$, with all common factors between M and n removed such that q is an odd integer (i.e., equivalent to Chu's code $\phi_k = q\pi k^2/P$). P is the periodicity of the modulation code, and $4P$ is the periodicity of the switching code. Thus, it can be seen that by choosing M to be the same as the number of samples, we are restricting the periodicity of the modulation code to M or less. The autocorrelation is unity for lags in multiples of P. The spectrum of the code has only P non-zero coefficients spaced M/P coefficients apart. If a weather signal time series is multiplied by the modulation code, the spectrum of the resulting time series is a convolution of the code spectrum and the signal spectrum. If the signal spectrum is unimodal, it is easy to visualize that for n=1, the modulated spectrum is noise-like, and for n=32, it is bimodal (see Fig. 5.1, for $\pi/4$ code, Part 1 of the report). For n=1, the noise-like spectrum yields $R(1)$=0 in the mean, but there is an upper limit for the suppression of $R(1)$ by modulation, for any given realization of the signal time series with a practical number of samples. However, for n=32, the bimodal spectrum yields much better suppression of $R(1)$ because of the matching property, which is obtained for each realization. The matching property, as discussed in Part 1 of this report, is the equality of the k^{th} and $(k+M/2)^{th}$ spectral coefficient magnitudes ($|s_k|=|s_{k+M/2}|$; k=1,2,...$M/2$). Only the difference power ($|s_k|^2-|s_{k+M/2}|^2$) contributes to $R(1)$. As n is increased from 1 to 32, the whitening property gradually changes to matching property.

From the results presented in Part 1 of this report, it is observed that the region of recovery of v_2 in the $\{p_1/p_2; w_1\}$ space is approximately demarcated by the residual power ratio, R_p, (for definition of R_p see list of symbols, page ii) for the notch filter width used in the decoding algorithm. The $sd(\hat{v}_2)$ in the region of recovery is dictated by the overall SNR that is achieved for the weaker signal after the notch filtering and cohering steps. With a larger value for the code parameter n, better overall SNR can be achieved, but with a smaller notch width, which reduces the region of recovery of v_2 in $\{p_1/p_2; w_1\}$ space. Although earlier simulation study (Part 1 of the report) indicated the SZ(8/64) code as the best, it is not necessarily the optimum when the window and the noise effects are included. In Fig. 5.13 of Part 1 of this report, the notch width was fixed at n_w=0.75, which is not the optimum for all n values. In fact, for a given n, there is a maximum value of n_w beyond which the cohering process breaks down. This limiting value of normalized notch width can be written as

$$(n_w)_{max} = | 1 - 2n/M | ; \quad 1 \le n \le M. \tag{2.2}$$

This limiting value of n_w is derived from the fact that the modulation spreads the power in each of the spectral lines of the signal into M/n spectral lines separated by n coefficients, and at least two of these spectral coefficients are required for cohering the signal without the loss of the mean velocity information. Assuming that the notch width is within the maximum limit, increasing n_w

increases the region of recovery of v_2 in $\{p_1/p_2;w_1\}$ space, but at the same time, increases the standard error in $\hat{v}_2$ for a given n. Thus, the optimum n_w is the one that yields a tolerable standard error in $\hat{v}_2$ with a maximum region of recovery. For the SZ(8/64) code, n_w=0.75 yields a $sd(\hat{v}_2)$ of about 1 m s^{-1} for w_1=4 m s^{-1}, and w_2=4 m s^{-1}, without the window and noise effects. This notch width is also the maximum that we can use with this code. For larger w_2, we need to reduce the notch width to keep the $sd(\hat{v}_2)$ within the tolerable limit. If the maximum notch width (Eq. 2.2) is used for each n, and the variance of $\hat{v}_2$ is computed using simulation results, we can see that the $sd(\hat{v}_2)$ decreases with increasing n, but the extent of p_1/p_2 over which v_2 can be recovered is also reduced (Fig. 2.1).

Although the code spectrum changes drastically as n is changed from an even to an odd number (see Fig. 5.12, Part 1 of this report), the reconstructed spectrum (after the notch filtering and cohering) changes in a systematic manner, and the performance of the decoding algorithm also changes smoothly. With increasing n, the $sd(\hat{v}_2)$ and the recovery region in the $\{p_1/p_2;w_1\}$ space decreases to a minimum if the maximum admissible notch width is used in processing. When the practical effects of the window, noise, and phase error are included, the optimum n is expected to be somewhere between 8 and 16. Therefore, in this report, we examine the SZ codes with n between 8 and 16. Specifically, results are given for SZ codes with n=8,12, and 16.

In the present application, in which the phase of $R(1)$ is used for velocity computation, it suffices to have a code with $R(1)$ equal to zero; hence, any n between 1 and 63 would satisfy this requirement. For n/M=8/64, the autocorrelation is unity for lags in multiples of 8, and is zero otherwise, whereas for n/M=16/64, the autocorrelation is unity for lags in multiples of 4 and is zero otherwise. The SZ(8/64) switching and the modulation phase codes have periodicities of 32 and 8, respectively (Table 2.1a and 2.1b). In the rest of the report, the discussion and the results presented are mostly for the SZ(8/64) code. Because the SZ(12/64) and SZ(16/64) codes are similar, the discussion on these codes has been kept brief, but the final performance results are given for all three codes for comparison.

2.2. Notch filtering and cohering - SZ(8/64) code.

The spectrum of the SZ(8/64) code has exactly 8 non-zero coefficients spaced $M/8$ coefficients apart, and all are of equal magnitude (Fig. 2.2a). If the weather signal complex time series samples, e_i, are multiplied by the modulation code, C_i= exp($j\phi_i$), the resulting spectrum is shown in Fig. 2.2c. It can be seen that the weather spectrum is split into 8 identical parts having 1/8th of the original power and are separated by n coefficients (note: the magnitude of the spectral coefficient is plotted and not the power). If the spectrum width is large (Fig. 2.2d), the overlapping of the spectral coefficients produces a spectrum resembling a white noise spectrum (Fig. 2.2e).

The notch filtering process removes the overlaid stronger signal to a large extent, and the weaker signal to a lesser extent. An examination of how the notch filtering and cohering processes affect the two signals gives us a good understanding of the working of the SZ coding scheme.

First, consider the weaker 2nd trip signal. Before notch filtering, this signal spectrum is modulated by the code, C_k= exp($j\phi_k$); thus, the k^{th} coefficient of the modulated spectrum is a

complex weighted sum of 8 coefficients of the unmodulated signal spectrum at $k_m=k+8m$; $m=0,1,...7$ (The DFT is cyclic; thus, if k_m is greater than M, it would be k_m-M.). The complex weights are from the modulation code. Now, assume the signal to be a d.c.; i.e., all the spectral coefficients are zero except the first coefficient. Thus, the spectrum before the notch filtering would be the spectrum of the code itself as shown in Fig. 2.3a. In the cohering process, each of the 8 non-zero coefficients is split into 8 parts and added with different phases at different locations. If any two adjacent non-zero coefficients remain after filtering, as in the case of $n_w=0.75$, the two components add in phase only at the first coefficient (i.e., the d.c. component), and in all other places, they add up to a smaller magnitude because of the phase difference. The spectrum after cohering is shown in Fig. 2.3c. There is a symmetry in the spectral coefficient amplitudes about the d.c. component; thus, the velocity estimate would not be biased. However, because of the remaining non-zero components, the width would be very large. It may be noted that there is no self noise generated in the process. To cohere one spectral coefficient, the maximum notch width that can be used is up to 0.86, beyond which only one non-zero coefficient remains, and the cohering process would break down. Even at $n_w=0.86$, the notch has to be positioned such that two adjacent non-zero coefficients are retained after notch filtering. In practice, this is not possible because the position of the notch is determined by the stronger signal spectrum, and also, the signal spectrum is not a single line but has significant width. Thus, to ensure at least two coefficients contribute in the cohering process for all the coefficients, the maximum notch width that can be used is $n_w=0.75$ (see Eq. 2.2). Perhaps one may operate with $n_w=0.8$ with some loss of coherency because the practical signals have widths of the order of 4 m s^{-1}, and one could afford to loose a few coefficients. But this will result in an increased error in the estimate because the incoherent part appears as noise.

At the outset, it appears that the SNR of the weaker signal is not affected by the notch filtering process because signal and the noise power are reduced by the same factor, $(1-n_w)$. However, in the present context of estimating the mean velocity from the phase of $R(1)$, only the part of the power contributing to $R(1)$ can be treated as the signal. How much of this cohered signal contributes to the autocorrelation, $R(1)$, can be assessed by a subtraction process in the power spectrum domain. The subtraction process is as follows: the spectral power coefficients $|s_k|^2$ and $|s_{k+M/2}|^2$ are taken at a time, and the lower of the two is subtracted from both coefficients; the process is carried out for $k=1,2,...M/2$. The subtracted part does not contribute to the $R(1)$, as can be seen from the relation between $R(1)$ and spectral coefficients (Eq. 2.7, Part 1 of this report). The subtraction process retains only three coefficients which contribute to $R(1)$: one at d.c. and one each at $+M/8$ and $-M/8$ from the d.c. component, with a reduced amplitude ($1/\sqrt{2}$ times the d.c. component; Fig. 2.3d). The signal power loss in the subtraction process is 2.19 dB. This loss factor is applicable to only the signal part because all the side bands replicate the original signal except for a complex multiplier, and it does not apply to the noise present in the signal. Thus, there is a net degradation in the SNR of the signal by 2.19 dB due to the notch filtering and cohering processes.

The signal loss computed in the previous paragraph is for a single spectral coefficient. In Fig. 2.4, the notch filtering and cohering processes are shown with a narrow width ($w_2=2$ m s^{-1}) weather signal. In this example, a narrow width is chosen to show the individual spectra after cohering. It is clear that the spectra shown in Fig. 2.4d and 2.4e are convolutions of the signal spectrum in Fig. 2.4a, with the spectra given in Fig. 2.3c and 2.3d, respectively. If the spectrum

width is large, the signal and the two side band spectra in Fig. 2.4e overlap; thus, they cannot be clearly identified as three different spectra. Because of the overlap, the power loss in the notch filtering and cohering processes varies for each realization of the weather spectra. A simulation study with varying spectrum widths (w_2=1 to 8 m s^{-1}) yielded loss values between 1.7 dB and 3.2 dB. Further, in the overlapped portion of the spectrum, the amplitudes of the side bands vary because of the random phases; hence, the second and the third side bands do not cancel completely in $R(1)$. This can be seen in Fig. 2.4e where the second side band is not completely eliminated. The residual power from the 1st trip signal is equivalent to noise and thus further degrades the SNR.

The overlapped part of the signal and the side band spectra contribute to the variance of the velocity estimate. The mean velocity is not affected because the side bands have a symmetry about the mean velocity. Because of the overlapped spectra, there is an increase in the $sd(\hat{v}_2)$ with respect to the $sd(\hat{v}_2)$ of the original signal using the autocovariance algorithm.

Now, we consider the notch filtering and cohering processes with respect to the 1st trip signal. Assume that the 2nd trip signal is absent, and the 1st trip signal has a Gaussian shape. The effect of notch filtering and cohering processes on the 1st trip signal is illustrated with an example of a simulated weather signal of w_1=6 m s^{-1} (Fig. 2.5a). Since the 1st trip signal is coherent before notch filtering, and the notch is centered on the mean velocity, the residual power is equal to (p_1/R_p), where

$$R_p = 1 \,/\, [1 - \mathrm{erf}\{n_w v_a/(w_1\sqrt{2})\}] \qquad (2.3)$$

is the residual power ratio (i.e., the ratio of the total power, p_1, to the residual power after notch filtering). Note that the expression (2.3) is for a Gaussian spectrum and not for the sampled signal spectrum with finite number of samples, but it is used here because it is a fairly good approximation up to n_w=0.9. The cohering of the 2nd trip signal after the notch filtering, modulates the 1st trip residual power; the modulation code in this case is the complex conjugate of C_k. If the notch width is zero, the spectrum would appear more like a white noise for large widths (as in Fig. 2.2e) because each coefficient is a complex weighted sum of 8 coefficients of the original spectrum before modulation. However, with increasing notch width, less coefficients are added, resulting in less of the white noise part and more of the colored noise. At the same time the match property improves with increasing notch width, and perfect matching is obtained for n_w = 0.875 because the overlap is zero. The match property is $|s_k|=|s_{k+M/2}|$, or the left and right halves of the spectrum have the same envelope (see eq. 5.4 of part-1 of this report). But we cannot use this notch width because of the reasons stated earlier. The maximum usable n_w=0.75 results in a less than perfect match. The matched part and the white noise part do not contribute to the autocorrelation, $R(1)$ and, thus, would not affect the mean velocity. With notch filtering, only the tail ends of the spectrum are retained; the power is suppressed by 42 dB by the notch filter of width n_w=0.75. In the cohering step, the residual signal is phase modulated resulting in a spread of the power into 8 identical spectra having 1/8 of the power. The matching property can be clearly seen in the spectrum shown in Fig. 2.5c. The part of the power that contributes to $R(1)$ can be obtained by the subtraction process, which accounts for another 8 dB of suppression (Fig. 2.5d). The subtraction is used only to compute the suppression of overlaid power. It is not used in the decoding algorithm (described in section 5.4) which automatically

accomplishes equivalent suppression in computing $R(1)$. The suppression of overlaid power is a function of the spectrum width w_1 and the notch width.

To get an idea of how much of the residual 1st trip noise in $R(1)$ is suppressed, a simulation study was conducted with only the 1st trip signal subjected to the notch filtering, cohering, and subtracting processes. The ratio of the residual power before and after the subtraction, μ, as a function of the notch width is shown in Fig. 2.6 for w_1=4 m s^{-1}. The mean value of μ remains fairly constant at 3.6 dB up to about n_w = 0.55 and then starts increasing; it is about 6.5 dB (mean value; a ±2 dB variation is observed in the simulation) at n_w = 0.75. This behavior is because of the improvement in the matching property for larger notch widths. The variation of the μ with the spectrum width is plotted in Fig. 2.7 for the selected n_w=0.75, which indicates that the μ increases with decreasing spectrum width because of the improvement in the matching property.

When both signals are present, there is a loss of the 2nd trip signal of about 7.7 to 9.2 dB (~8.5 dB, of which 6 dB is caused by the notch filter) with the notch filtering and cohering processes (as discussed earlier in this section), and there is a reduction in the 1st trip residual signal (noise-like) by about 5 to 8 dB (~6.5dB) in addition to the reduction by the residual power ratio, R_p. The net improvement in SNR is (R_p+6.5-8.5) dB on average, at a n_w=0.75 and w_1=4 m s^{-1}, which is about 2 dB less than the R_p. Approximate overall SNR for n_w=0.75 can be written as

$$\text{overall SNR} = (10^{-0.25}/4) \,/\, [0.25/\text{SNR}_2 + 10^{-0.65}\, p_1/(p_2 R_p)] \qquad (2.4)$$

The improvement in SNR is made possible by the notch filtering and cohering processes because the residual power of the stronger signal decreases much faster than the weaker signal power, as a function of notch width. It must be noted here that (2.4) includes the SNR degradation due to the signal power loss alone in the processing. There is some amount of noise generated due to the overlapped part of the spectrum after notch filtering and cohering processes, as indicated earlier in this section, which is a function of the spectrum width of the signal. Thus, in practice, the overall SNR would be lower than that given by (2.4).

2.3. Deconvolution procedure for spectrum width estimation - SZ(8/64) code.

So far, not much attention has been given to the spectrum width estimate of the weaker signal. The six undesirable side bands generated by the notch filtering and cohering processes produce a bias error in the spectrum width $\hat{w}_2$. The estimated width is always larger than the actual width.

An examination of the spectrum after the notch filtering and cohering processes (Fig. 2.4d) shows that the spectrum consists of the actual signal and three symmetrically placed side bands on either side, each with different amplitudes. These are shifted versions of the signal (with shifts in multiples of M/8 coefficients) multiplied by a complex number. Therefore, there is an amplitude change and phase shift associated with the multiplier. The magnitude spectrum appears as a convolution of the spectrum of the 2nd trip signal with the code spectrum obtained after notch filtering and cohering (see Fig. 2.3c), but it is not exactly a convolution because of the notch filter. A deconvolution in the complex domain is not possible because the embedded notch

filtering process makes the matrix associated with convolution singular. In fact, the rank of the associated matrix is determined by the notch width and is given by $(1-n_w)M$; for example, the rank of the MxM matrix is $M/4$ for $n_w = 0.75$. An alternative is to deconvolve using only the magnitudes, which does not result in exactly the same signal spectrum but is fairly close to it. For narrow widths (w_2<2 m s $^{-1}$), the restored shape is almost like the original, but for larger w_2, the shape is not reproduced exactly. An example of the magnitude deconvolution is given in Fig. 2.8, for a narrow spectrum (w_2=2 m s^{-1}); the spectrum at different stages of the processing is shown. The power levels indicated on the figure are nominal values but can vary with each realization. For larger widths, the spectrum overlap combined with in-exact magnitude domain deconvolution produces a variation in power levels; it is about 6±1 dB after notch filtering, and about 0.5 to 4 dB additional loss in the deconvolution, depending on the spectrum width. The spectrum width is computed using this restored spectrum. A simulation study indicates that there is no bias in the width estimate, but the variance is larger than that obtained with an autocovariance algorithm in the absence of the overlaid signal. Therefore, this procedure is adopted for width estimation in the stand-alone version of the SZ decoding algorithm (SZ-1 algorithm).

The convolution matrix (magnitude only) is a MxM real matrix. The first row vector of the convolution matrix is obtained as follows. The spectrum of the modulation code is notch filtered and cohered (Fig. 2.3c), and then the normalized magnitude spectrum is computed (total power is normalized to unity). The notch filter width is the same as that used in the SZ decoding algorithm, but the position can be anywhere because the magnitude spectrum is independent of the position; only the phases are dependent on the position. All other rows of the matrix are obtained by shifting cyclically the first row by $(n$-1) coefficients to the right for the n^{th} row. The matrix, thus obtained, is inverted to get the deconvolution matrix. The deconvolution process consists of pre-multiplying the magnitude spectrum (Mx1 -column matrix), obtained after the notch and cohere processes, by the deconvolution matrix. The result is a column matrix which is the recovered magnitude spectrum. The deconvolution matrix is pre-computed and is input to the SZ decoding algorithm.

The deconvolution procedure allows us to cohere all the side band power which otherwise would correspond to a 6 dB loss for n_w=0.75. However, since the deconvolution is carried out in the magnitude domain, the power in the spectrum is not conserved. There is a loss of the signal which is a function of the spectrum width. The loss is about 0.5 dB for w_2=1 m s^{-1} and can be as large as 4 dB for w_2=8 m s^{-1}. For a median width of 4 m s^{-1}, the loss is about 2.5 dB. It is shown later that there is a corresponding loss in the residual stronger signal also by about the same factor (see 2 paragraphs below). Thus, the net improvement is still 6 dB.

To evaluate the efficacy of the deconvolution process in recovering the weaker signal spectrum, especially the spectrum width, a simulation study was carried out with the SZ(8/64) coded 2nd trip signal subjected to the notch filtering and cohering processes. The 1st trip signal is assumed to be absent. Fig. 2.9a is a scatter plot of the spectrum width recovered after notch filtering, cohering, and deconvolution processes, versus the input width to the simulation program. The mean and the standard deviation is also shown on the plot. In generating this plot, the following parameters are used: v_a=32 m s^{-1}, M=64, SNR$_2$=40 dB, n_w=0.75, and v_2 is randomly selected within ±28 m s^{-1}. The spectrum width is computed using the ratio of *R(0)/R(1)* (Eq. 2.6 of part 1 of this report). Compare this with Fig. 2.9b which is a similar plot with the same

parameters for the simulation, but the width is estimated from the uncoded time series using the autocovariance algorithm. The standard deviation of the width estimate is increased to some extent by the notch filtering, cohering, and magnitude domain deconvolution processes.

It is important to examine the effect of the deconvolution procedure on the 1st trip residual signal, especially the effect on the residual power and the nature of the residual spectrum after deconvolution. In Fig. 2.10, a series of spectra of the 1st trip signal are shown at different stages of processing. The 2nd trip signal is assumed to be absent, and a large spectrum width of 6 m s^{-1} is chosen for the 1st trip signal so that the residual power after notch filtering is substantial for demonstration purposes. After the notch filtering and cohering processes, the spectrum has an appearance of white noise but has a matching property because of the systematic code. The last spectrum in the figure is after the deconvolution. It can be seen that the spectrum still has the appearance of a white noise, but the power is less by about 7 dB. The power loss is because of the magnitude domain deconvolution process. The power levels shown on the figure are nominal values and may vary for each realization of the spectrum. The reduction in the residual power is a function of the spectrum width. The loss and its variation due to the deconvolution procedure is larger for larger spectrum widths. A simulation study yielded loss values between 3 dB and 8 dB for widths between 1 and 8 m s^{-1}. The loss of the residual power improves the SNR; however, this is partly off-set by the loss of weaker coherent signal as well, as discussed earlier (see 2 paragraphs above). On the other hand, if the residual power loses its white noise property or the matching property due to deconvolution, then it can introduce bias error in the velocity estimate of the recovered signal. Again, a simulation study using different widths indicates that the mean velocity of the residual spectrum is zero; thus, the deconvolution does not introduce bias error in $\hat{v}_2$. However, the variance of the mean velocity estimate increases due to the deconvolution process because the reconstructed magnitude spectrum is not exact. Therefore, the deconvolution step is used only for spectrum width computation, and the velocity is estimated before the deconvolution.

Now, if both 1st and 2nd trip signals are present in the spectrum, the magnitude domain deconvolution procedure would affect the two signals in a somewhat similar manner, but the composite result may vary because the magnitude spectrum is the magnitude of the vectorial sum of the two spectra. Fig. 2.11 demonstrates the recovery of the weaker 2nd trip signal in the presence of a strong 1st trip signal. The parameters used are shown in the figure. It can be seen that the recovered spectrum (Fig. 2.11e) does not have exactly the same shape as the original 2nd trip signal (Fig. 2.11b) but has nearly the same mean velocity and width.

Table.2.1a. Modulation phase code sequence for *n/M*=8/64 in degrees.

k	ϕ_k	k	ϕ_k	k	ϕ_k	k	ϕ_k
0	0.0	16	0.0	32	0.0	48	0.0
1	22.5	17	22.5	33	22.5	49	22.5
2	90.0	18	90.0	34	90.0	50	90.0
3	-157.5	19	-157.5	35	-157.5	51	-157.5
4	0.0	20	0.0	36	0.0	52	0.0
5	-157.5	21	-157.5	37	-157.5	53	-157.5
6	90.0	22	90.0	38	90.0	54	90.0
7	22.5	23	22.5	39	22.5	55	22.5
8	0.0	24	0.0	40	0.0	56	0.0
9	22.5	25	22.5	41	22.5	57	22.5
10	90.0	26	90.0	42	90.0	58	90.0
11	-157.5	27	-157.5	43	-157.5	59	-157.5
12	0.0	28	0.0	44	0.0	60	0.0
13	-157.5	29	-157.5	45	-157.5	61	-157.5
14	90.0	30	90.0	46	90.0	62	90.0
15	22.5	31	22.5	47	22.5	63	22.5

Table.2.1b. Switching phase code sequence for *n/M*=8/64 in degrees.

k	ψ_k	k	ψ_k	k	ψ_k	k	ψ_k
0	0.0	16	180.0	32	0.0	48	180.0
1	22.5	17	-157.5	33	22.5	49	-157.5
2	112.5	18	-67.5	34	112.5	50	-67.5
3	-45.0	19	135.0	35	-45.0	51	135.0
4	-45.0	20	135.0	36	-45.0	52	135.0
5	157.5	21	-22.5	37	157.5	53	-22.5
6	-112.5	22	67.5	38	-112.5	54	67.5
7	-90.0	23	90.0	39	-90.0	55	90.0
8	-90.0	24	90.0	40	-90.0	56	90.0
9	-67.5	25	112.5	41	-67.5	57	112.5
10	22.5	26	-157.5	42	22.5	58	-157.5
11	-135.0	27	45.0	43	-135.0	59	45.0
12	-135.0	28	45.0	44	-135.0	60	45.0
13	67.5	29	-112.5	45	67.5	61	-112.5
14	157.5	30	-22.5	46	157.5	62	-22.5
15	180.0	31	0.0	47	180.0	63	0.0

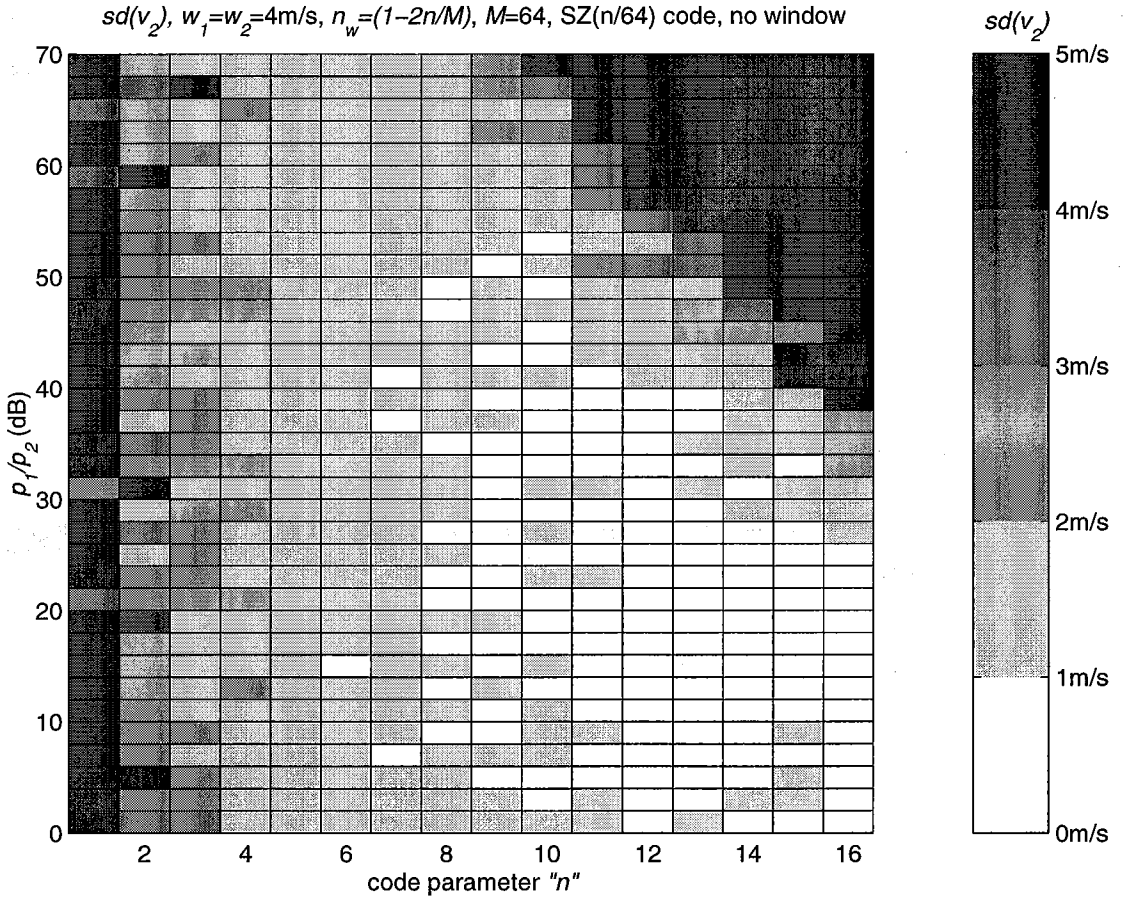

Fig. 2.1. $sd(\hat{v}_2)$ as a function of the code parameter n. The notch width is n_w=|1-2n/M|, the maximum allowable value for each n.

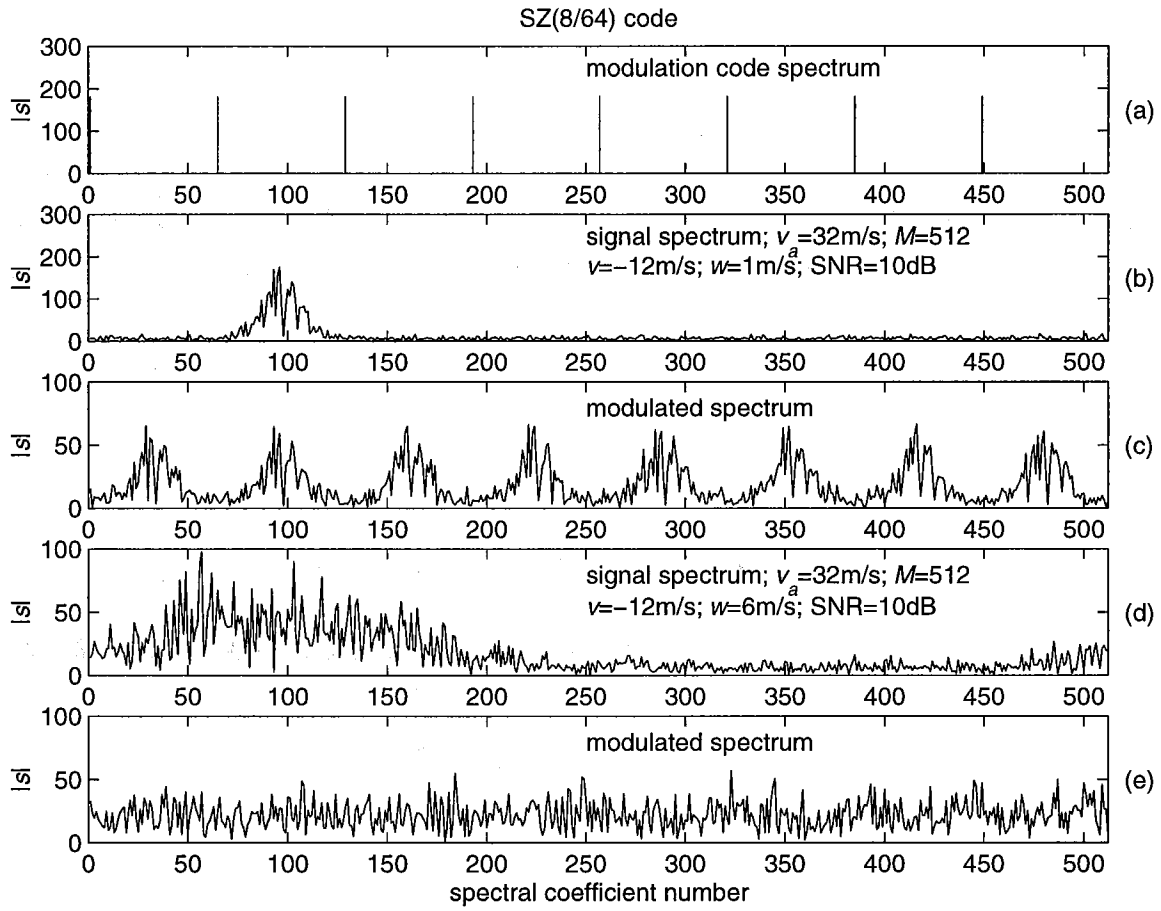

Fig. 2.2. Illustration of the SZ(8/64) phase coded signal spectra.

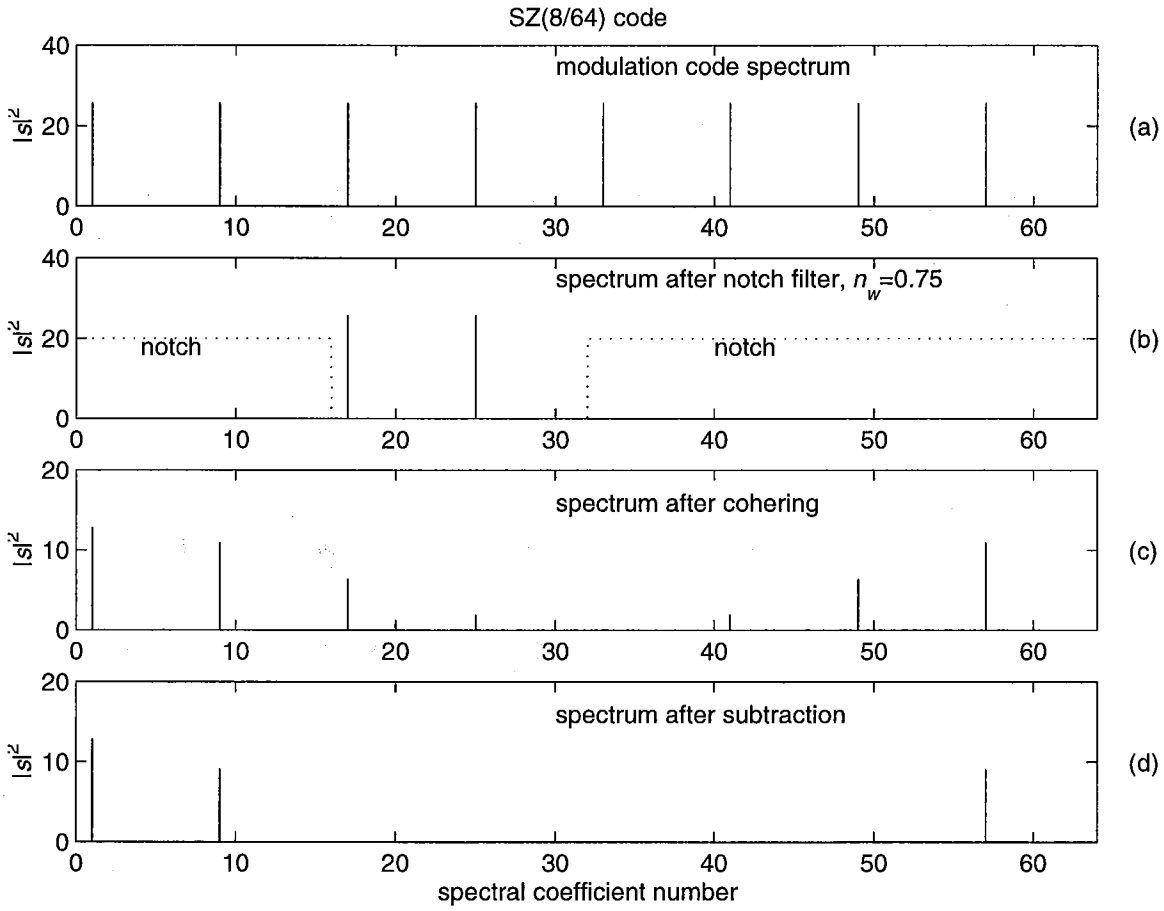

Fig. 2.3. Modification of the code spectrum using the notch filtering and cohering processes.

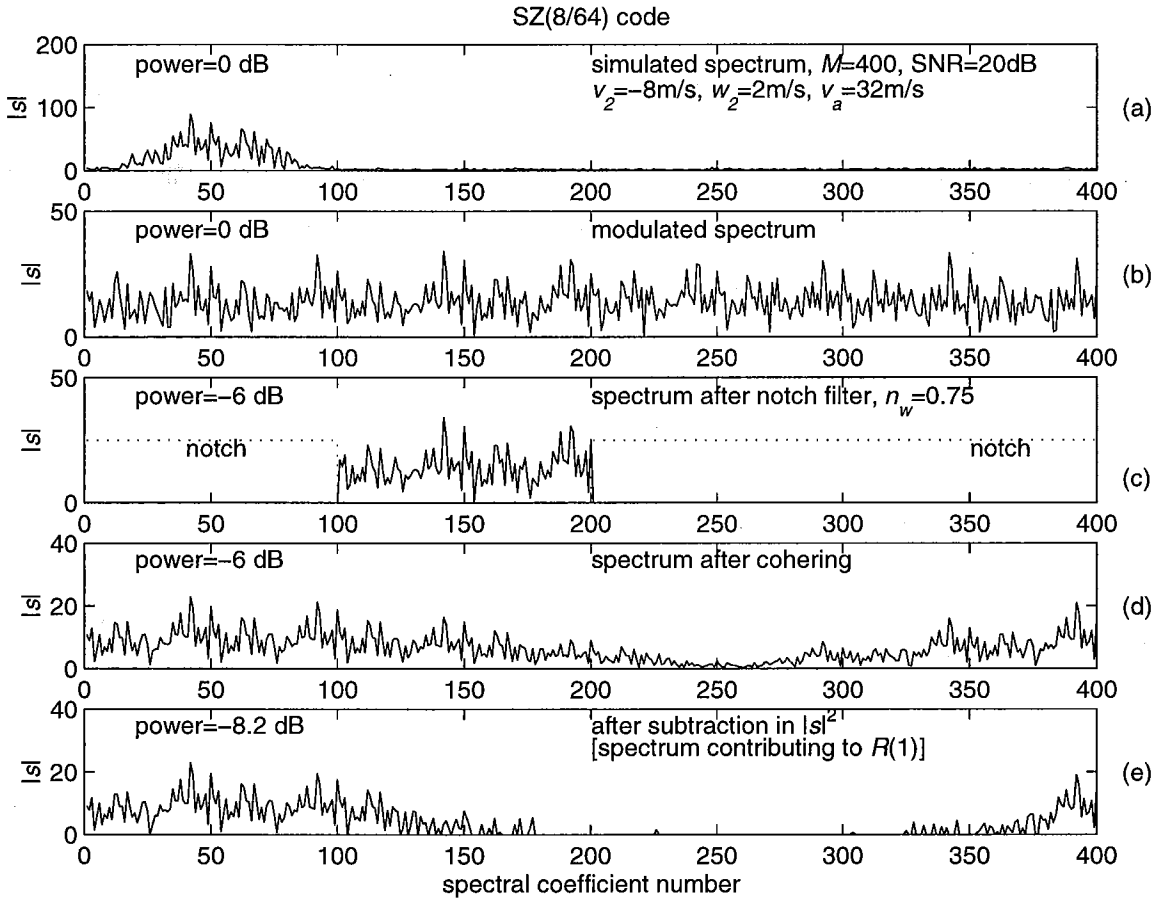

Fig. 2.4. Spectra illustrating the effect of the notch filtering and cohering on the weaker 2nd trip signal.

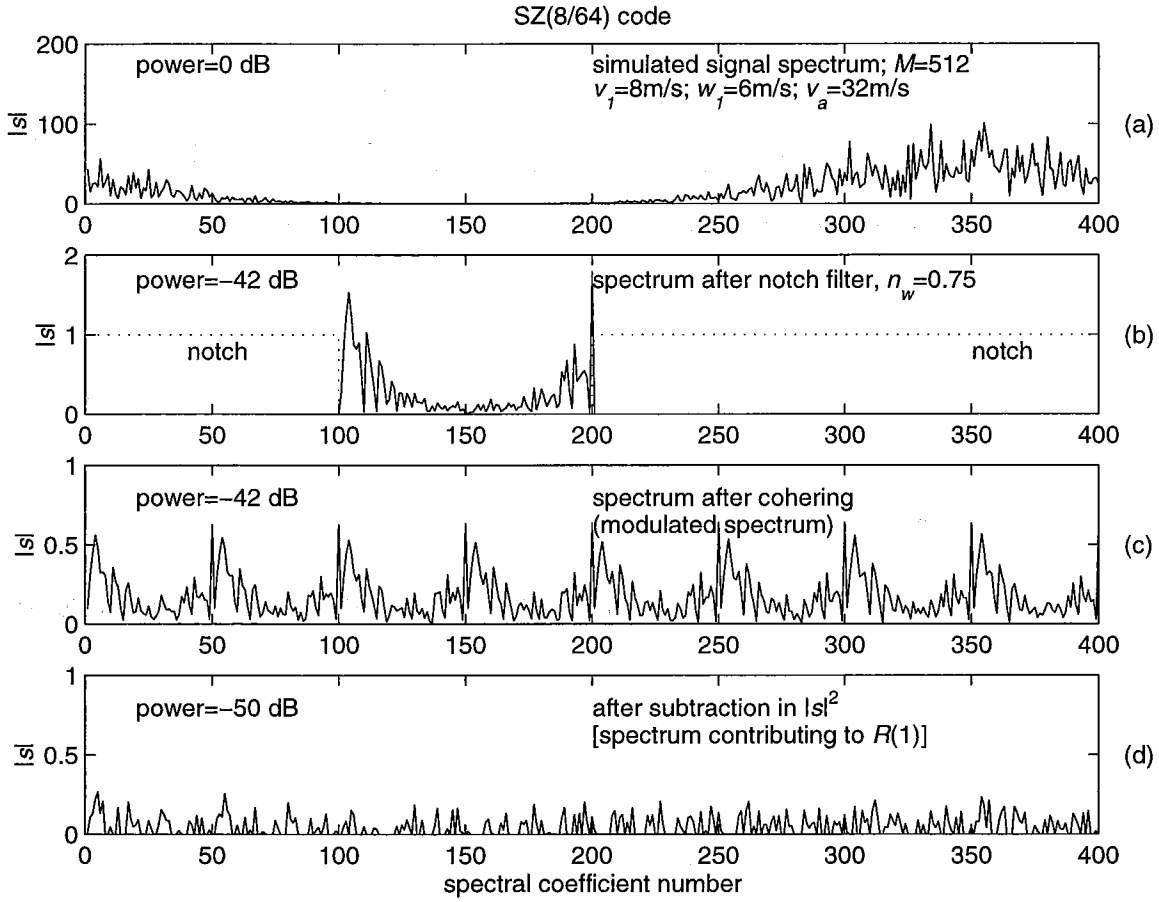

Fig. 2.5. Illustration of the notch filtering and cohering on the stronger 1st trip signal.

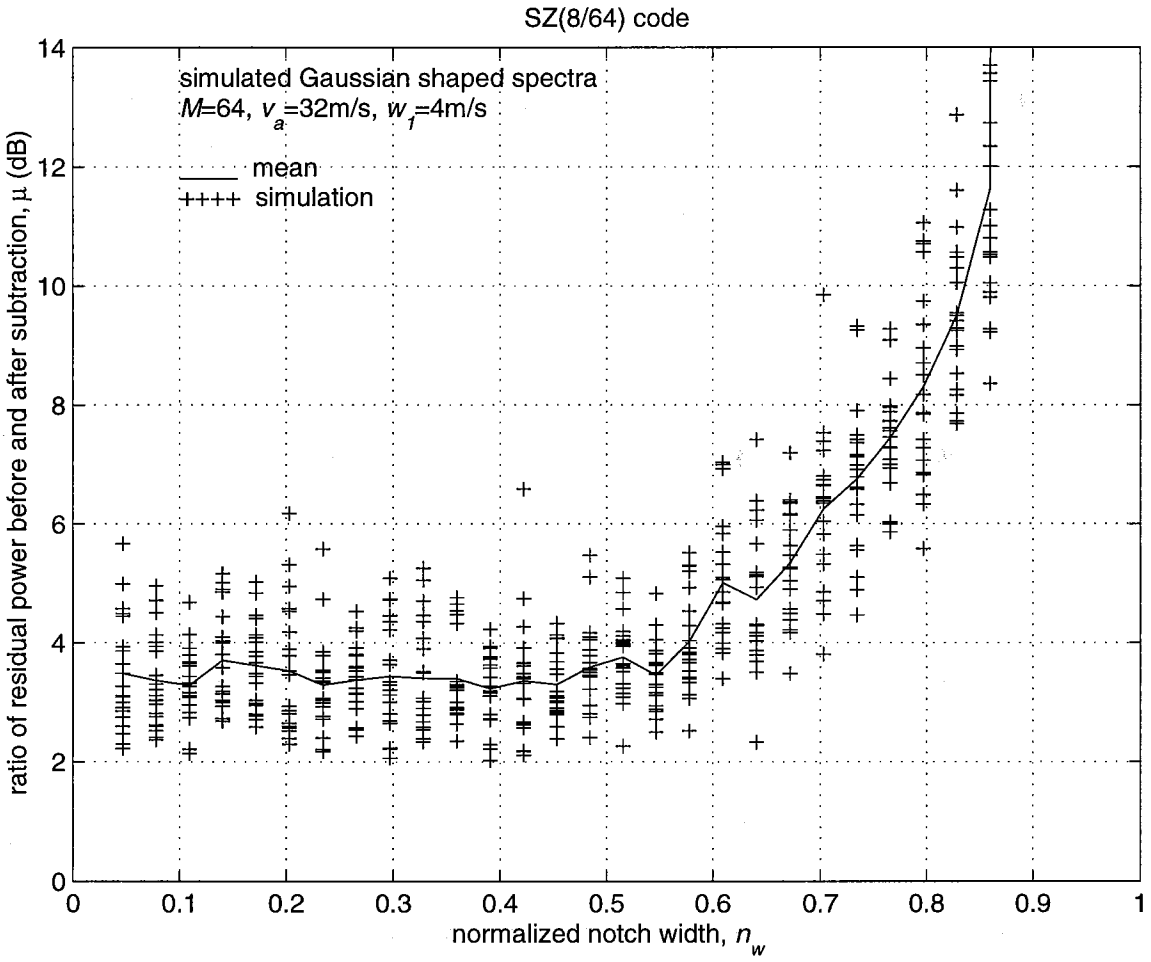

Fig. 2.6. Effective suppression of the residual power in $R(1)$ as a function of normalized notch width.

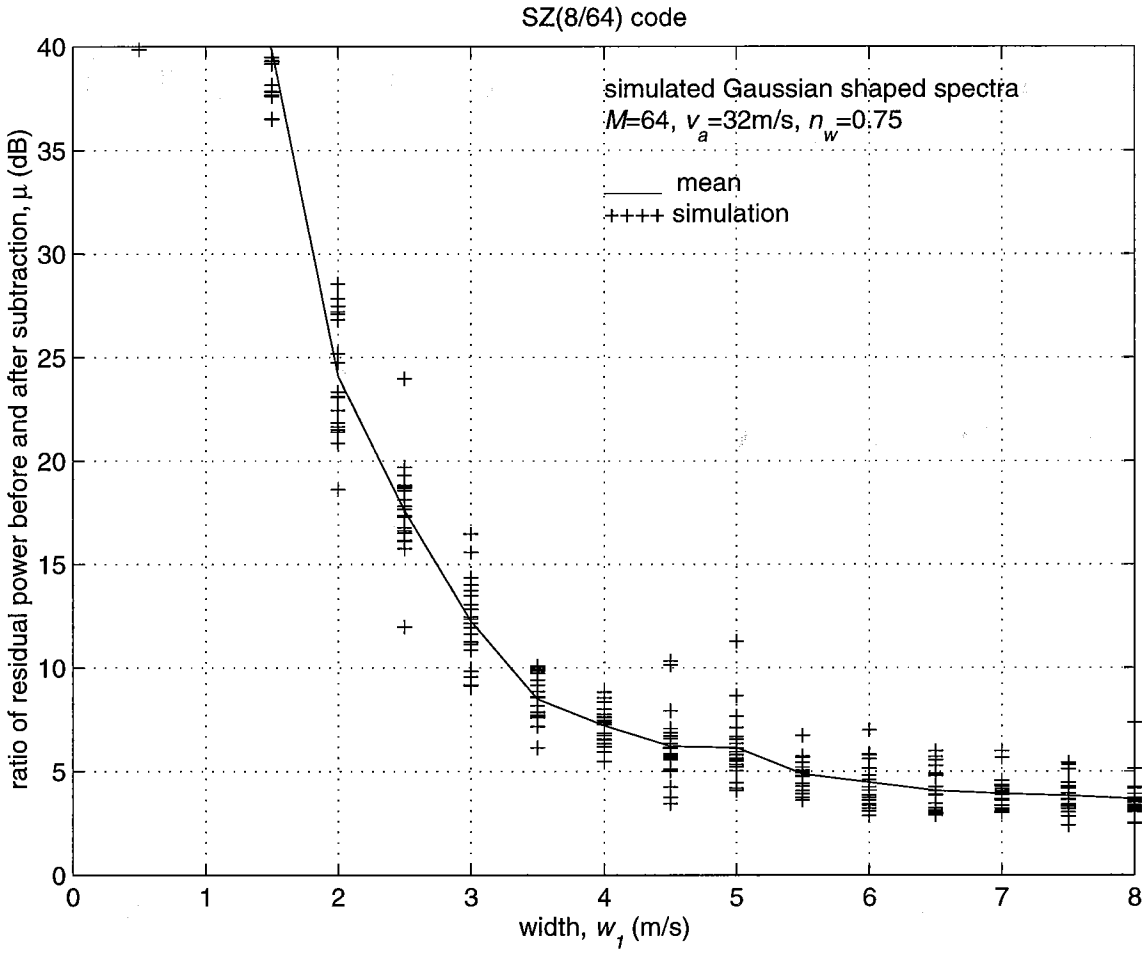

Fig. 2.7. Effective suppression of the residual power in $R(1)$ as a function of spectrum width for n_w=0.75.

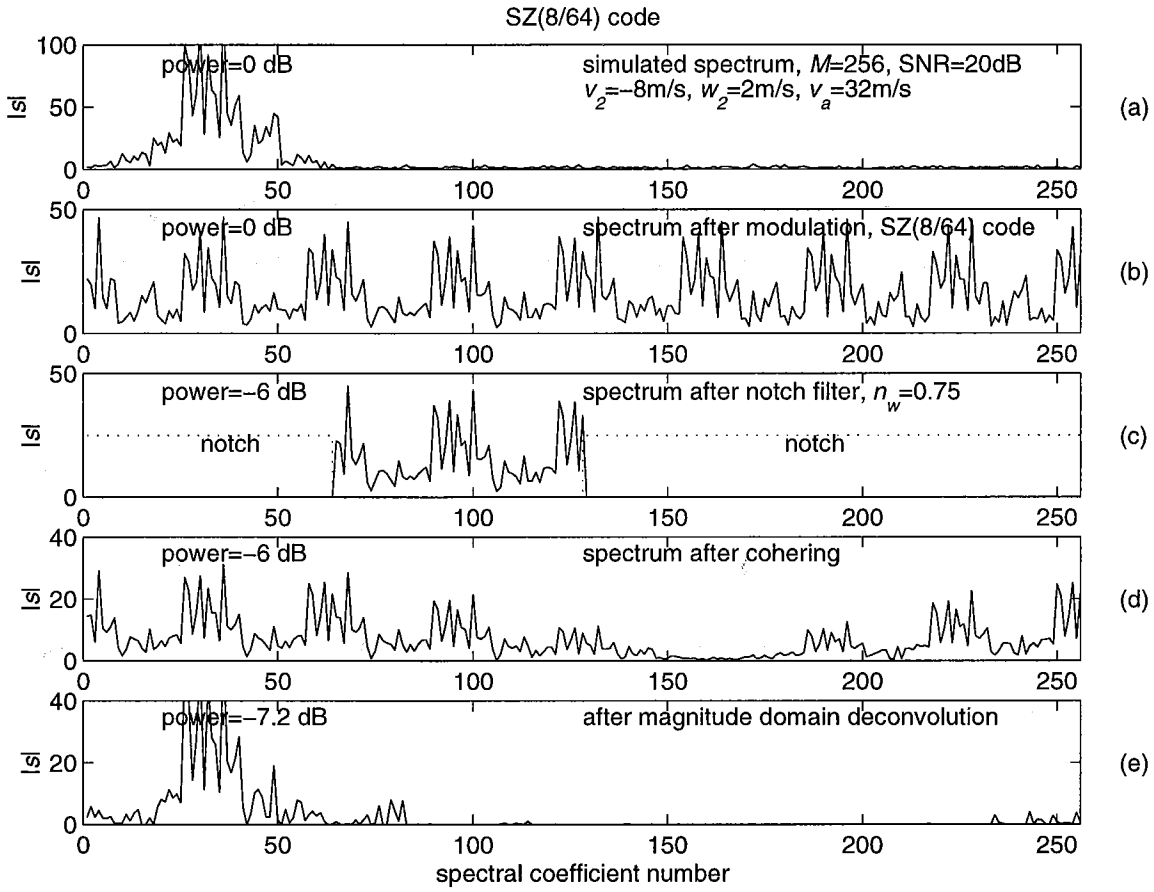

Fig. 2.8. Illustration of the processing steps in the SZ(8/64) decoding algorithm.

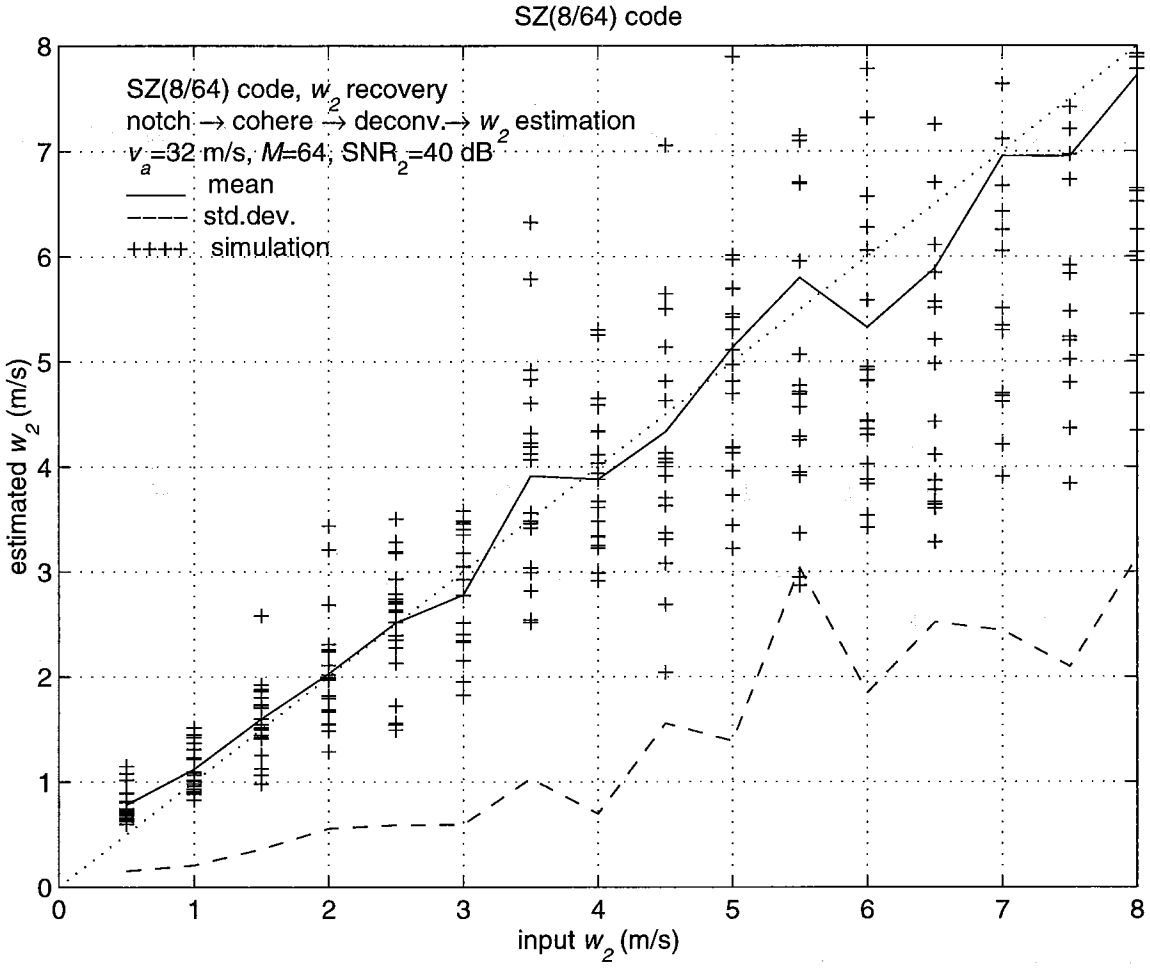

Fig. 2.9(a). Performance of the magnitude domain deconvolution procedure in the recovery of the spectrum width w_2.

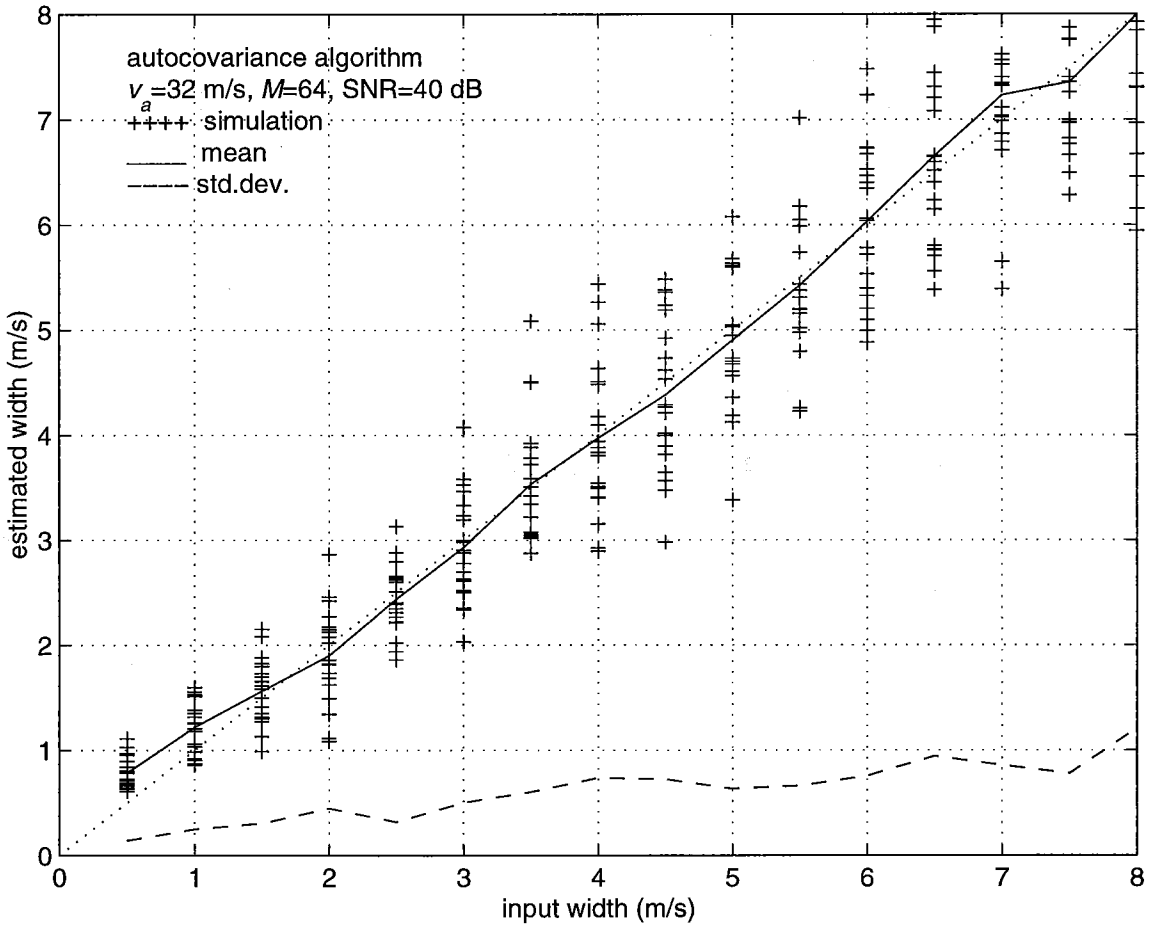

Fig. 2.9(b). Performance of the autocovariance algorithm in the recovery of the spectrum width.

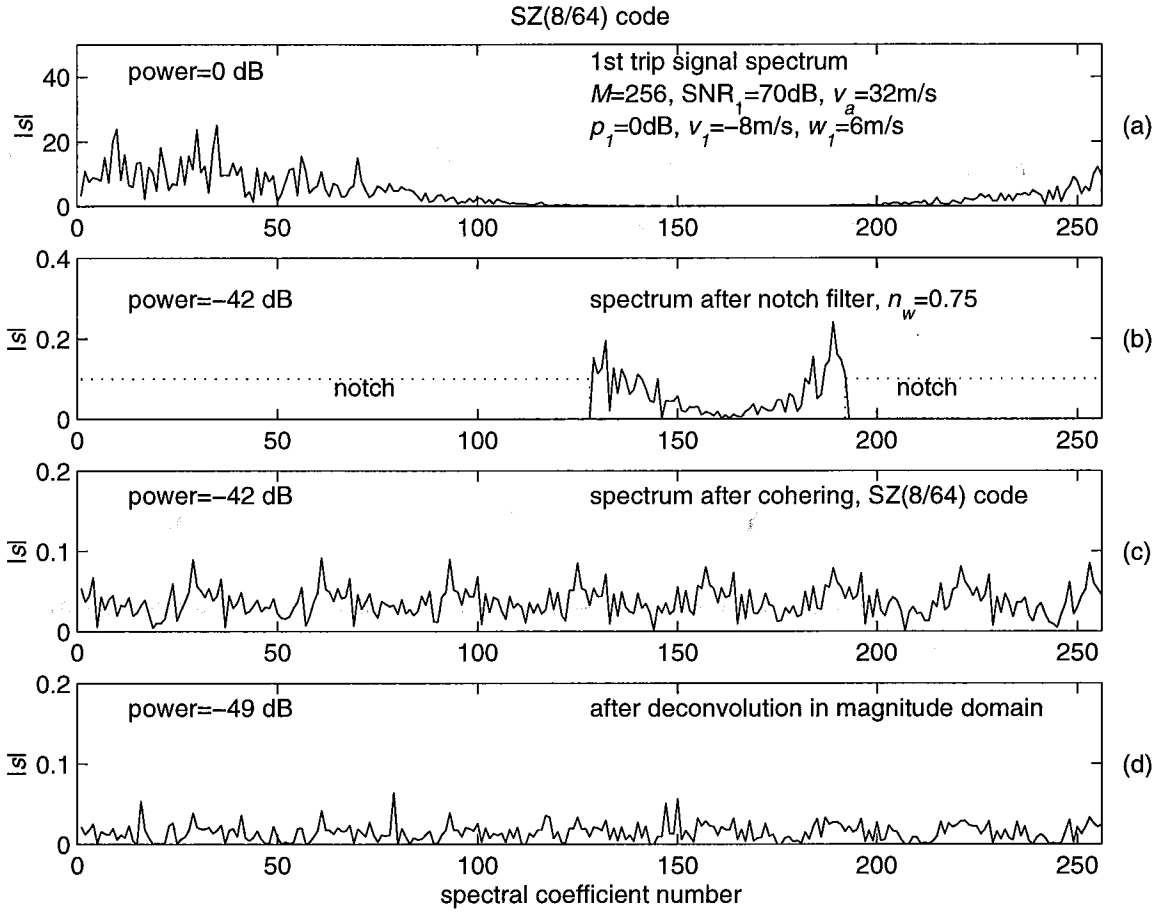

Fig. 2.10. Illustration of the effect of the deconvolution step on the stronger 1st trip signal. In (c), the cohering is for the second trip signal which, in this case, is absent. Similarly, the deconvolution is for the missing second trip signal

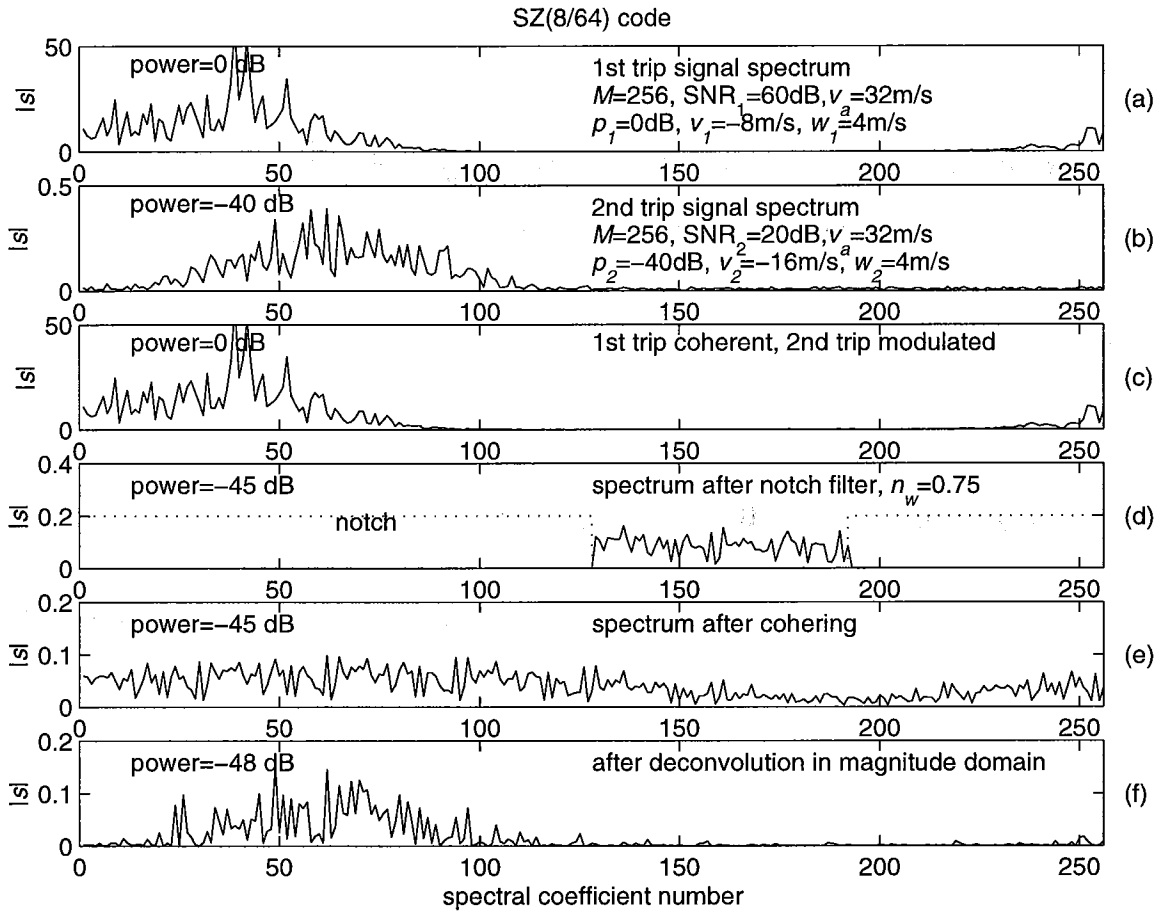

Fig. 2.11. Illustration of the effect of the deconvolution step on the weaker 2nd trip signal.

3. PRACTICAL ASPECTS OF THE RADAR SIGNAL

3.1. Window effect.

All the results presented in Part 1 of this report and in Section 2 were derived from simulated weather signals having a Gaussian shaped spectra. It is also amply clear from the results that the performance of the velocity recovery algorithm depends on the residual overlaid power after notch filtering the stronger signal, which in turn depends on how good is our assumption of a Gaussian shape for the weather signal, especially in the tail ends of the spectrum. The conclusion based on the observation of the weather spectra, that the shape is Gaussian in the mean, does not guarantee that the spectral skirts have this shape. However, this may not be a serious drawback because the window effect is likely to control the power in the spectral tails, rather than the actual weather signal.

The finite length of the time series collected using the radar automatically introduces a rectangular window, resulting in a spread of the power through the side lobes of the window function. In the spectral parameter estimation, this window effect shows up as an increase in the spectrum width estimate. It is generally reduced by introducing a weighted window function which controls the error between the actual and the estimated spectrum. Whatever error remains is not of very serious concern in the estimation of spectral parameters of echo from a single range. However, in the present context of an overlaid signal recovery, the performance of the algorithm for estimating the mean velocity of the weaker signal can be significantly affected. A proper choice of the window weighting function is very important to maximize the region of recovery in the $\{p_1/p_2;w_1\}$ space, especially for narrow spectrum widths.

The rectangular window effect is simulated by generating a long time series and truncating it. Our simulation shows that it is not necessary to generate very long time series; it is sufficient to generate 2 or 3 times the required length and then truncate both ends of the time series to retain only the desired number of samples. A uniformly weighted narrow width signal with a Gaussian spectrum has a far side lobe level of about 40 dB with respect to the peak. This significantly increases the residual power ratio, R_p, of the signal for any given notch width, as compared to the ideal Gaussian spectrum. It has been established earlier that R_p is the limiting factor for the recovery of mean velocity of the weaker signal (for example, see Fig. 5.15 of Part 1 of this report).

A second effect that can be expected is an increase in the standard deviation of the estimation error in the velocity, resulting from the loss of the power due to the window weighting function. To minimize these two effects, we need to retain as much power as possible in the spectrum while suppressing the far side lobe power which will contribute to R_p for the selected notch width. Note that the optimality criteria in the present application is different from the commonly used criteria of maximum energy concentration, minimum energy moment, etc. However, no effort has been made here to optimize the window weights with this new criterion. The well known window functions available in the literature have been evaluated for their suitability, and the one that performed best was selected. This decision was based on the practical considerations, and it will be clear from the results presented later in this section.

The window functions readily available in the literature are the Chebyshev, the Hamming, the von Hann, the Kaiser, the Bartlett, the Blackman, etc. (see MATLAB toolbox software). Since

our interest here is in suppressing the far side lobes, we can evaluate the windows based on their side lobe level and choose the one that has the lowest far side lobes. The Chebyshev window has a variable side lobe level that can be set to any desired value, but it may not be the optimum from the point of minimizing the power loss. We will look at the R_p versus spectrum width plots for these windows, in addition to the side lobe levels, to substantiate our choice. And finally, we shall examine some simulation results with selected spectral parameters to ascertain the suitability of the window for the present purpose.

Fig. 3.1a shows the simulated power spectra with different windows applied. A narrow width is selected to show the side lobe degradation due to the window effect. From the side lobe level consideration, the Blackman window is the choice. The von Hann window also can be chosen with nearly the same performance. The Gaussian signal spectrum without the window is also shown for comparison.

It is important to note that the side lobe level is a function of the number of samples, M. For example, the windowed spectrum departs from the Gaussian spectrum at about -100 dB for the von Hann window, with M=300. For M=64, this point would be -80 dB (see Fig. 3.1b). A similar plot for a wider spectrum (w=4 m s^{-1}) is shown in Fig. 3.2. Note that for spectrum widths 4 m s^{-1} and larger, the signal itself has a larger spread; hence, many of the window functions give the same side lobe power, which shows that the selection of the window is not critical for larger widths.

The effect of the window weighting on the residual power ratio, R_p, is depicted in Fig. 3.3 for n_w=0.75 and different window weights. Simulated spectra are used in computing the R_p. It is clear from this figure that the best choice is the Blackman or the von Hann window. The difference between these two is marginal with respect to the side lobe performance. With respect to the power loss due to the weighting, the von Hann window has about 1 dB lower loss. For the same side lobe level setting (about -100 dB), the Chebyshev window has much higher power loss. With M=64, the power loss associated with different windows are 4.19 dB for von Hann, 5.23 dB for Blackman, 5.72 dB for Chebyshev (side lobe level=-100 dB), 5.33 dB for Kaiser(9), 4.075 dB for Hamming, and 4.84 dB for the Bartlett window.

The window effect is equivalent to a decrease in the SNR of the signal because the residual power from the stronger signal appears as noise when the weaker signal is cohered. Therefore, we can expect an increase in the standard deviation of the error in the recovered mean velocity of the weaker signal as well as some bias error in the mean power estimate of the weaker signal, especially for large p_1/p_2. This is found to be true. The errors in $\hat{v}_2$, obtained from simulations without the window effect, and with the von Hann window weights, are compared in Fig. 3.4 which shows an increase in the standard error from approximately 1.1 m s^{-1} to 1.6 m s^{-1} for w_1=4 m s^{-1} and w_2=4 m s^{-1}, with zero system noise. A similar study with the Blackman window results in a standard error of 2 m s^{-1}; hence, the von Hann window is selected.

The overall performance of the decoding algorithm, with and without the window effect included, is given in Figs. 3.5a and 3.5b, for w_2=4 m s^{-1}. Note that the results reported in Fig. 3.5a are not the same as those reported in Fig. 5.15 of Part 1 of this report; it is different because the error in v_2 is with respect to the input parameters in Fig. 3.5a. Comparing Fig. 3.5a with Fig. 3.5b, it is clear that the window effect increases the standard error in $\hat{v}_2$ by about 0.5 m s^{-1}, but the region of recovery is still as much as that without the window effect. The major difference is that with the window, there is an upper limit for the p_1/p_2, which is independent of the width

w_1. This limit is fairly high (about 90 to 100 dB for M=64 see Fig. 3.3) and for all practical purposes, is more than adequate. The standard error in the region of recovery is larger for w_2>4 m s^{-1} and is less for widths smaller than 4 m s^{-1} (Figs. 3.6, 3.7, 3.8).

The window also affects all other spectral parameters to some degree. The effect of the von Hann window weighting on the estimated parameters v_1, p_1, p_2, w_1, and w_2, is shown in Figs. 3.9 through 3.13, respectively. Widths of both signals are kept constant (4 m s^{-1}) in all these simulations, and the system noise is zero. The upper plots are without the window, and the lower ones are with the window. In all cases, there is an increase in the standard error. The following table gives the mean value of the standard errors with and without the window effect.

Table. 3.1. Mean values of standard deviation of the error in the estimated parameters without window effect and with the von Hann window. (SZ(8/64) code, w_1=w_2=4 m s^{-1}, p_1/p_2 values are varied from 0 to 70 dB.)

parameter	std. err. no window effect	std. err. with window	increase in std. err.	units
$\hat{p}_1$	1.20	1.62	0.42	dB
$\hat{p}_2$	1.51	2.10	0.59	dB
$\hat{v}_1$	0.81	1.10	0.29	m s^{-1}
$\hat{v}_2$	1.16*	1.64*	0.48	m s^{-1}
$\hat{w}_1$	0.61	0.80	0.19	m s^{-1}
$\hat{w}_2$	0.87*	1.25*	0.38	m s^{-1}

Note: * indicates that the mean is computed for p_1/p_2 values over 0 to 50 dB only, the region of recovery for v_2 and w_2.

The increase in standard error is mainly caused by the power loss due to window weighting, which is equivalent to a decrease in the number of samples. For the von Hann window, the 4.19dB loss is equivalent to averaging only 38 percent of the available samples.

A second effect of the window weighting is the loss of power, which results in lower estimates (i.e., bias error) for powers p_1 and p_2. With the choice of the von Hann window, the mean power estimates, p_1 and p_2, have to be compensated by adding 4.19 dB to the estimated values. This is incorporated in the SZ decoding algorithm.

3.2. Receiver noise.

The receiver noise and the background thermal noise received by the antenna are always present in the radar signal. In a receiver system design, the noise figure is sought to be minimized so that further degradation in the input SNR is kept to a minimum possible value. The WSR-88D radar receiver has a noise floor of -113 dBm (Doviak and Zrnic, 1993, p.47), which enables us to get good SNRs for weather signals of interest to meteorologists. For example, at

a 230 km range a reflectivity factor of 25.75 dBZ gives a SNR of 20 dB. The effect of the noise on the spectral parameters estimated using autocovariance processor has been well studied and is available in the literature (see Zrnic, 1977; Doviak and Zrnic, 1993). The standard errors in the velocity estimate, both theoretical and simulated, using an autocovariance processor, are shown Fig. 3.14. (The theoretical $var(\hat{v})$ is computed using Eq. 6.21 of Doviak and Zrnic, 1993, p. 133.) It is seen that a SNR of about 5 dB or better is required for estimating the velocity with an accuracy that is relatively independent of the SNR, using a finite number of samples (M=64). For a SNR >16 dB, the variance of the velocity estimate is mainly due to the signal width, itself. This is the standard deviation of the error in velocity estimate with no window effect present. If the von Hann window is used, the variance almost doubles (for SNR>10 dB), and we require a SNR of at least 10 dB for obtaining a similar performance, i.e., $sd(\hat{v})$ independent of SNR (Fig. 3.15). Fig. 3.15 is generated using simulated weather signals with von Hann window and autocovariance algorithm. A second degree polynomial is fitted to the simulation results to obtain smooth curves.

In the case of overlaid signals with SZ(8/64) phase coding, the SNR_1 required for the stronger signal for the recovery of v_1 is 10 dB (Fig. 3.14). Since the weaker signal is subjected to notch filtering and cohering processes, a degradation in the SNR_2 takes place as discussed in Section 2; thus, the required input SNR_2 is about 20 dB to obtain the lowest possible standard error in the velocity estimate (Fig. 3.16). Note that this lowest error is much larger than that for the autocovariance algorithm without overlay (compare Figs. 3.15 and 3.16). Therefore, the weaker signal power has to be at least -98 dBm (the noise floor of the receiver is -113 dBm) for v_2 estimation. The effect of the receiver noise cannot be eliminated by any of the steps in the algorithm or by the phase coding.

3.3. Ground clutter filtering and its effects.

In the low elevation scans, there is always the ground clutter in the 1st trip returns at close ranges (typically 0 to 20 km), which also affects the recovery of the 2nd trip signal, corresponding to these ranges. The clutter in a weather radar is generally classified into two categories: normally propagated (NP) clutter and anomalously propagated (AP) clutter (generally at longer ranges). The clutter returns can be from fixed scatterers, such as terrain, buildings, trees, vegetation, etc., which produce returns around zero Doppler. For a weather radar, the returns from moving vehicles, birds, insects, air crafts, ocean waves etc., are also considered as clutter, but these echoes will have non-zero Doppler and, hence, need to be identified so that they are not mistaken for the meteorological phenomena. The characteristics of the ground clutter are normally different from that of the weather signal. The width of the ground clutter signal is generally very narrow; however, antenna scanning widens the clutter spectrum. For the scan rates used in the WSR-88D (18 to 20 deg/sec), the width is of the order of 0.35 m s^{-1} (Doviak and Zrnic, 1993, Fig. 7.32; Cornelius et.al., 1995).

Since we are using a uniform PRT, the ground clutter can be easily filtered with a notch filter of sufficient band width centered on the zero Doppler. The ground clutter filter (GCF) can be implemented in the time domain or in the frequency domain. Here, we have chosen to use the frequency domain filtering since spectral processing is used in the algorithm. The GCF is

implemented by simply deleting from the weather spectrum the required number of spectral coefficients centered on the zero Doppler. The spectral peak of the clutter signal can be as large as 70 dB with respect to the noise floor of the receiver, and the clutter power can spread to the rest of the spectrum via the side lobes of the window function. The clutter filtering can affect the recovery of the spectral parameters of the 1st and the 2nd trip signals in several ways. The following discussion on the effect of ground clutter filtering on the spectral parameters is with respect to the SZ decoding scheme. Further, we assume that the echo signal consists of the 1st and 2nd trips and the ground clutter.

The processing in the SZ decoding algorithm branches off along two different paths, depending on whether the 1st trip signal is stronger or weaker, than the 2nd trip signal. These two situations require separate considerations because the ground clutter is present always in the 1st trip range interval.

First, we consider the case of the 1st trip signal stronger than the 2nd trip signal. In this situation, the 1st trip signal parameters are obtained by autocovariance processing the time series with the 1st trip signal coherent (square law power, pulse pair velocity, and logarithm of pulse pair $R(1)/R(2)$ width), and the 2nd trip parameters are obtained at different stages of the notch filtering, cohering, and deconvolution processing steps. The effect on the parameters p_1, v_1, and w_1 is similar to that in the case of an uncoded radar. The ground clutter filter (GCF) notch, centered on the zero Doppler, removes some part of the signal if v_1 is small and has spectral coefficients near zero Doppler. This loss of signal underestimates the mean power (or the reflectivity gets a negative bias), and if the clutter is wide and not completely filtered, the residual clutter power can produce a positive bias in $\hat{p}_1$ (Sirmans, 1992). The mean velocity, $\hat{v}_1$, can get biased away from the zero Doppler, when there is signal loss due to clutter filtering, or towards zero Doppler when there is a residual clutter. These bias errors can be minimized by an appropriate choice of ground clutter filter notch width, w_{cf} (in m s^{-1}). The velocity bias is not a very serious problem, but the reflectivity bias due to the signal loss is important enough to require compensation or correction (Cornelius et. al., 1995).

The effect of GCF on the 2nd trip signal parameter estimates depends on the mean velocity of the first trip signal, v_1. In the SZ(8/64) decoding algorithm, the signal spectrum is notch filtered to recover the weaker signal spectrum. The filter width is $3v_d/2$ centered on the mean velocity $\hat{v}_1$. This filter we refer to as the process notch filter (PNF). If v_1 is in the interval $\pm\, 3v_d/4 \mp w_{cf}/2$, then the two notch filters, viz., the GCF and the PNF, completely overlap; hence, the 2nd trip parameters are affected only to the extent of clutter power spreading due to the window effect (Fig. 3.17a). This effect can be neglected if v_1 is close to zero but can be significant when v_1 is near the limit of the velocity interval specified above.

If v_1 is outside the interval $\pm\, 3v_d/4 \mp w_{cf}/2$, the GCF and the PNF notch do not overlap completely; thus, after these two filters are applied, there are not enough spectral coefficients left for the 2nd trip signal to cohere effectively (a minimum of $M/4$ coefficients are needed for cohering the weaker signal). Therefore, it is necessary to change the PNF notch width or location, or both, to retain at least $M/4$ coefficients in the spectrum (Fig. 3.17b). This, of course, would increase the variance of the spectral parameters but cannot be avoided. The minimum standard error in v_2 is obtained when the residual power from the ground clutter and the 1st trip signal, remaining in the spectrum after the GCF and the PNF have been applied, is the lowest. The residual power ratio is denoted by R_{pr}, which is the ratio of total power, (p_1+p_c), and the residual

power after the GCF and the PNF are applied. The two filters together can have a maximum spread of $3v_a/2$, and the optimum location for the PNF center, v_c, is a function of the 1st trip signal-to-clutter ratio ($SCR_1=p_1/p_c$); the clutter filter width, w_{cf}; the 1st trip signal width, w_1; and the mean velocity, v_1. A typical variation of the R_{pt} with respect to the PNF notch center, v_c, for w_1=4 m s^{-1}, v_1=20 m s^{-1}, and GCF notch width, w_{cf}=5 m s^{-1}, shows that there is an optimum PNF center shift, (v_c-v_1), which is more than the minimum shift required to cohere the 2nd trip signal fully (Fig. 3.18). Both ground clutter and the 1st trip signal are assumed to be Gaussian shaped with w_c=0.35 m s^{-1}, and w_1=4 m s^{-1}; the von Hann window with M=64 is applied in the computations. Figs. 3.19 and 3.20 are similar plots for v_1= 24 m s^{-1} and 32 m s^{-1}, respectively. The GCF notch width and the minimum PNF shift required are also shown in the figures. For negative velocities, the shift is positive. The optimum shift which maximizes the R_{pt} is zero for velocities between $-v_a/2$ and $v_a/2$ and is larger than the minimum shift. Fig. 3.21 shows the normalized optimum filter offset, $(v_c-v_1)/2v_a$, (v_c is the PNF notch center in the velocity scale) as a function of normalized velocity, $v_1/2v_a$.

Now, consider the second situation where the 2nd trip signal is stronger. Before the clutter filtering, the 2nd trip is modulated; hence, after clutter filtering, the 2nd trip power is less by a factor $(1 - w_{cf}/2v_a)$. Note that this factor is derived with the assumption that the modulated spectrum has a uniform distribution of the power across the spectrum, which may not be exactly satisfied for narrow w_2 (<3 m s^{-1}). This error in $\hat{p}_2$ can be easily corrected since the factor is known. However, a more serious problem is in the recovery of velocity $\hat{v}_1$ of the weaker 1st trip signal because the stronger 2nd trip signal does not cohere fully due to the loss of the spectral coefficients around zero Doppler after GCF. This is equivalent to a decrease in the SNR because the incoherent part appears as noise, and thus, results in a larger variance in the v_1 estimate. The other effects on the 1st trip signal parameters $\hat{p}_1$, $\hat{v}_1$, and $\hat{w}_1$ are similar to that in the previous situation; i.e., if v_1 is close to zero, there is a significant loss of the power, and there will be bias in $\hat{p}_1$, $\hat{v}_1$, and $\hat{w}_1$ because of the GCF notch. The parameters, v_2, and w_2, are estimated after cohering the 2nd trip signal, which is not affected by the GCF notch filtering. In this situation, there is no need to change the location or the width of the PNF notch (the PNF is centered on $\hat{v}_2$).

The GCF notch width required to effectively remove the clutter depends on the clutter width. Fig. 3.22 plots the clutter suppression ratio, R_c, as a function of the GCF notch width for three different clutter widths: w_c=0.2, 0.35, and 0.5 m s^{-1}. The theoretical curve is for a Gaussian signal without the window effect, and the data points indicated by a Δ symbol are obtained using simulation with M=1024, zero noise, and the von Hann window. It can be seen that the window introduces an upper limit for the clutter rejection ratio, R_c (see the limit for clutter width=0.2 m s^{-1}). The noise is set to zero to show this effect. If the SNR of the signal is lower than this upper limit, then SNR will be the upper limit for the recovery of v_2. It is important to note that this upper limit for the R_c is a function of the number of samples, M.

In order to study the effect of ground clutter on the velocity recovery using the SZ coding scheme, we again resort to the simulation. The ground clutter is simulated by introducing a narrow Gaussian shaped spectrum centered on the zero Doppler with a specified clutter-to-noise power ratio (CNR). Since the noise floor of the receiver generally remains constant (-113 dBm for WSR-88D), we take the noise level as the reference to specify the clutter power and the 1st and 2nd trip signal powers. The following abbreviations are used: $CNR=p_c/p_n$, $SNR_1=p_1/p_n$, $SNR_2=p_2/p_n$, $SCR_1=p_1/p_c$, and $SCR_2=p_2/p_c$ (p_n- noise power; p_c - clutter power; p_1/p_2 - overlaid power ratio; SCR

- signal to clutter ratio).

Let us examine the effect of the window on the clutter spectrum using the example given in Fig. 3.23. The first spectrum is a simulated spectrum without the window effect. The second one shows a significant spread of the power due to a uniformly weighted rectangular window. The third spectrum is with the von Hann weights. It can be seen that the spectrum shape is nearly restored by the von Hann weights, except for a loss of about 4.19 dB in the signal power. A 4 m s^{-1} wide notch filter would remove almost all the clutter from this spectrum. However, the situation is not as good in practice because the spectral spread by the von Hann window increases with a decreasing number of samples. In the example discussed above, M=512 is used. The spectrum shape is not restored to the original shape when CNR=50 dB and M=64 (Fig. 3.24). There is a significant spreading of the spectral power which needs a much wider filter to achieve the same rejection ratio. Therefore, the clutter filter width has to be increased to get better rejection. This will lead to a larger loss of the 1st trip signal and would increase the bias error in $\hat{v}_1$ if it is close to zero.

If the 1st trip signal is stronger, there is an optimum clutter filter width and PNF notch location with respect to v_2 recovery. However, this clutter filter width may not be the optimum with respect to minimizing the bias error in the $\hat{v}_1$ and $\hat{p}_1$. It is always a compromise between these two that we have to arrive at while selecting the clutter filter width. In a practical implementation, it is perhaps better to retain the clutter filter selection, as it is done presently in the WSR-88D, and select an optimum PNF shift to optimize the v_2 recovery.

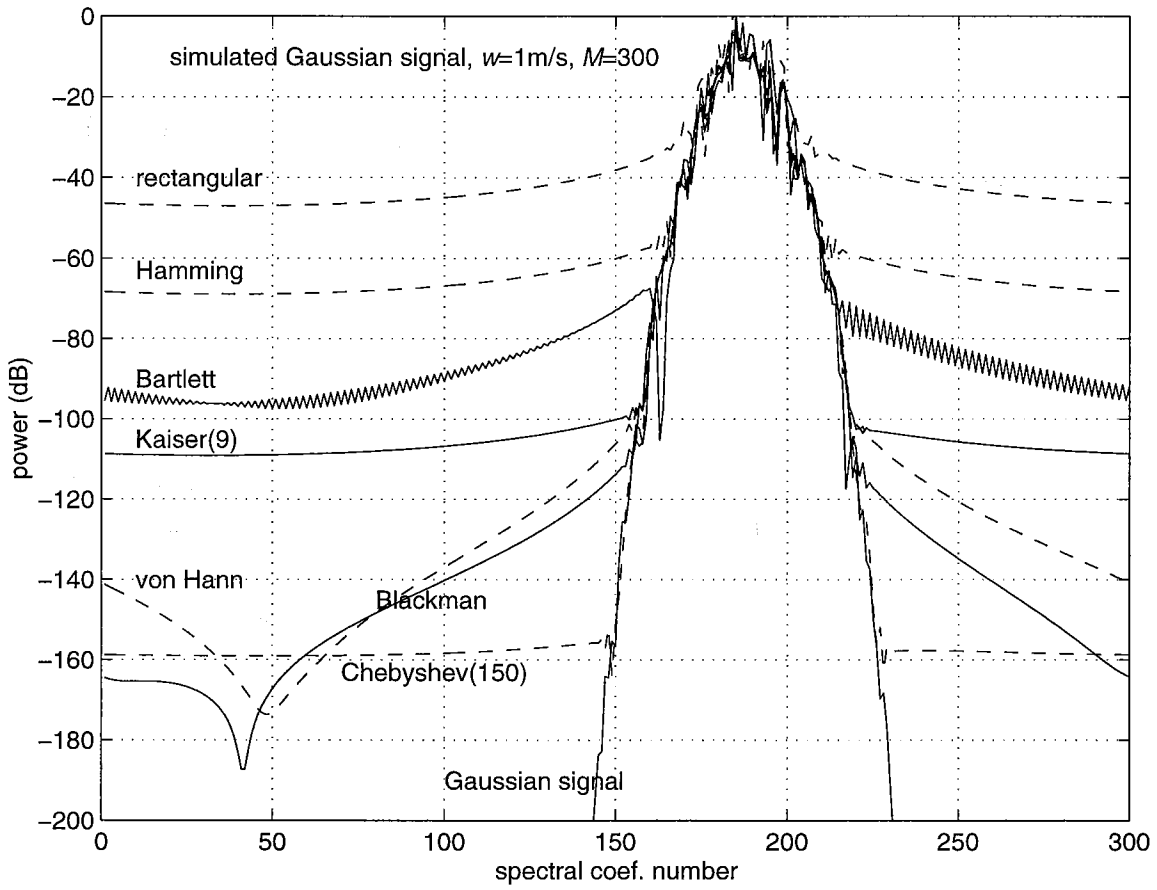

Fig . 3.1(a). Effect of the window on a narrow width Gaussian shaped simulated weather signal spectrum (v_a=32 m/s, w=1 m/s, M=300).

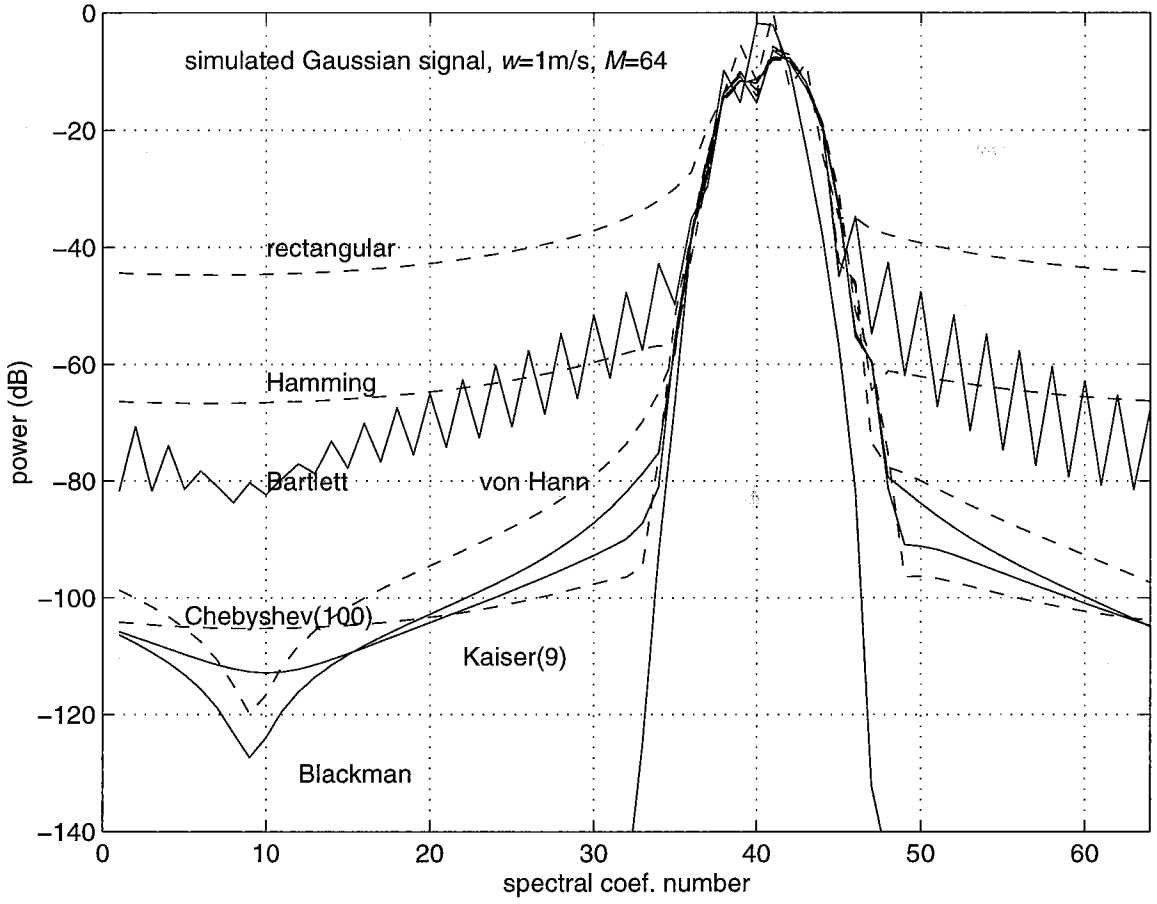

Fig . 3.1(b). Spectrum broadening effect due to a limited number of samples (v_a=32 m/s, w=1 m/s, M=64).

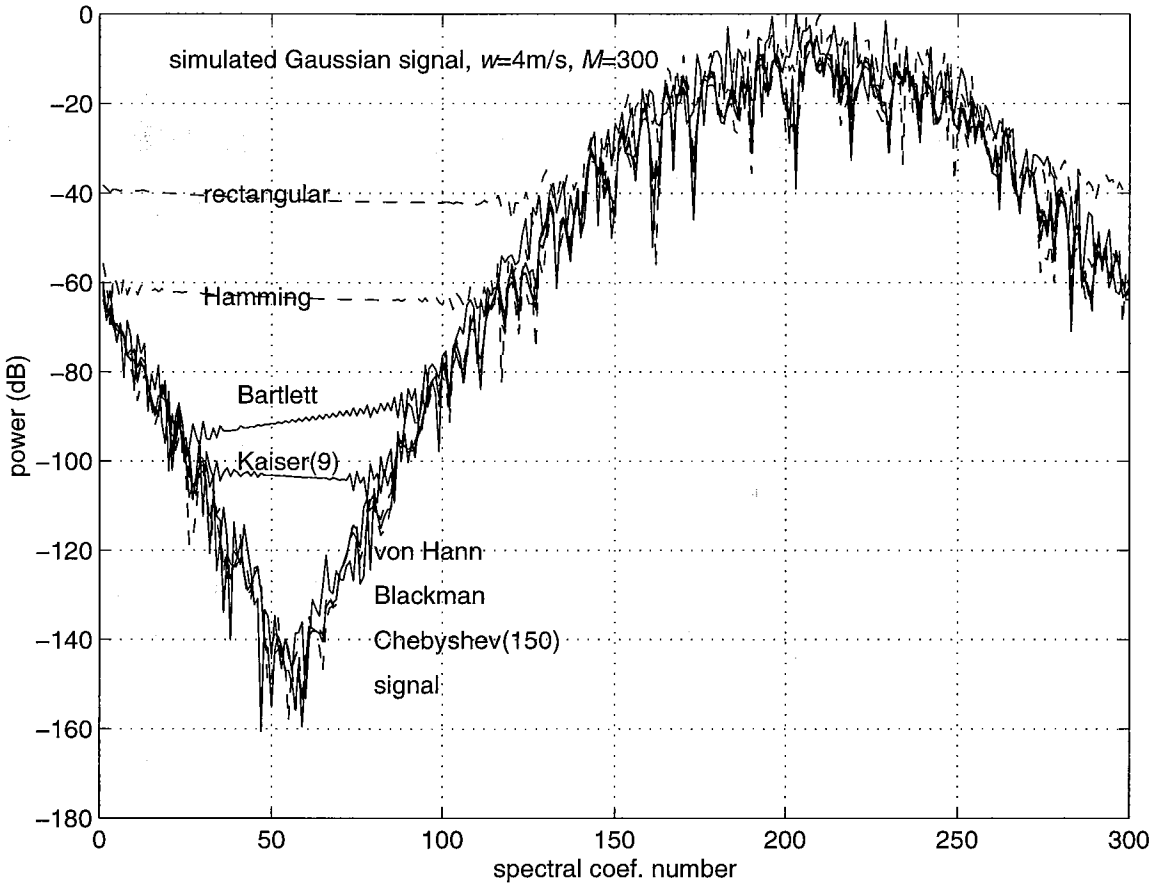

Fig. 3.2. Effect of different windows on a broader spectrum (v_a=32 m/s, w=4 m/s, M=300).

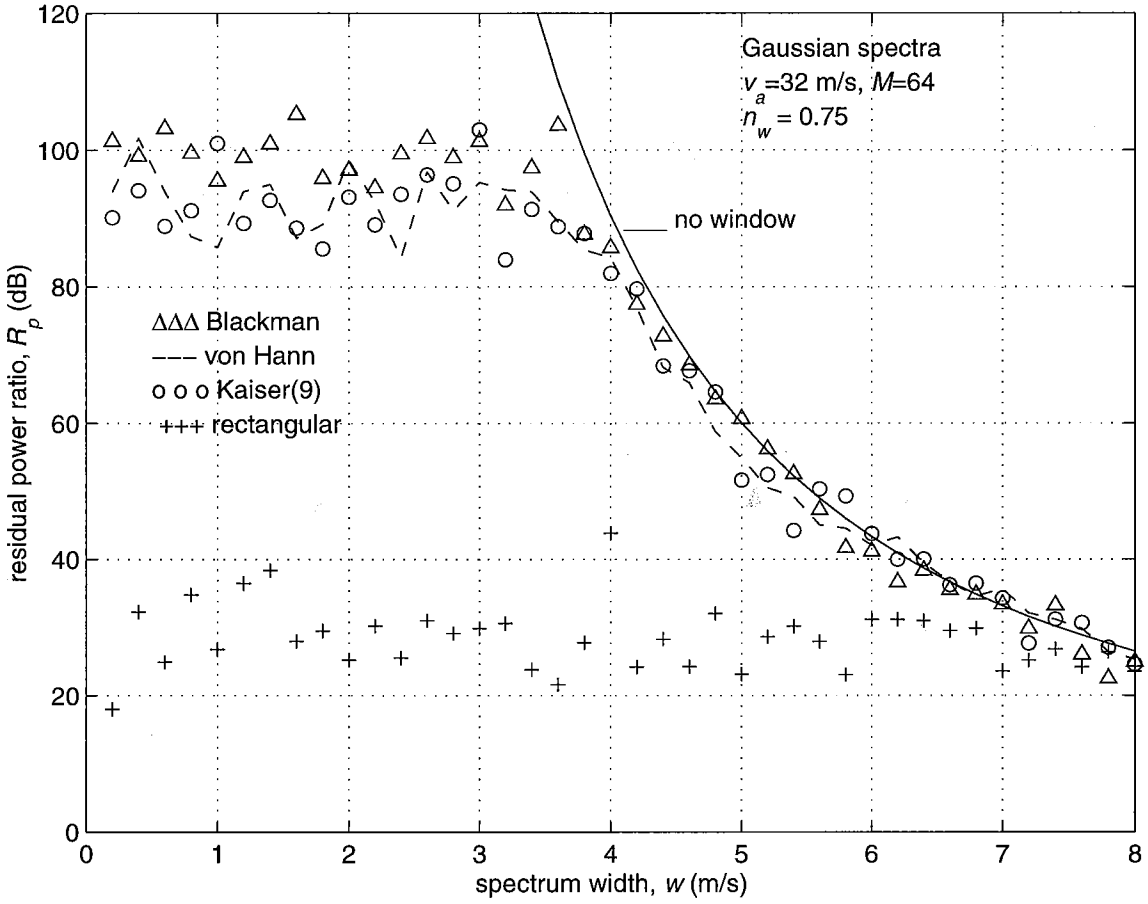

Fig. 3.3. Theoretical and simulated residual power ratios as a function of the spectrum width for different windows.

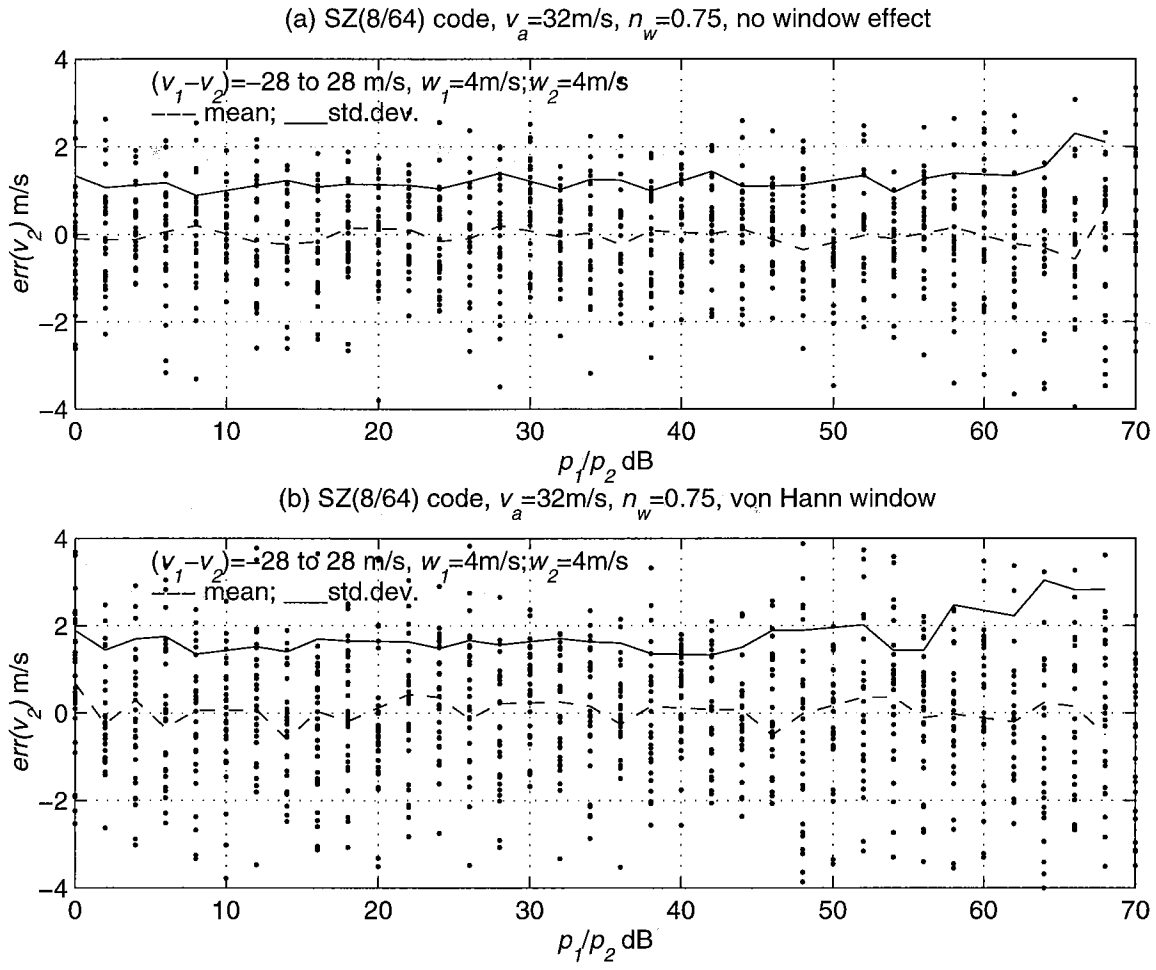

Fig. 3.4. A comparison of the error in v_2 estimate; (a) without the window effect, and (b) with the von Hann window.

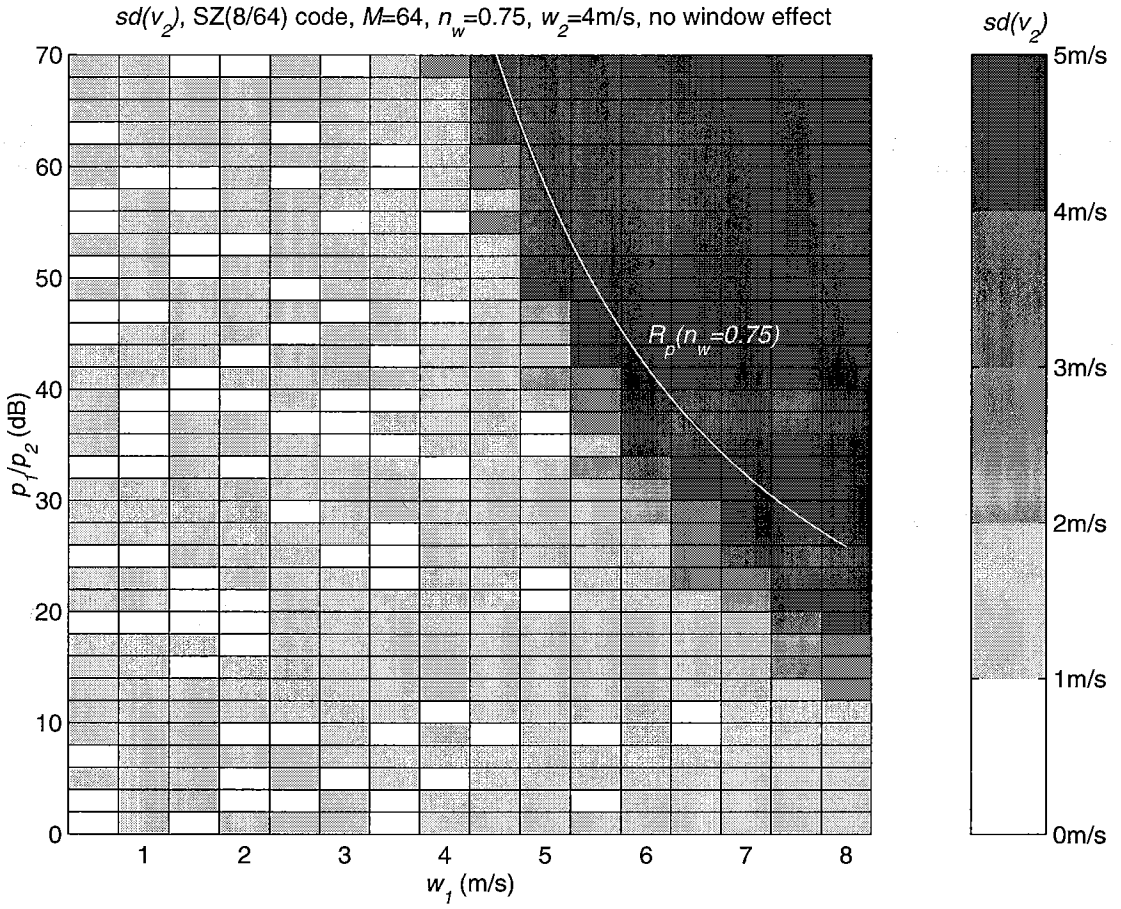

Fig. 3.5(a). Plot of $sd(\hat{v}_2)$ as a function of p_1/p_2 and w_1 without the window effect (w_2=4 m/s, v_a=32 m/s).

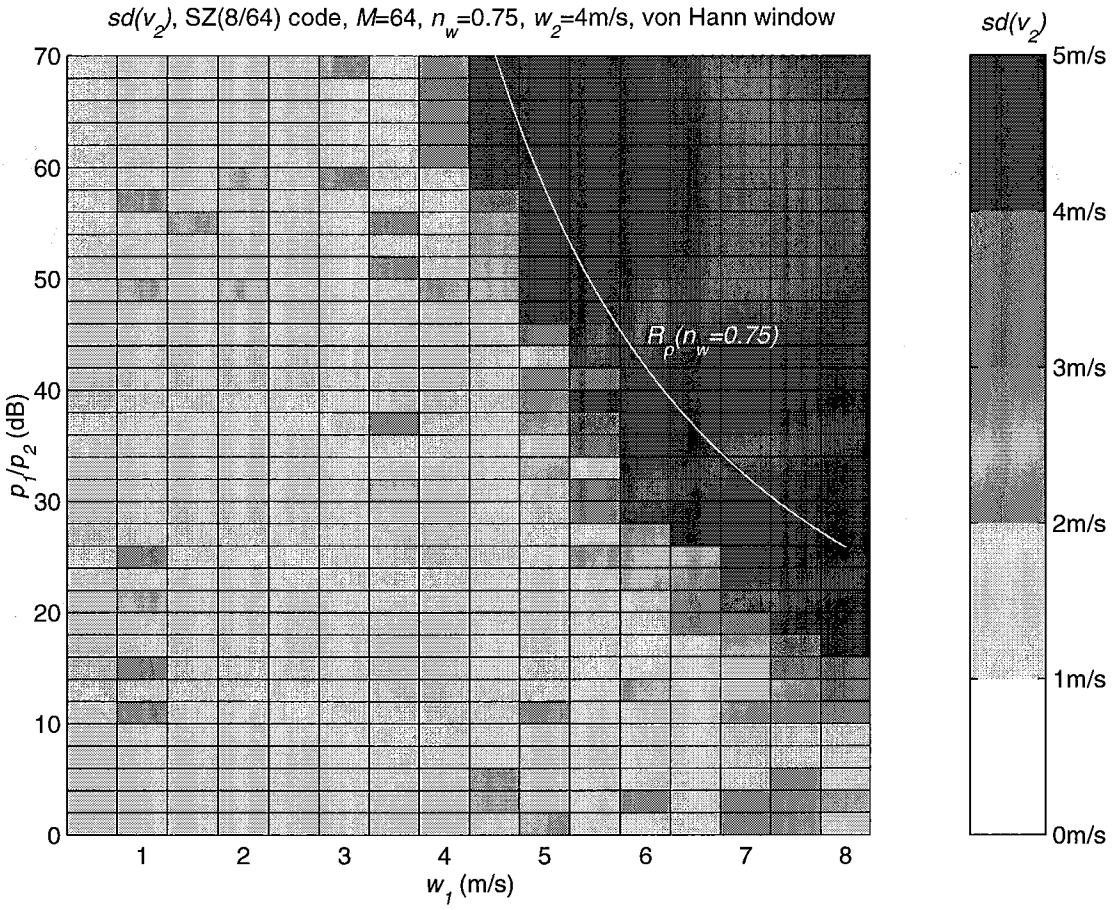

Fig. 3.5(b). Plot of $sd(\hat{v}_2)$ as a function of p_1/p_2 and w_1 with the von Hann window (w_2=4 m/s, v_a=32 m/s).

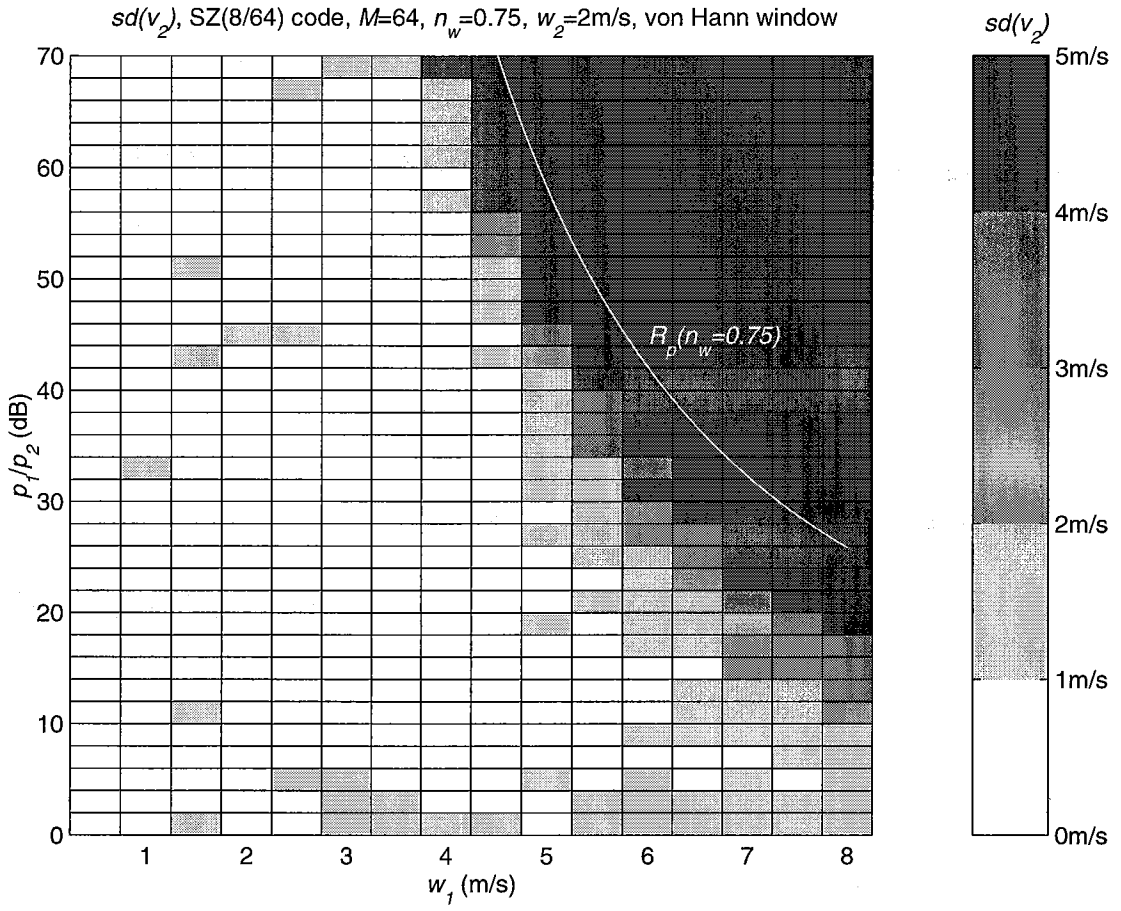

Fig. 3.6. Plot of $sd(\hat{v}_2)$ as a function of p_1/p_2 and w_1 with the von Hann window (w_2=2 m/s, v_a=32 m/s).

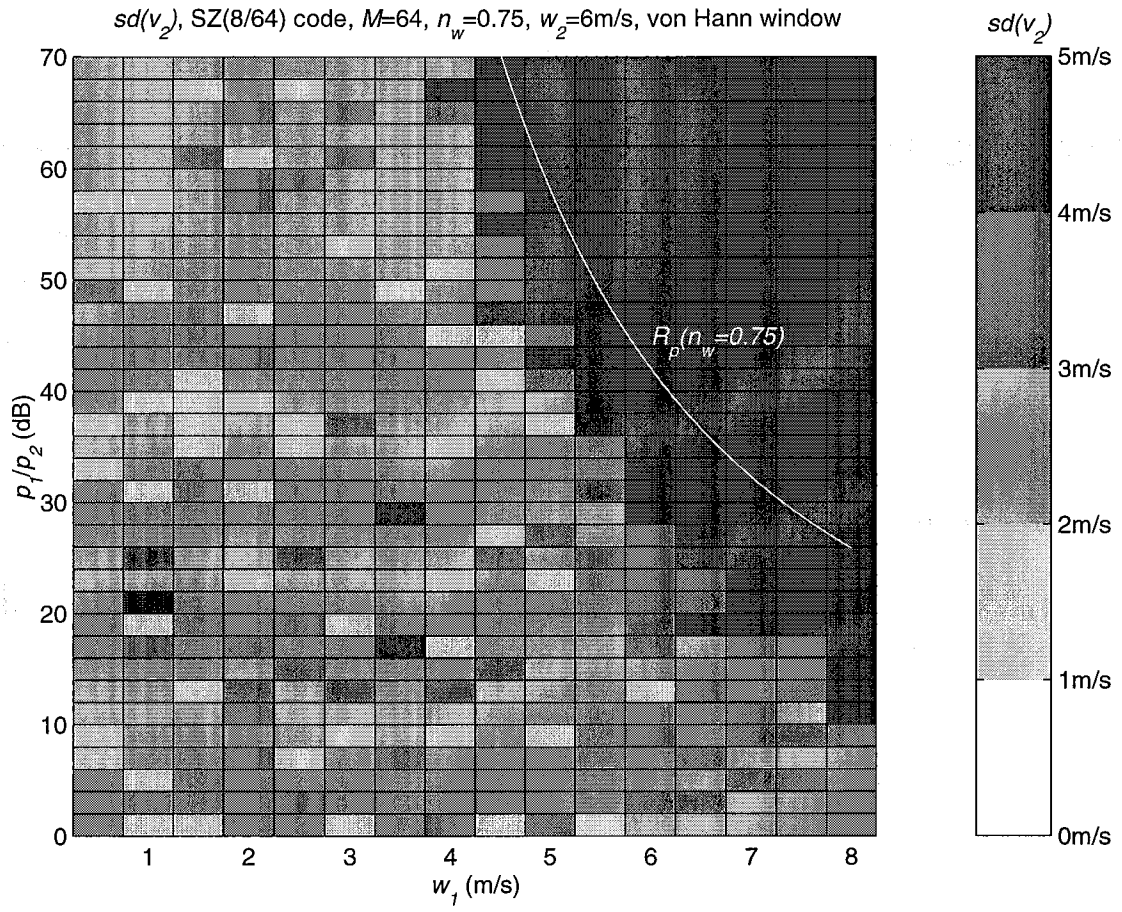

Fig. 3.7. Plot of $sd(\hat{v}_2)$ as a function of p_1/p_2 and w_1 with the von Hann window (w_2=6 m/s, v_a=32 m/s).

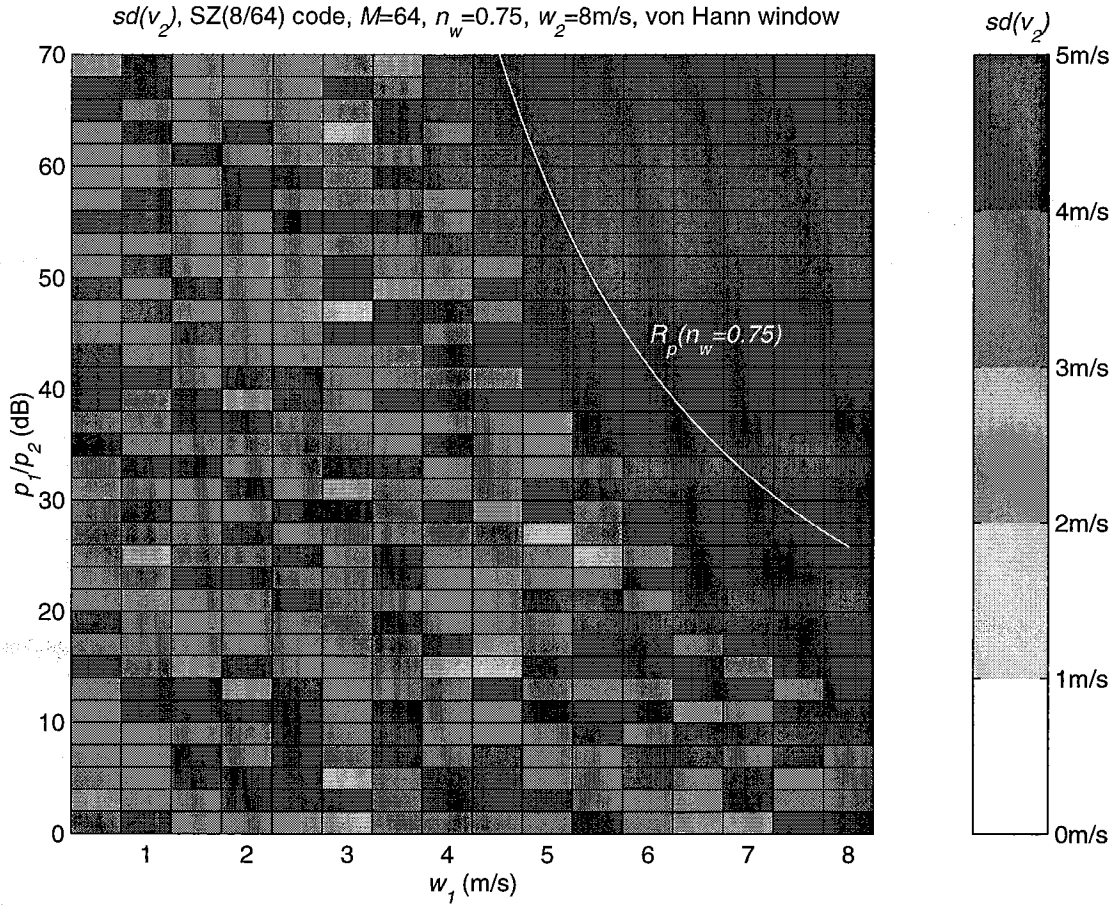

Fig. 3.8. Plot of $sd(\hat{v}_2)$ as a function of p_1/p_2 and w_1 with the von Hann window (w_2=8 m/s, v_a=32 m/s).

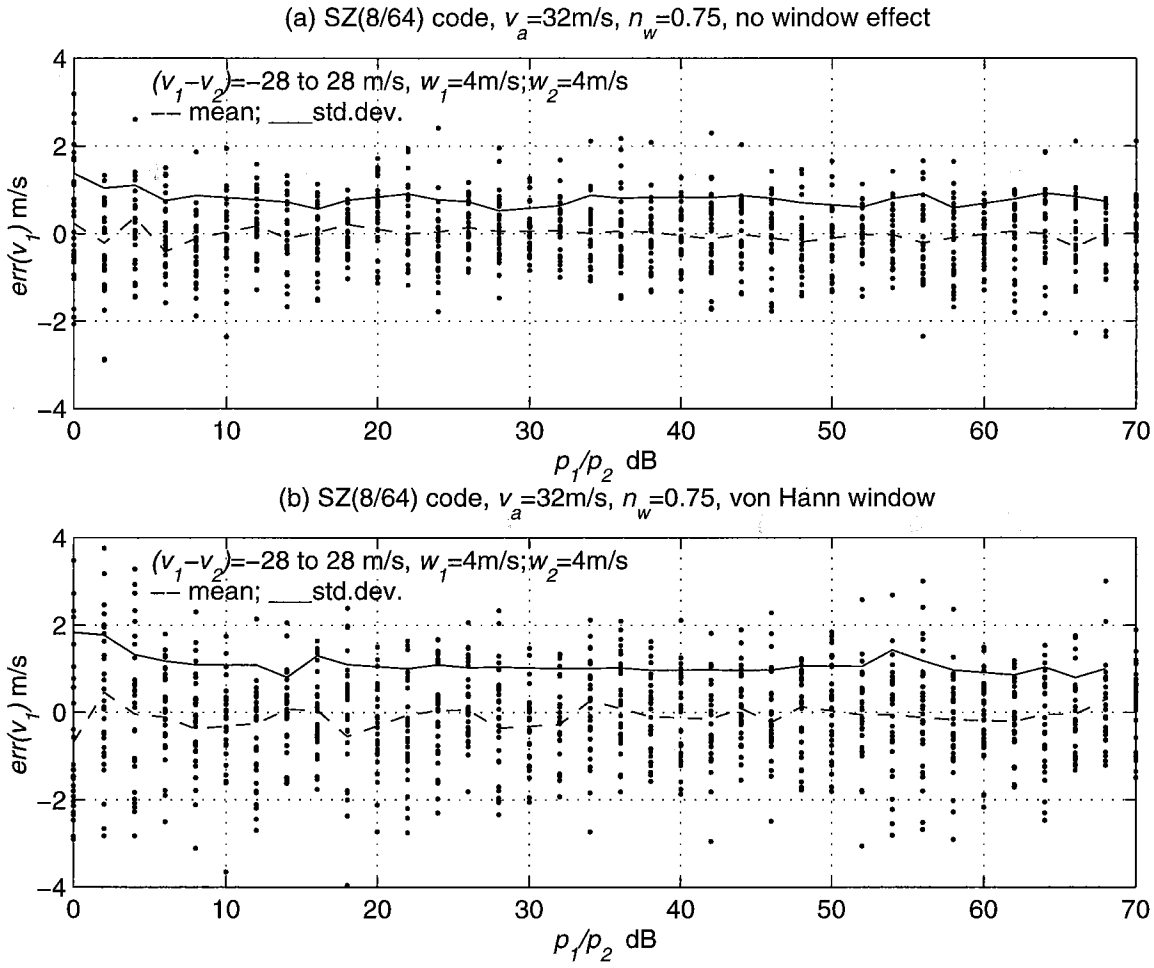

Fig. 3.9. A comparison of the error in v_1 estimate, (a) without the window effect and (b) with the von Hann window.

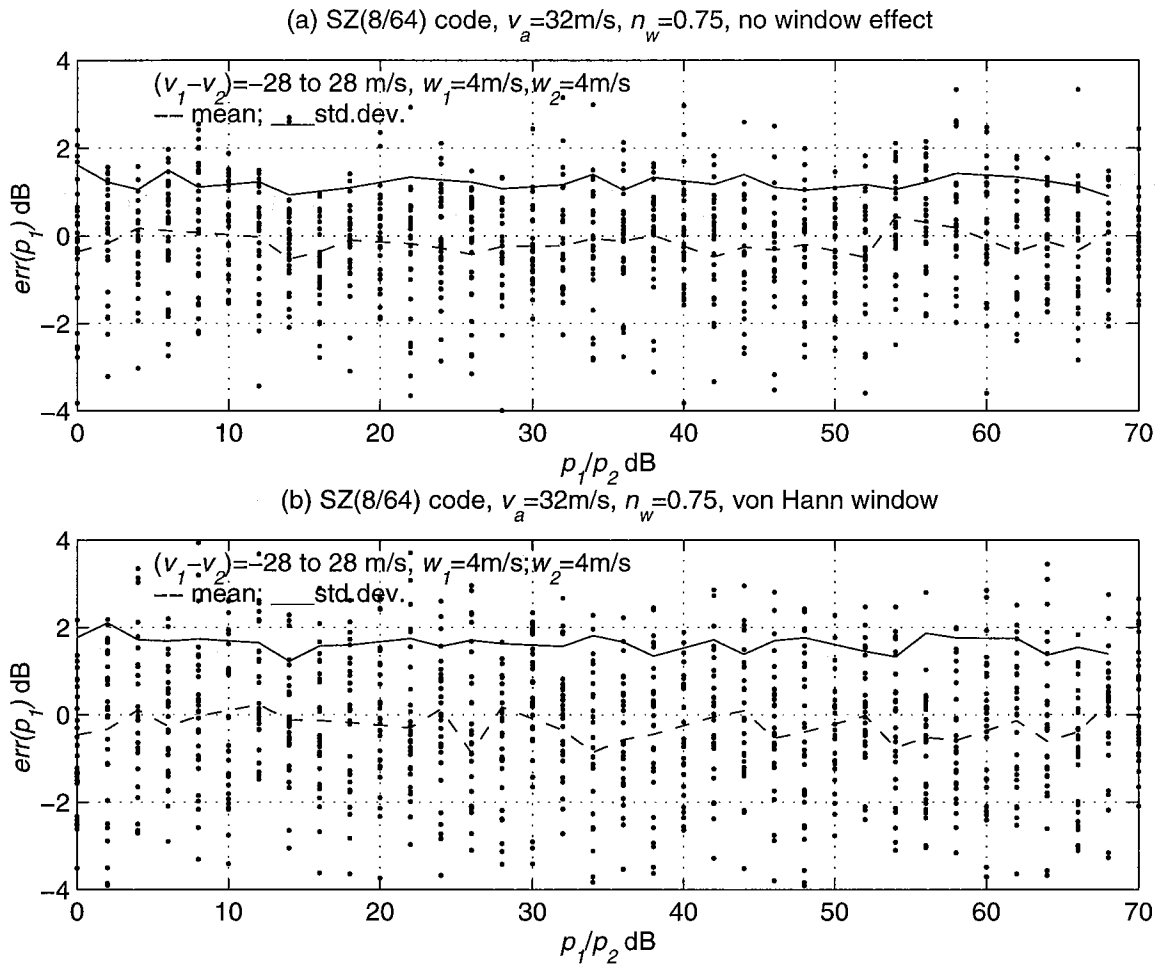

Fig. 3.10. A comparison of the error in p_1 estimate, (a) without the window effect and (b) with the von Hann window.

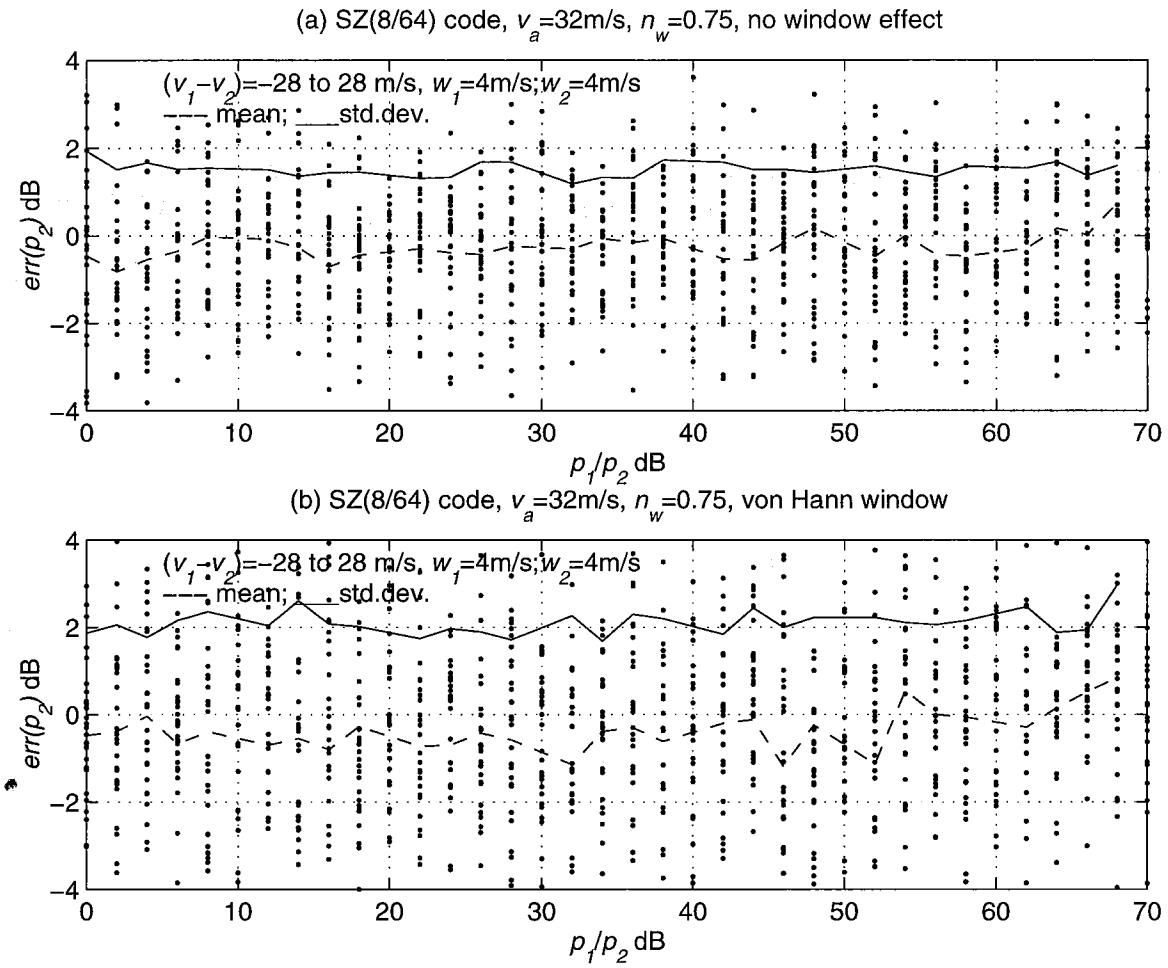

Fig. 3.11. A comparison of the error in p_2 estimate, (a) without the window effect and (b) with the von Hann window.

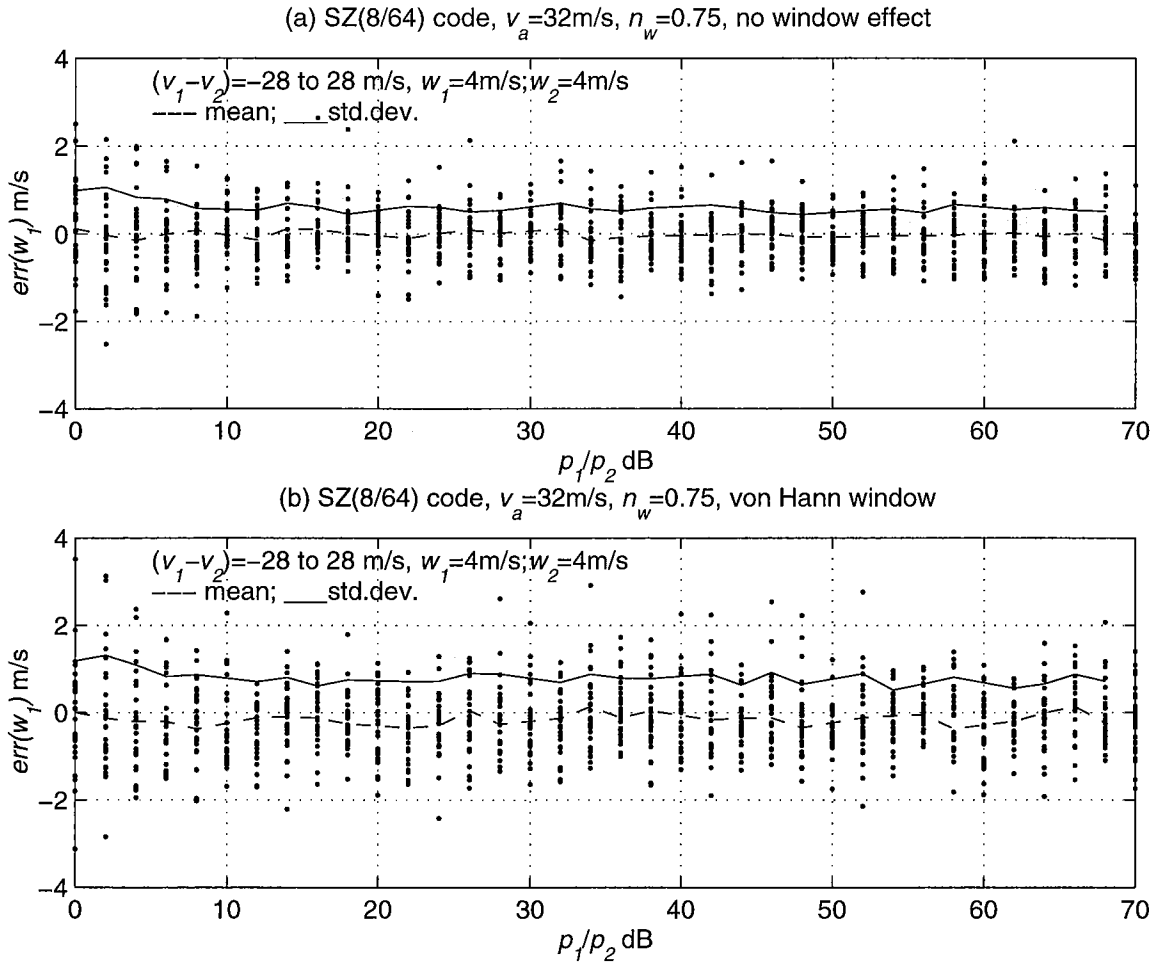

Fig. 3.12. A comparison of the error in w_1 estimate, (a) without the window effect and (b) with the von Hann window.

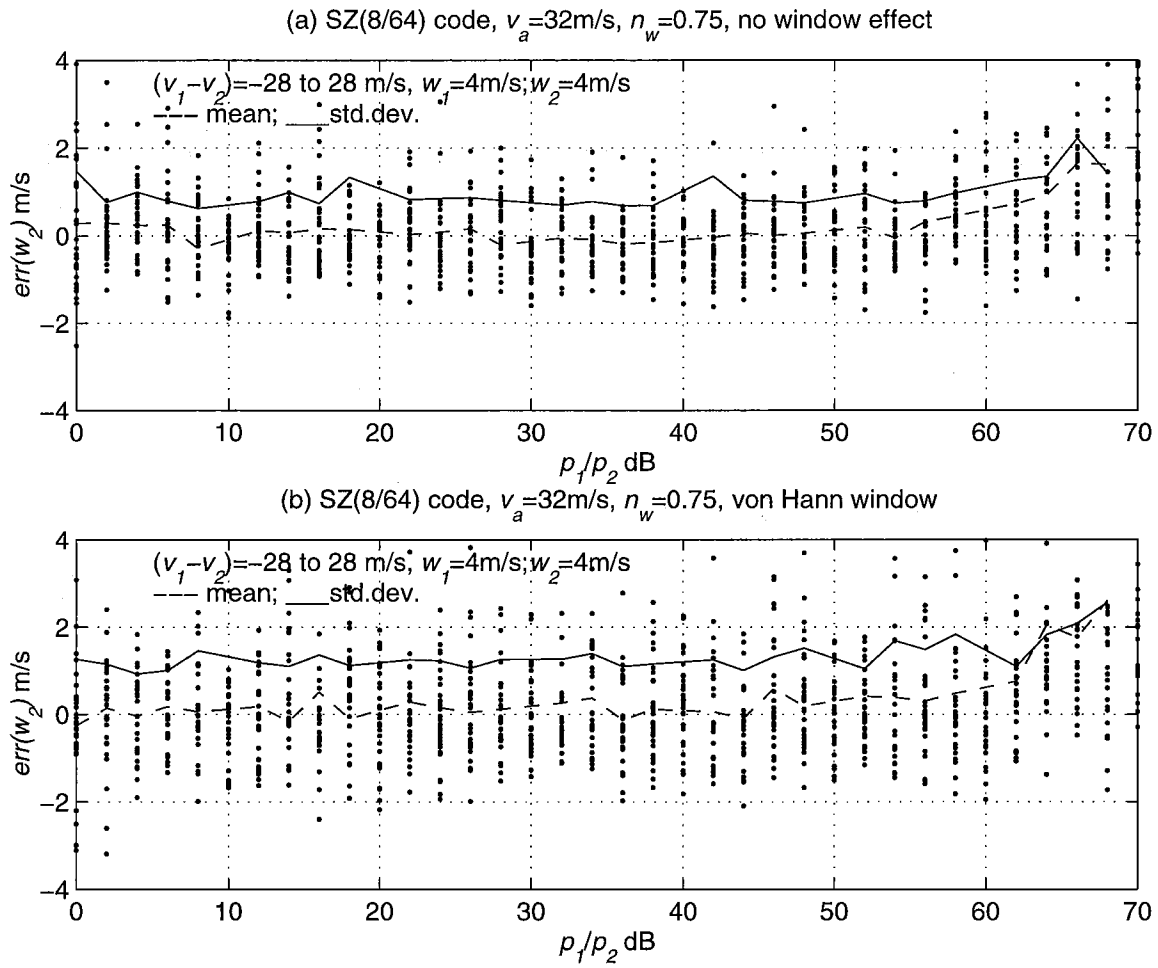

Fig. 3.13. A comparison of the error in w_2 estimate, (a) without the window effect and (b) with the von Hann window.

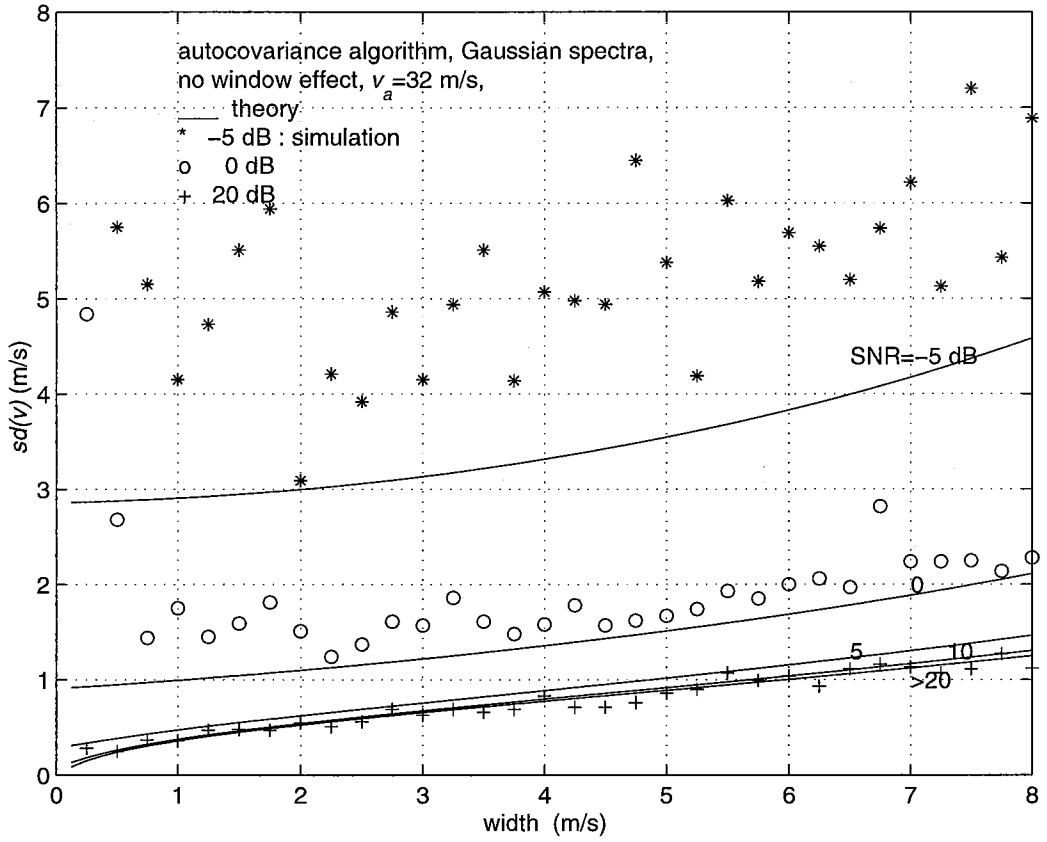

Fig. 3.14. Theoretical and the simulated $sd(\hat{v})$ using the autocovariance algorithm. (Theoretical values are computed using Eq. 6.21. of Doviak and Zrnic, 1993.)

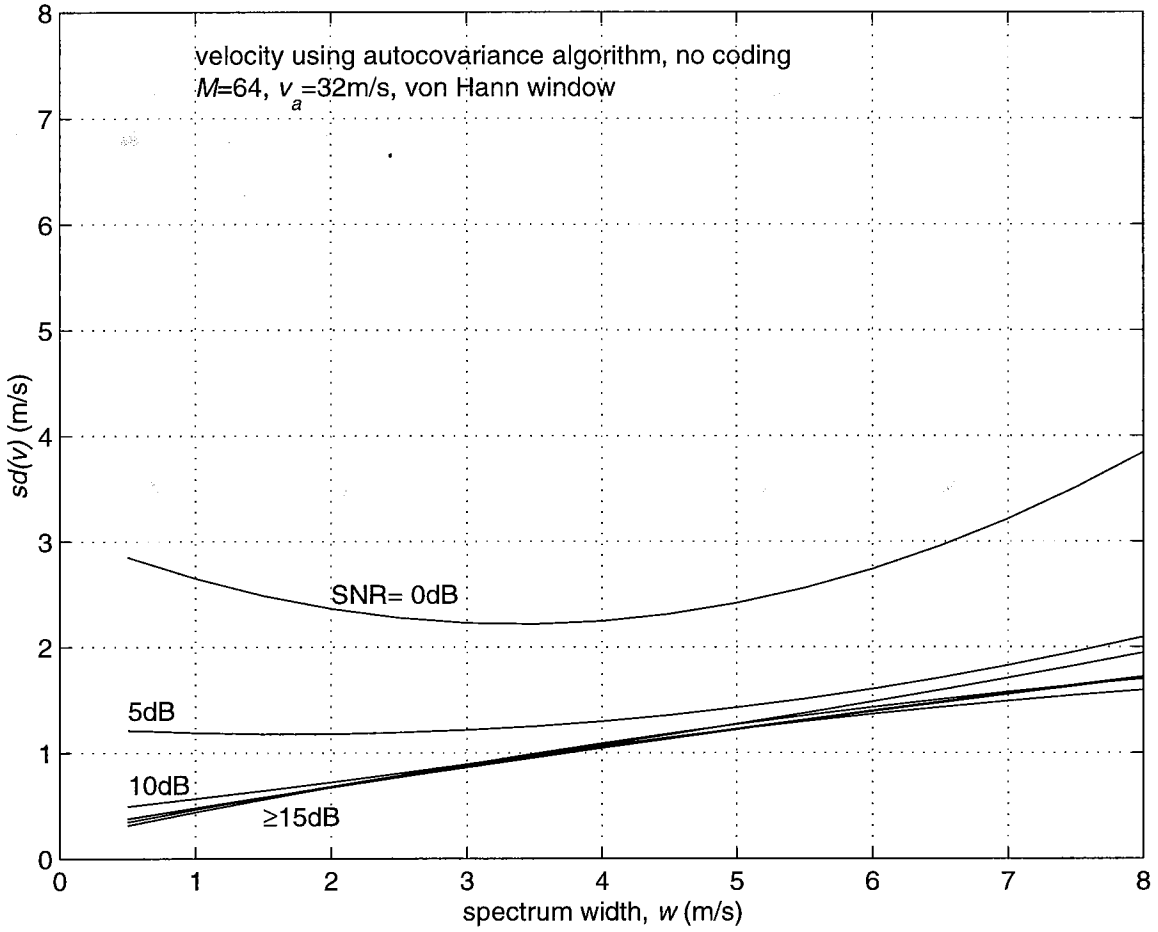

Fig. 3.15. $sd(\hat{v})$ versus spectrum width, w, with the von Hann window for the autocovariance algorithm. 100 simulations are used for each w and SNR to compute $sd(\hat{v})$, and a 2nd degree polynomial is fitted to smooth the curve.

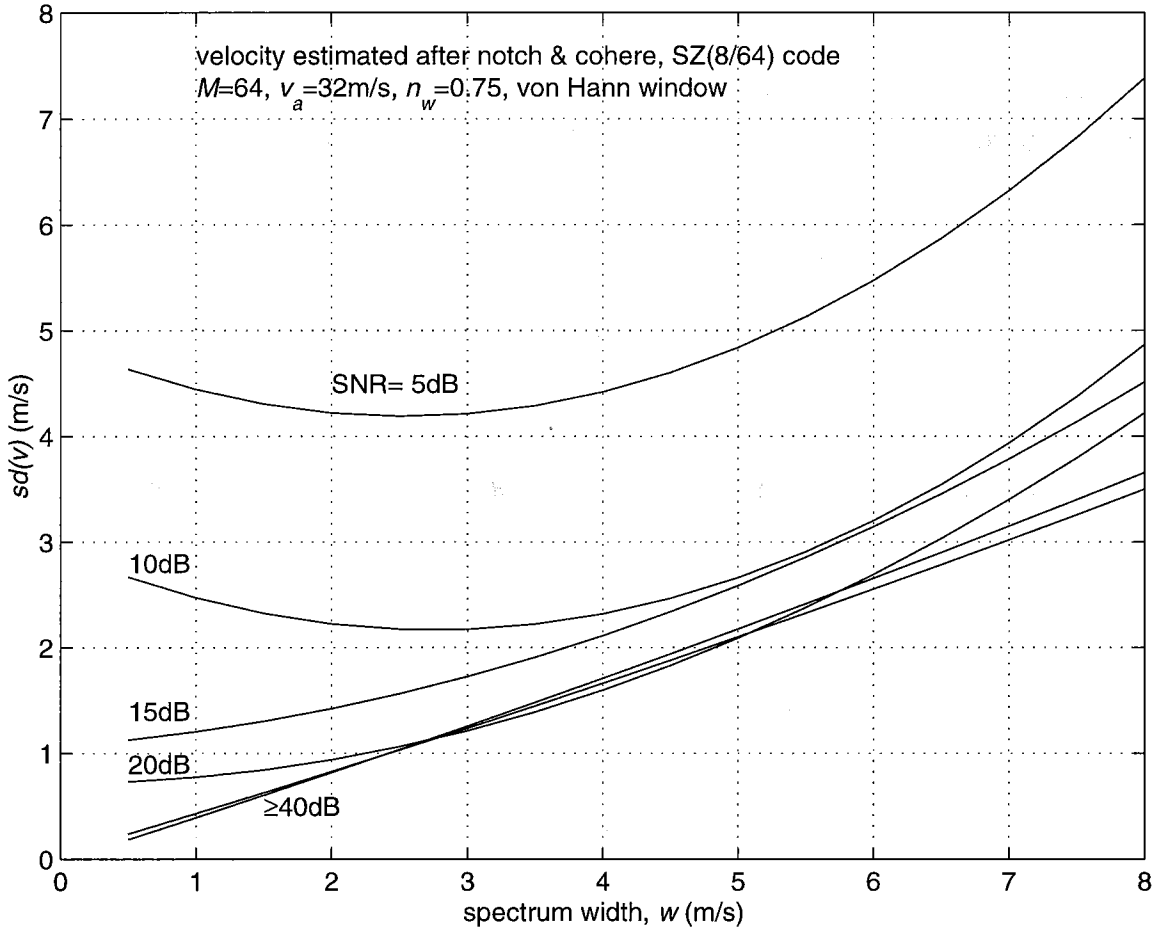

Fig. 3.16. $sd(\hat{v})$ versus the spectrum width w with the von Hann window for the SZ(8/64) algorithm. 100 simulations are used for each w and SNR to compute $sd(\hat{v})$, and a 2nd degree polynomial is fitted to smooth the curve.

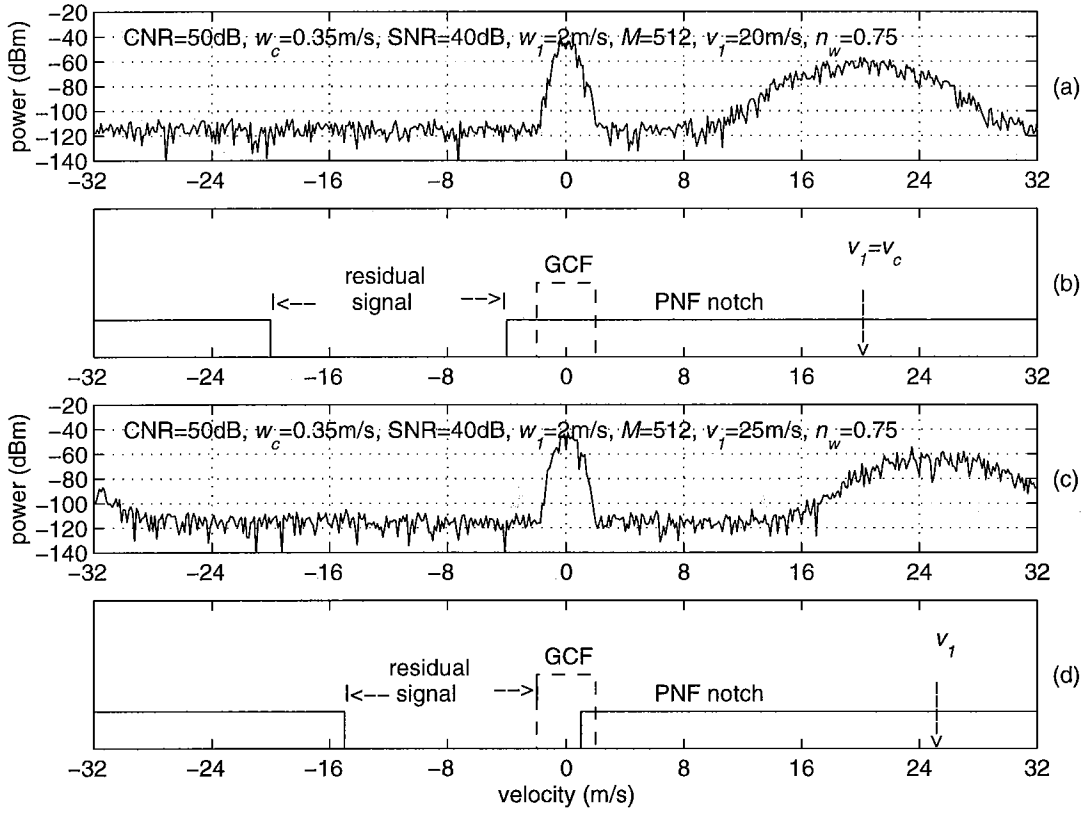

Fig. 3.17. (a) 1st trip signal and the clutter spectra, v_1=20 m/s. (b) Ground clutter and the process notch filter positions for $(-3v_d/4 + w_{cf}/2) < v_1 < (3v_d/4 - w_{cf}/2)$. (c) 1st trip signal and the clutter spectra, v_1=25 m/s. (d) Ground clutter and the process notch filter positions for v_1 outside the interval $(\pm 3v_d/4 \mp w_{cf}/2)$.

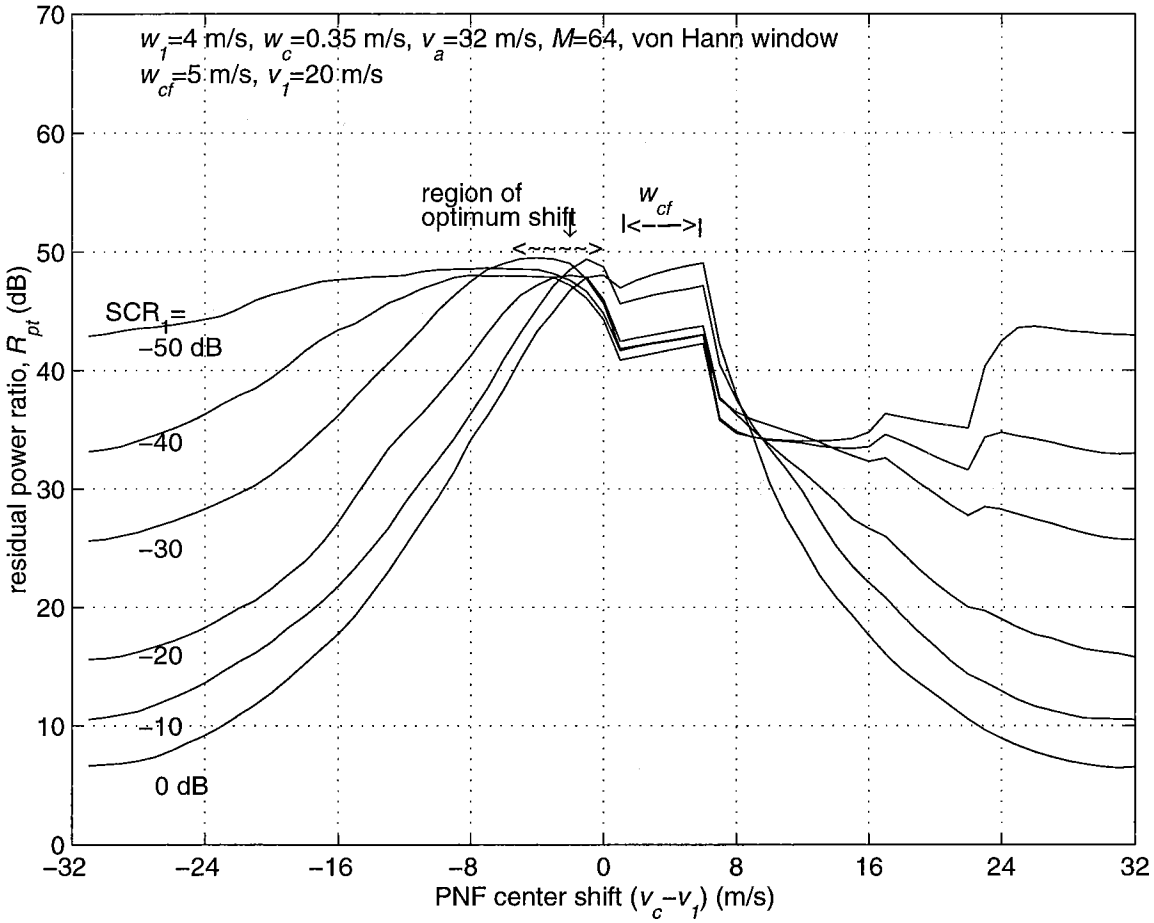

Fig. 3.18. Variation of the residual power ratio, R_{pt}, as a function of the PNF center shift for v_1=20m/s, w_1=4m/s, and w_c=0.35 m/s; with SCR_1 as a parameter.

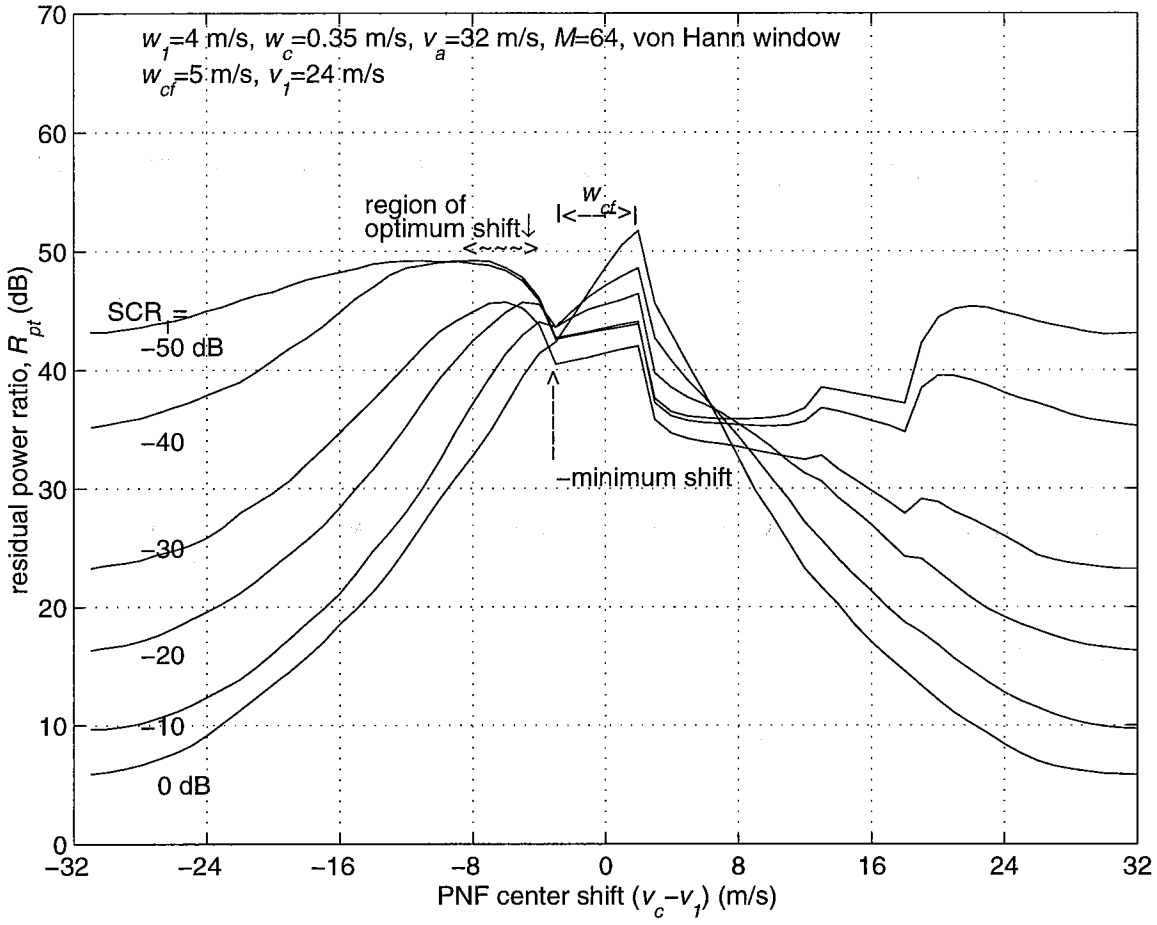

Fig. 3.19. Variation of the residual power ratio, R_{pt}, as a function of the PNF center shift for v_1=24m/s, w_1=4m/s, and w_c=0.35 m/s; with SCR_1 as a parameter.

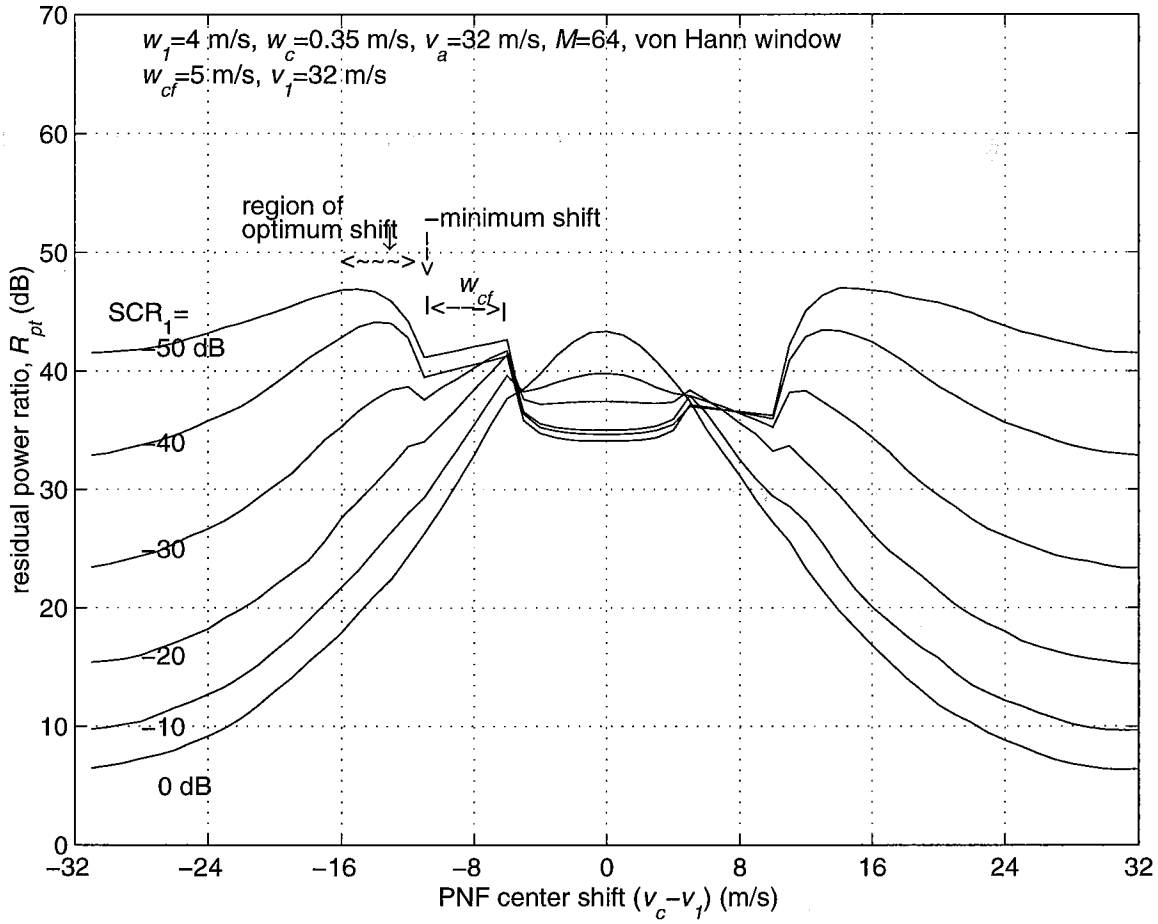

Fig. 3.20. Variation of the residual power ratio, R_{pt}, as a function of the PNF center shift for v_1=32m/s, w_1=4m/s, and w_c=0.35 m/s; with SCR_1 as a parameter.

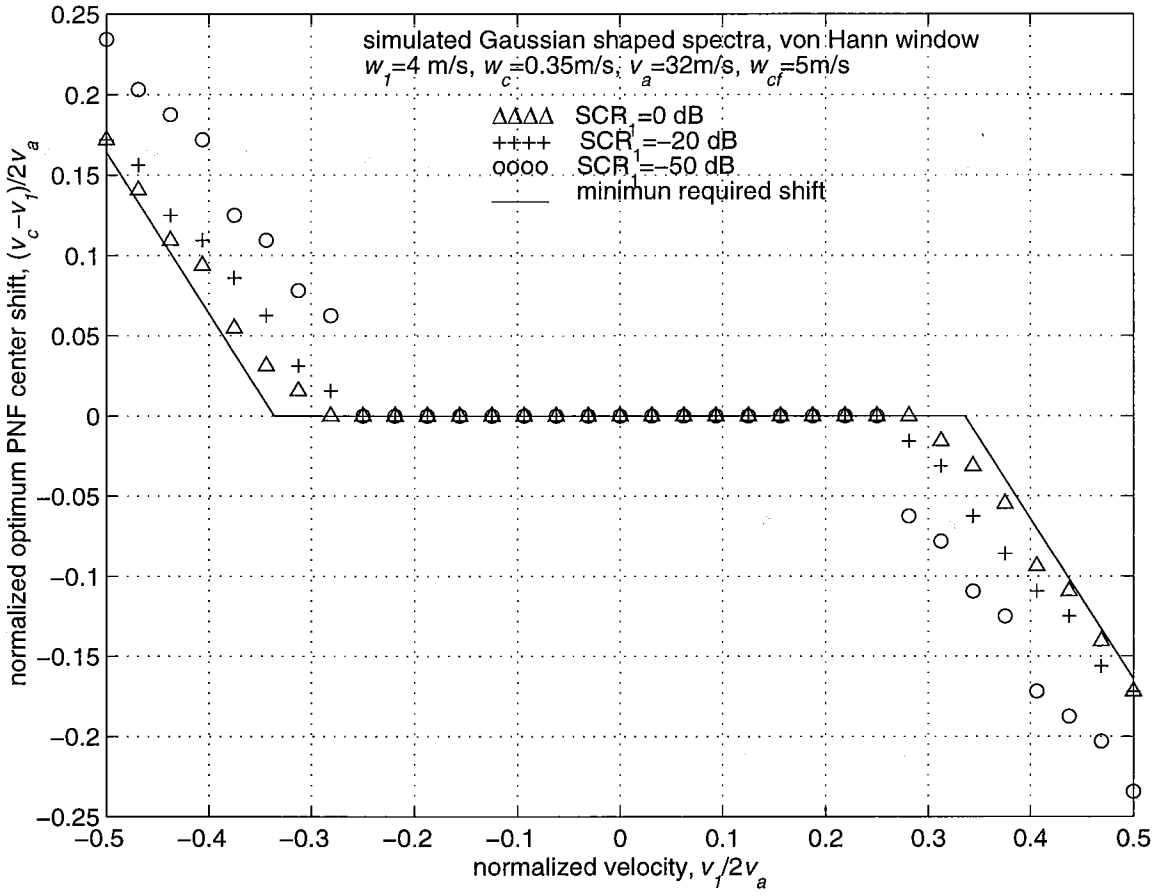

Fig. 3.21. Optimum normalized PNF shift as a function of the normalized velocity. The minimum shift required for fully cohering the 2nd trip signal is also shown.

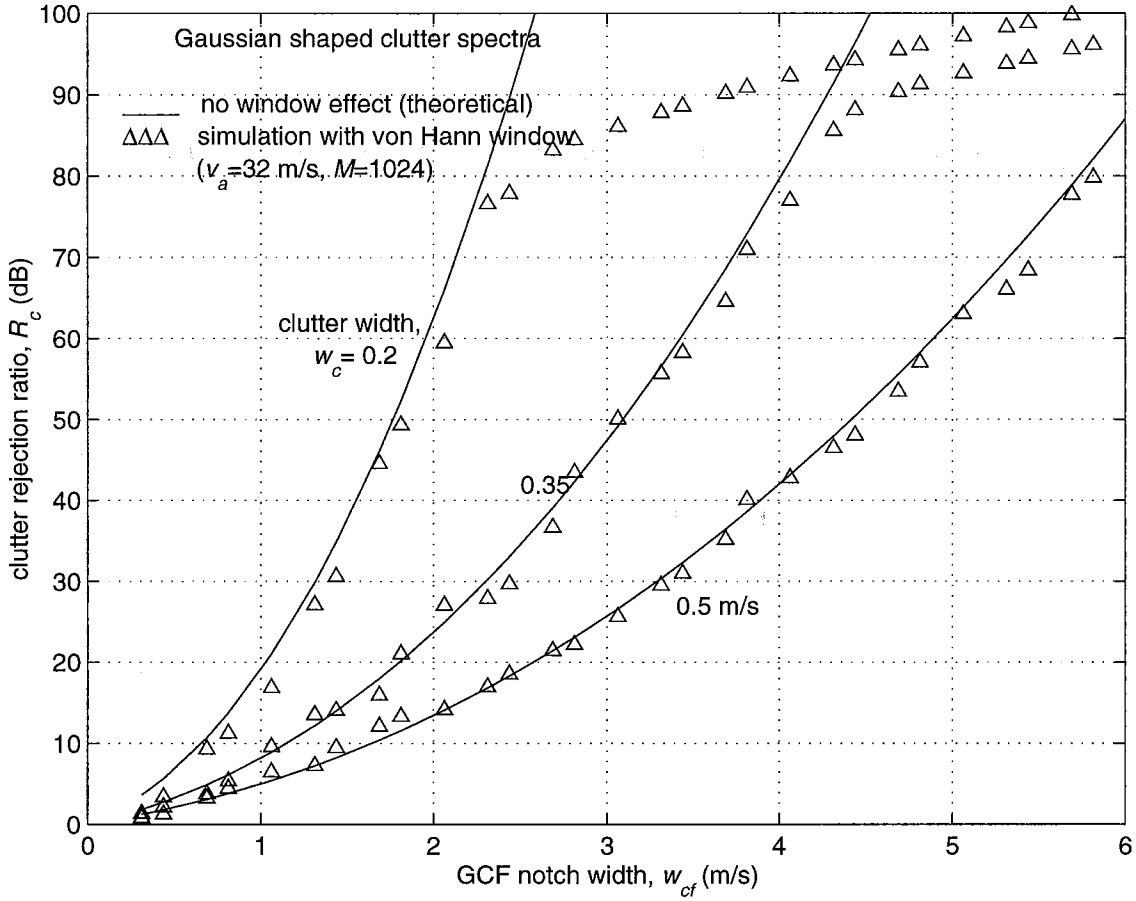

Fig. 3.22. The clutter rejection ratio, R_c, as a function of GCF notch width.

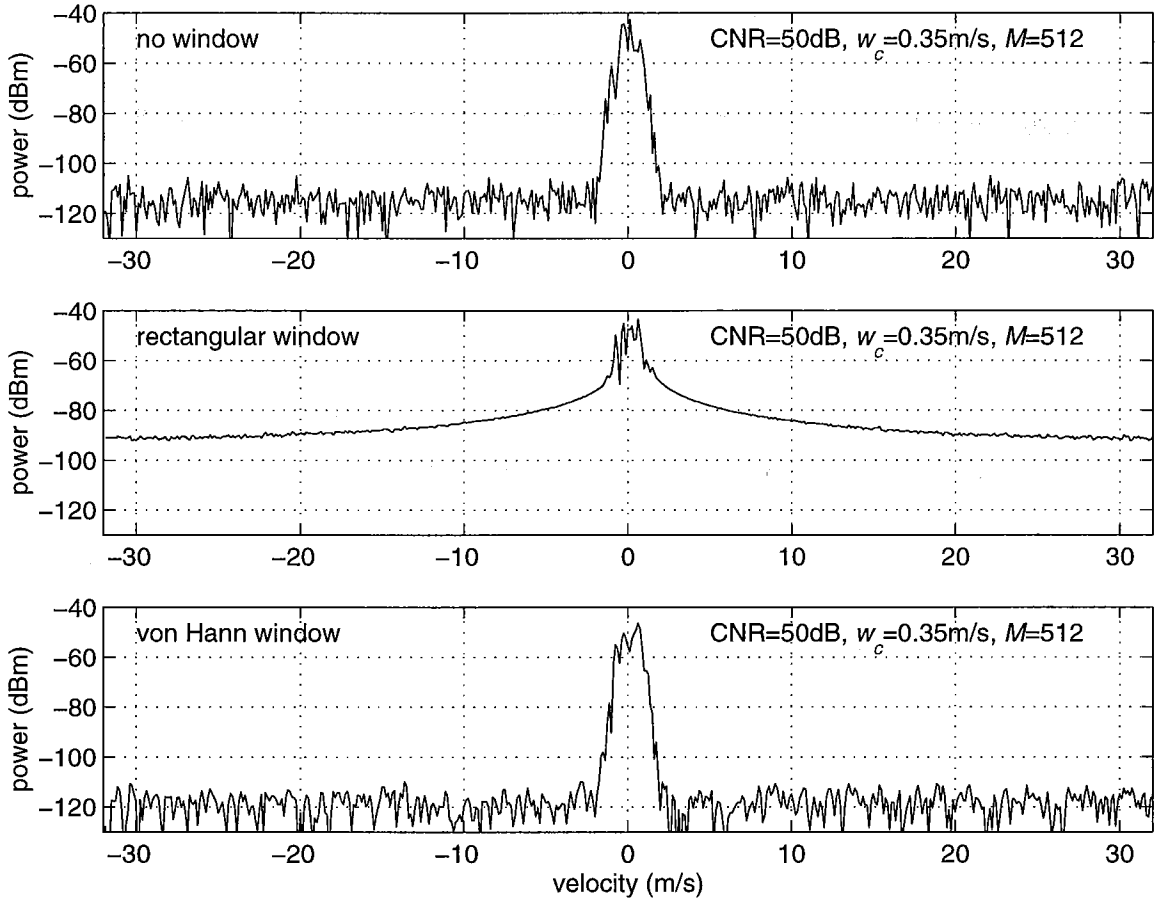

Fig. 3.23. An illustration of the effect of the von Hann window weights in restoring the spectrum (M=512).

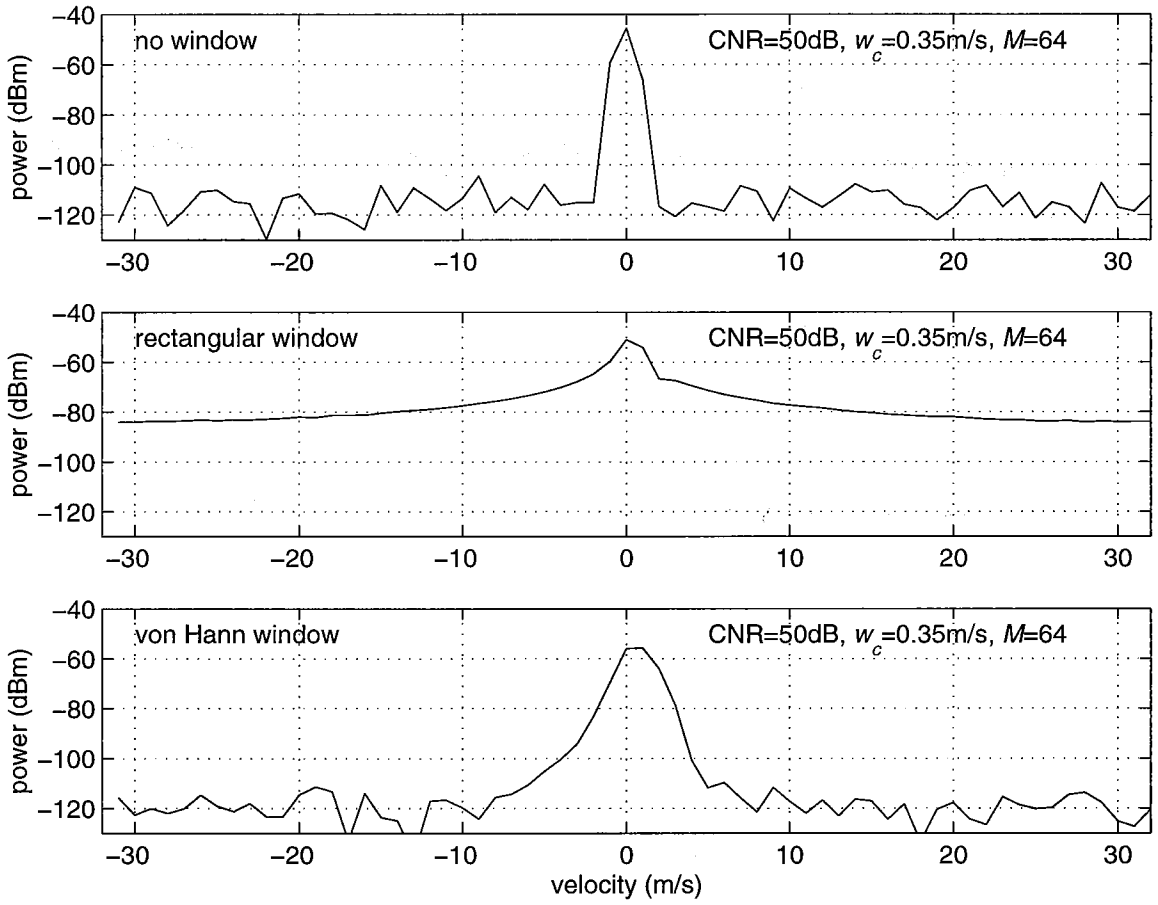

Fig. 3.24. An illustration of the increased side lobe power due to a limited number of samples (M=64).

4. CONSIDERATIONS FOR THE IMPLEMENTATION OF THE SZ-CODE ON THE WSR-88D RADAR

4.1. Phase accuracy and sensitivity analysis.

In the phase coded radar, the transmitted pulses are phase shifted according to the SZ code, and the received samples are phase shifted in the opposite direction to cohere the first trip signal. The phase shifting of the transmitted pulses is carried out using an electronic phase shifter which generally has an accuracy specification. It is important to know how this error in the phase affects the performance of the phase coded radar. There are two kinds of phase errors that can occur in practice; these are random and fixed.

The random error is due to the transmitter phase jitter, fluctuations in the phase shifter drive voltage, system transmit path phase changes due to moving parts such as the rotary joints, stress induced distortions in the wave guides and scanning antenna, etc. The fixed phase error can be due to the phase quantization in the digital phase shifter. The random error is time dependent; therefore, if this error is significant, one way to correct it is to measure the transmitted phase of every pulse and use these phases in the cohering process. The fixed error can be minimized by a proper selection and calibration of the phase shifter. But it is important to know how sensitive the decoding procedure is to these errors before we attempt a correction.

Consider the first type of error (assume zero error due to phase quantization). The transmitted phases have random phase error, but for cohering the first trip, the exact code phases with no random error are used. This leads to a partial cohering of the first trip signal, and a small part of the power appears as noise, spread over all the coefficients (because the spectrum of the switching code is also nearly white). The weaker 2nd trip signal is also affected to the same extent; i.e., when it is cohered during the processing, a small part of the power does not cohere. Thus, a small part of the 1st and 2nd trip signals is converted to noise. Effectively, the residual power ratio for the 1st trip signal, R_p, decreases for any given notch filter width. From the results obtained using simulations, it has been established that $p_1/p_2=R_p$ is the upper limit for the recovery of the mean velocity of the weaker signal (Part 1 of this report). The effect on the recovery of v_2 would be similar to the window effect.

To compute the effective residual power ratio, R_{pe} of the stronger signal in the presence of the first type of phase error, let us assume the distribution of the phase error, $\delta\psi_i$, to be uniform with a specified maximum amplitude of ϵ radians. Let $|E_i|$ and θ_i be the magnitudes and phases of the complex samples of the first trip (stronger) signal. It is well known that the magnitudes, $|E_i|$, are Rayleigh distributed, and the phases, θ_i, are uniformly distributed (Doviak and Zrnic, 1993, p.71). The SZ code phases, $(\psi_i+\delta\psi_i)$, are added to the transmitted pulses, where $\delta\psi_i$ are the phase errors uniformly distributed over $\pm\epsilon$. Hence, the received samples will have phases $(\theta_i+\psi_i+\delta\psi_i)$. In the cohering process, ψ_i are removed, while $\delta\psi_i$ remain. The incoherent part of the signal samples can be approximated as $|E_i\delta\psi_i| \exp\{j(\theta_i+\psi_i+\pi/2)\}$ for small values ($< 5°$) of ϵ ($\delta\psi_i$ part in the exponent is neglected). For a normalized notch filter width, n_w, $(1-n_w)$ fraction of this incoherent power remains in the spectrum after the notch filtering (assuming that the SZ code, ψ_i, produces a white spectrum), along with the residual of the coherent power.

Assuming E_i to be Rayleigh distributed and $\delta\psi_i$ to be uniformly distributed, the expected value of the incoherent part of the power is

$$\mathcal{E}\{ p_{inc}\} = \int_{-\epsilon}^{\epsilon} \int_{0}^{\infty} |E|^2 \, \mathcal{P}\{E\} \, (\delta\psi)^2 \, \mathcal{P}\{\delta\psi\} \, dE \, d(\delta\psi), \tag{4.1}$$

where $\mathcal{P}$ is the probability density distribution of the parameters shown in brackets. Because the incoherent part of the power is like white noise, $(1\text{-}n_w)$ part of this power remains in the spectrum after the notch filtering. The expected value of the total power, p_1, is given by the integral

$$\mathcal{E}\{ p_1 \} = \int_{0}^{\infty} |E|^2 \, \mathcal{P}\{E\} \, dE. \tag{4.2}$$

Thus, the coherent part of the power is obtained by subtracting the incoherent part; i.e.,

$$\mathcal{E}\{p_{coh}\}=\mathcal{E}\{p_1\}-\mathcal{E}\{p_{inc}\}. \tag{4.3}$$

Assuming a Gaussian shape for the coherent spectrum, the residual coherent power after the notch filtering is obtained by multiplying by a factor $[1\text{-erf}\{n_w v_d/(w_1\sqrt{2})\}]$, in which w_1 is the spectrum width, and erf{ } is the error function. Inserting appropriate distribution functions and evaluating the integrals in (4.1) and (4.2), we get the expression for the effective residual power ratio, R_{pe}, as

$$\begin{aligned} R_{pe} &= p_1/[\mathcal{E}\{p_{inc}\}(1\text{-}n_w)+ \mathcal{E}\{p_{coh}\}(1 - \text{erf}\{n_w v_d/(w_1\sqrt{2})\})] \\ &= 3/\{(3 - \epsilon^2)[1 - \text{erf}\{n_w v_d/(w_1\sqrt{2})\}] + \epsilon^2(1\text{-}n_w)\}. \end{aligned} \tag{4.4}$$

A plot of this function for n_w=0.75 and different values of phase error parameter ϵ shows that there is an upper limit for the R_{pe} for any given notch width and the spectrum width (Fig. 4.1). With the von Hann window and zero phase error (ϵ=0), the upper limit is at 90 dB for $w_1/(2v_d)$ < 4/64, and M=64. With 0.1° error, the limit falls sharply to about 66 dB.

In the above theoretical expression, we have assumed that the incoherent part of the 1st trip signal is like white noise (the factor $(1\text{-}n_w)$ in Eq. 4.1). This is a valid assumption because the phase error term, $\delta\psi$, is random; hence, produces white noise-like spectrum. The power distribution is nearly uniform only for the modulation code and not for the switching code. The theoretical expression (Eq. 4.4) agrees well in the mean with that from simulation using M=64. The R_{pe} (Eq. 4.4) for the simulated Gaussian signal is found to have a variation of about ±5dB (Fig. 4.1, simulation results) because of the small number of samples used. The effect of random phase error is similar to the window effect which spreads the power across the spectrum.

Now, in the present case, we cannot assume that the R_{pe} is the upper limit for the recovery of v_2 because the phase error produces noise (the incoherent part of the signal is like noise), and we need to consider SNR degradation before we can come to definite conclusions. The SNR_1 of the 1st trip signal after cohering can be written as $SNR_1=\{p_1/p_{inc}\text{-}1\}$, assuming that the SNR due to the system noise is infinity. Using equations 4.1 and 4.3, we can derive the expression for the SNR_1 as

$$SNR_1 = 10 \log_{10}(3/\epsilon^2 - 1) \quad (dB). \tag{4.5}$$

The SNR_2 of the weaker 2nd trip signal is less by a factor p_2/p_1. Fig.4.2 shows the effective SNR_2 of the 2nd trip signal as a function of the random phase error parameter ϵ (in degrees). The p_1/p_2 ratio is shown as a parameter. The curve corresponding to p_1/p_2=0 dB is also the SNR of the 1st trip signal after cohering. Comparing the values of R_{pe} and the SNR_2 as a function of the phase error parameter ϵ, it is seen that the SNR_2 is lower than R_{pe} by about 6 dB and, hence will put an upper limit on the p_1/p_2 for which v_2 can be recovered with an acceptable error. For example, the R_{pe} is 60 dB for ϵ=0.2°, and $w_1 < 4.5$ m s^{-1}, but the SNR_1 is 53.9 dB, which is about 6 dB lower. The SNR_2=0 dB for p_1/p_2=53.9 dB. For the v_2 estimate to have a standard error less than 1 m s^{-1} (for w_2=4 m s^{-1}), we require a SNR of at least 15 dB (see Fig. 3.16). Therefore, the upper limit for p_1/p_2 is about 40 dB with 0.2° phase error. For 0.5° phase error, the limit is about 33 dB.

From Fig. 4.1 and Fig. 4.2, it is clear that we need to maintain a phase error less than 0.2° so that v_2 can be recovered for p_1/p_2 up to 40 dB. This is a stringent requirement which necessitates measurement of the transmitted phases from pulse to pulse and uses these phases in the decoding algorithm.

To verify these conclusions and to evaluate the effect of the phase error of the first type on the velocity recovery, a simulation study was carried out with a random error introduced during simulation of the overlaid signal time series. The phase error was modeled by adding a uniformly distributed random phase sequence to the SZ code phases.

The random phase error was introduced using a random number generating program, rand(1,n), available with MATLAB software. With the error included, the phase switching sequence is

$$\psi_k = -\sum_{m=0}^{k}(n\pi m^2/M) + [2\, r(k) - 1]\, \epsilon \;; \quad k=0,1,2,....M-1, \tag{4.6}$$

where $r(k)$ is a random number uniformly distributed over (0 to 1), and ϵ is the maximum error in radians. In the decoding program, the code is assumed to be the first term of (4.6) alone without the random error. That is, the phase error has occurred in the phase shifter (or in the entire system), but no measurement of the actual transmitted phase is made, and the phase is assumed to be the exact SZ code in the decoding algorithm. The simulation program is executed with different values of ϵ, and the standard deviation of the most crucial parameter, v_2, is computed for ϵ values of 0°, 0.2°, 0.5°, 1°, 2°, and 5° (Fig. 4.3). It can be seen that the error in $\hat{v}_2$ has a behavior similar to the one observed with the window effect (see Fig. 3.3); i.e., there is a limit to the p_1/p_2 beyond which the error in $\hat{v}_2$ increases steeply. From Fig. 4.3, it follows that with a system phase accuracy of the order of ±0.5°, we can recover v_2 for p_1/p_2 up to about 35 dB. This is about 5 dB lower than that predicted by the theory (Eq. 4.4), for w_1=4 m s^{-1}; the limit is lower for larger widths.

The fixed error due to the quantization is less serious because of two reasons. The recovery of v_2 using the algorithm (SZ code) is not very sensitive to this error, and also it can be removed. The fixed error can be simulated by introducing a uniformly distributed phase error in the switching code (see Eq. 4.6) and use the same phases in the decoding algorithm. This situation is similar to the one in which the transmitted phases are measured, and these phases

are used in the decoding algorithm. The standard error in $\hat{v}_2$ is plotted in Fig. 4.4 for different phase errors in the code. It is seen that the quantization error can be as large as 5° to 10° without much degradation of the standard error in the recovered $\hat{v}_2$. The simulation study of these two types of phase errors indicates that it is necessary to measure the transmitted phases accurately (to an accuracy of 0.5° or better) and use these phases for cohering the signals. The accuracy of the phase shifter settings is not very critical. The 7-bit PIN diode phase shifter in WSR-88D has a quantization step size of 2.8°; hence, the maximum quantization error is about 1.4°, which is within the tolerable value, provided the phase shifter is calibrated after each volume scan.

4.2. Effect of ADC quantization.

The WSR-88D receiver uses a 12 bit analog-to-digital converter (ADC). The saturation and quantization noise of ADC degrades the SNR of the signal. Fig. 7.20 of Doviak and Zrnic (1993) gives the maximum achevable SNR for optimized clipping level of the ADC. From this figure, we get a maximum SNR achievable as 62 dB for a 12 bit ADC. Therefore, the SNR of the stronger signal would have an upper bound equal to 62 dB. If a SNR of at least 15 dB is required for weaker signals, this would put an upper bound for the p_1/p_2 at 47 dB, beyond which v_2 is not recoverable with reasonable accuracy, even when SNR_2 is large.

4.3. Code synchronization and code length.

To cohere the echo samples, one needs to know the transmitted phase for each of the samples. This requires synchronizing the switching phase sequence with the decoding phase sequence in the algorithm. But the starting point can be anywhere in the code sequence because it is cyclic. The performance of the algorithm is independent of the shift in the code, and this was confirmed by the simulation study (Fig. 4.5). Since the modulation code has a periodicity of 8, 0 to 7 sample shifts cover all the possible shifts that can result from an arbitrary starting point. All shifts result in nearly the same mean and standard errors in $\hat{v}_2$. Therefore, if the transmitter is continuously transmitting, any M contiguous sample sequence can be used for decoding by appropriately synchronizing the code sequence. If there is a dead zone between radials where the transmitter is switched off for a time interval greater than 1 PRT (e.g., if alternating long and short PRT transmissions are used as in the batch mode), then it is important to have at least one pulse more than the code length and process the second sample onwards. This is because the first sample will have only the 1st trip signal.

The WSR-88D radar operates in different modes, and in each mode, the scan parameters are automatically selected to be some preset values. For example, the sample lengths in the short PRT mode at the lowest elevation angle scan are preset to one of the values, 44, 52, 56, 61, or 66. We explored the possibility of processing the available sample lengths without changing the code. The SZ(8/64) switching code was selected, and a truncated time series with sample lengths equal to 44, 52, 56 and 60 were used to recover $\hat{v}_2$ by the decoding algorithm. Truncating the time series resulted in an increase in the standard error (Fig. 4.6). This increase is slightly more than the increase expected from a reduction in the number of samples for estimation, but the mean of the error in $\hat{v}_2$ is still zero. For comparison, the values for M=64 are also shown (continuous line). Therefore, to achieve as small a variance as possible, it is best to keep the time series length the same as the code length for which it is optimized.

It is possible to optimize the code for each M, but it has some disadvantages. First, the phase shifter settings may not be exactly realizable, and secondly, for each M, the notch width and the deconvolution matrix have to be changed in the processing algorithm. If M/n is less than 8, the maximum notch width that can be used in the SZ algorithm has to be correspondingly reduced from n_w= 0.75 to completely cohere the weaker signal. To obtain the optimum value of M/n, it is necessary to study the standard error in $\hat{v}_2$ as a function of the parameter n, which would involve a large number of simulation runs. This was done only for M=64 (Fig. 2.1) because there is a more attractive alternative to handle shorter sequences that is discussed next. The disadvantages of selecting a different code for each sample sequence length outweigh the disadvantages of the alternative scheme. With the alternative scheme suggested below, it is not necessary to change the existing scan parameters of the WSR-88D. The modification is only in the way the sample lengths are selected for processing.

There are several practical advantages in selecting the code with M=64 and n=8, which are discussed in the following paragraphs. The switching code phase shifts are integral multiples of $\pi/8$ radians (22.5°), which is a standard in digital phase shifters (phase shifts are generally integral multiples of $360/2^n$ degrees for a n bit phase shifter; this smallest phase increment is called a phase bit). For other M/n, the phase bit will have a value which is not generally a standard phase bit available in commercial phase shifters. However, this is not a serious problem because the readily available 7-bit PIN diode phase shifter in WSR-88D has a smallest phase bit of 2.8°, and the algorithm tolerates a phase setting deviation as large as 10°. Another advantage with the SZ(8/64) code, which perhaps is the **most important** one, is the saving in computation time required for FFT. The computation time is the shortest when M is a power of 2 and can be several times slower if M is a prime number.

Another aspect is the periodicity of the phase switching sequence ψ_k and modulation sequence ϕ_k (when one of the signals is made coherent). In general, the phase shifts are in integral multiples of $(n\pi/M)$ radian, and the multiplier increases quadratically (0, 1, 4, 9, 16, 25, ...etc.) in the modulation code, and in the switching sequence, the multiplier increases as the sum of squares(Σp^2, with summation over 0 to k). These phases, when mapped onto $[0,2\pi)$, will have different periodicity depending on the value of M/n. For example, the SZ(8/64) code has a periodicity of 8 and 32 for the modulation and the switching sequence, respectively, and for SZ(7/64), the modulation and switching sequences have a periodicity of 64 and 256, respectively. To make use of the cyclic property of the code (i.e., to be able to select any M contiguous samples for processing), it is necessary to maintain the complete cycle of the switching sequence.

A feature common to all codes (for any M & n) is an even symmetry in the modulation sequence and an odd symmetry in the switching sequence within the periodicity of the codes. This plays an important role in obtaining the matching property, and it is best when the time series length is an even multiple of the periodicity of the modulation code.

To take advantage of all the above mentioned points, and also to retain the scan parameters as they are in WSR-88D, one strategy is to use the SZ(8/64) code and process 64 samples centered on any radial with overlap onto the adjacent radials; i.e., process M=64 samples with center to center separation of m=52 samples, for example (Fig. 4.7). There will be an overlap of 12 samples on either side. This amounts to averaging over a wider angular sector than is currently done. This excess smoothing should not be a serious problem because the von Hann window weighting significantly suppresses this overlapped portion. For the example shown in

Fig. 4.7, for M=64 and m=52, the ratio of overlapped power to the total power, R_o = 0.0114, with the von Hann window, and is equivalent to an overlap of R_ox64=0.73 samples only, on either side. For m=44, the equivalent overlap is 6.4 samples on either side. In fact, this is an advantage because the scheme effectively makes use of more of the sample power, while keeping the computation time the shortest. This scheme can be implemented because of the cyclic nature of the SZ code whose performance is independent of the shift.

A suggested schematic of the data storage and flow, to accomplish the sorting of the echo samples to obtain 64 samples with a center to center separation of 52 samples, is shown in Fig. 4.8. The horizontal axis is the range time, and the vertical axis is the sample time. The long horizontal rectangles can be thought of as a stack of registers for storing the complex samples for all the gates, one for each pulse transmission, along with the phase shifter setting (SZ phase code) and the antenna azimuth angle (it may include other information also). The stack falls by one every time the data from each transmission is loaded onto the top register, so that at any given time, we have 64 samples available for each gate. The data in all the 64 registers is read by the processor for computing the spectral moments, every 52 pulse transmissions. The computed spectral parameters are assigned to the radial at the antenna angle corresponding to the 32nd register entry at the time the data is transferred to the processor.

4.4. Integration of long and short PRT data.

The discussion in this section pertains to the SZ-2 algorithm which uses the long PRT scan data, preceding the short PRT scan. The SZ algorithm, in the stand alone mode (i.e., SZ-1), decides which of the two signals is stronger by autocovariance processing the two time series, the one with the first trip coherent and the other with the second trip coherent. This step can be eliminated if reflectivity data from the long PRT scan is used for making this decision. This can eliminate one autocovariance processing and one cohering step. However, sometimes this will lead to unacceptably large errors in the velocity estimates of both trip signals when the p_1/p_2 ratio is within about ±5 dB. Refering to Fig. 3.9, it can be observed that there is a small increase in the $err(\hat{v}_1)$ for p_1/p_2 values near zero. An extrapolation onto the negative axis (i.e., p_1/p_2 <0 dB) indicates that the $err(\hat{v}_1)$ increases sharply beyond the acceptable error limits. Because of the statistical nature of the weather signals and the fact that the long and the short PRT data are separated in time (by one azimuth scan time of the antenna, in the lowest elevation scans), there can be a difference of several dB in the p_1/p_2 estimates from the long and short PRT data. This poses a problem, especially if p_1/p_2 is around zero. If the long PRT data is used to estimate p_1/p_2 and used in the algorithm, nearly 50 percent of the time the computation proceeds along the wrong path for low values of p_1/p_2, resulting in an increased $err(\hat{v}_1)$ as well as $err(\hat{v}_2)$, for -5dB< p_1/p_2<5dB. Therefore, both algorithms (i.e.,SZ-1 and SZ-2) presented in this report use the autocovariance processing method. But the long PRT data is processed for the spectrum width in addition to the reflectivity. Thus, the computation time required for the SZ-2 algorithm can be reduced by restricting it to the recovery of velocities only. Because the width is obtained from the long PRT data, the deconvolution step can be eliminated.

The implementation of this scheme is straightforward for the lowest two elevation scans. The long PRT can be used for the reflectivity and spectrum width computation over the 460 km range (spectrum width computation can be restricted to 230 km). The short PRT Doppler scan

is phase coded, and the SZ-2 algorithm is used to recover the mean velocities of both trips. The sample overlap scheme (Fig. 4.7) can be implemented to obtain the 64 samples required for the processing.

For intermediate elevations (2.5° to 6.5°), the batch mode presents some problems because the short PRT mode is interrupted alternately by the long PRT mode, and the number of samples available in the short PRT mode does not correspond to the required 64. Thus, we cannot implement the scheme presented in section 4.3. In the volume coverage pattern-11 (VCP-11), the number of samples available are 34, 41, 43, 46, or 50, and in the VCP-21, they are 59, 70, 76, 82, or 88 for different Doppler PRF number selections. The option of selecting different PRF numbers is to reduce the overlaid echo regions. With the phase coding, this option may not be needed; hence, the prt can be fixed for the phase coded transmission. For the SZ(8/64) code, a minimum of 65 samples are needed (64+1, because the 1st sample does not contain the 2nd trip signal and, hence, cannot be used in processing).

Another alternative, perhaps a less attractive one, is to replace the batch mode with the Doppler scan mode and use the SZ-1 algorithm (SZ algorithm in the stand alone mode) to recover all the spectral parameters. This is possible because the maximum range requirement is within 230 km for all elevations greater than 2.5°. The improved data rate can be used to reduce the scan time. The only limitation would be the error in the recovered weaker echo parameters if the p_1/p_2 is greater than 40 dB. Since all returns are treated as overlaid signals, and processed using SZ-1 decoding algorithm, there is likely to be a ghost effect on the display. Whenever there is a strong reflectivity core in one of the trips, the other trip region can be expected to have a ghost image because the residual power after notch filtering the stronger signal is treated as the weaker signal power. This produces a bias error in the weaker signal power estimate. If this is to be avoided, it is imperative to retain the long PRT reflectivity measurement mode and use the SZ-2 decoding algorithm for velocity. The SZ-2 algorithm is also computationally less demanding than the SZ-1 stand alone algorithm.

A fourth alternative is to use a staggered/variable PRT method for the 2.4° to 6.5° elevation scans because the ground clutter is not a major problem for these elevation scans. This option is part of a concurrent study to be described in a separate report.

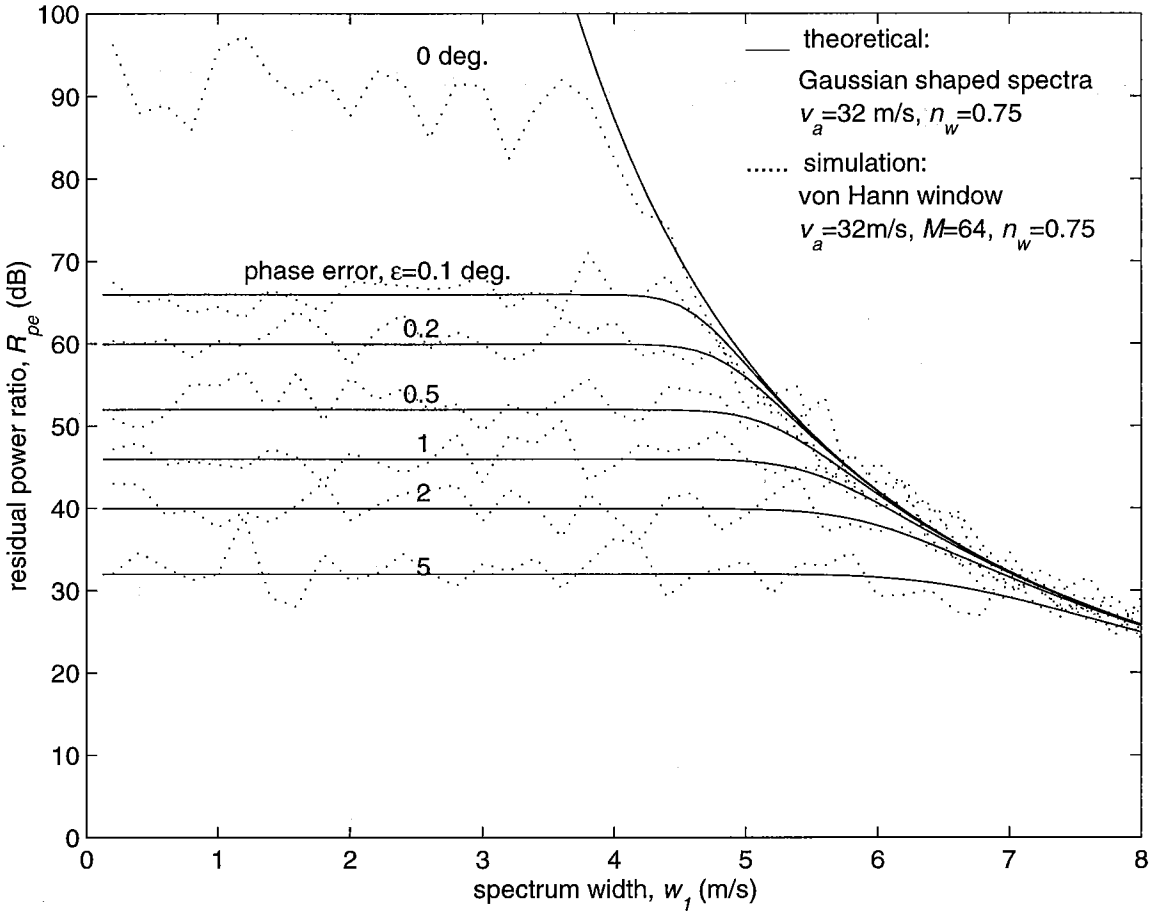

Fig. 4.1. Theoretical and simulated residual power ratio, R_{pe}, as a function of the spectrum width, w_1, for different values of the phase error parameter.

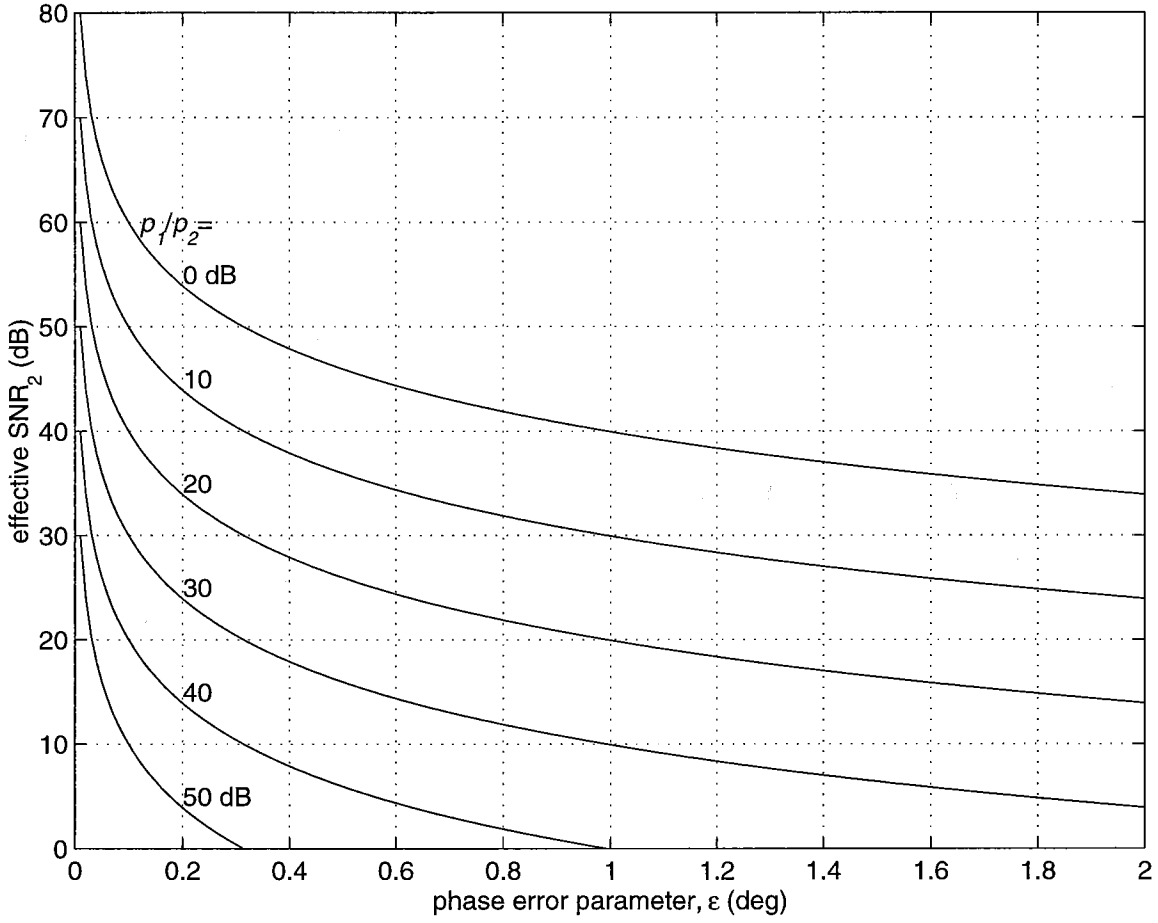

Fig. 4.2. The effective SNR of the 2nd trip signal as a function of the phase error parameter, ϵ, with p_1/p_2 as a parameter.

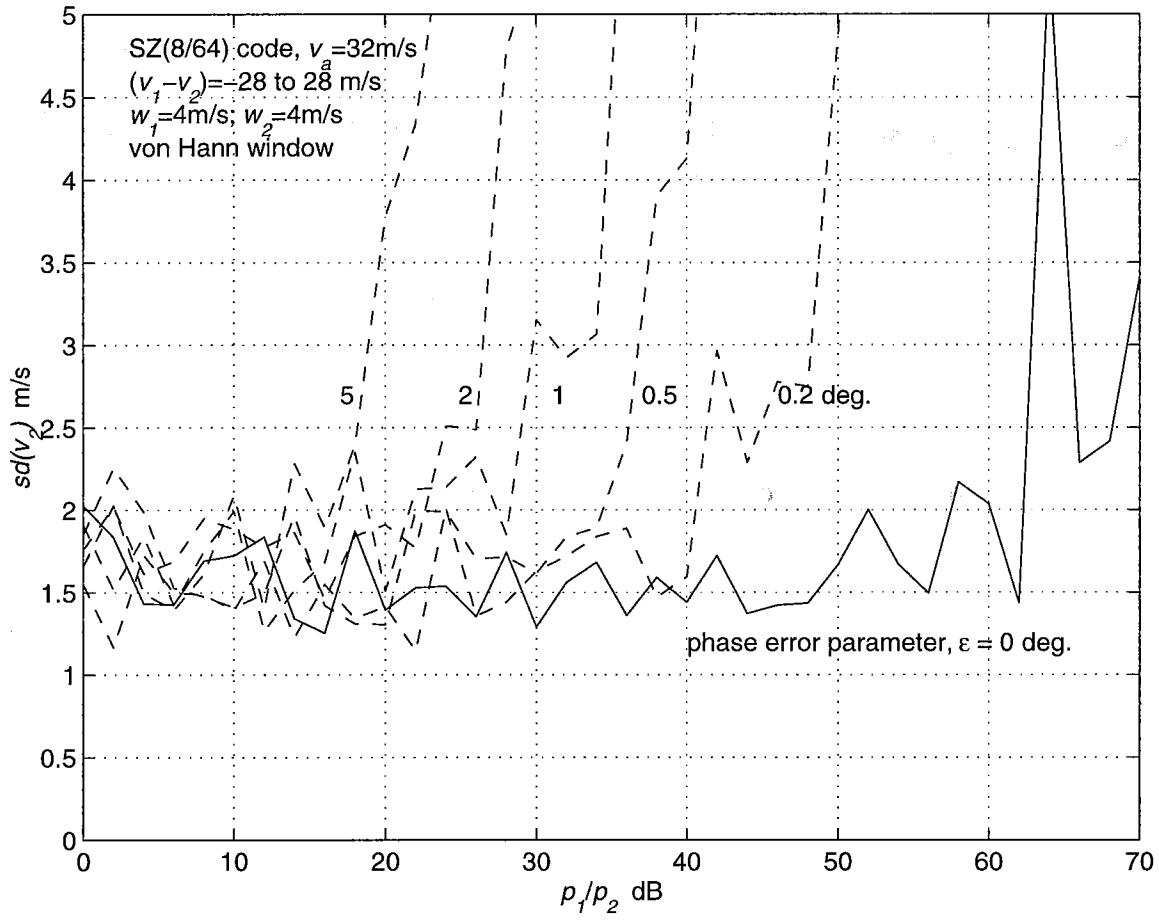

Fig. 4.3. The standard deviation of the error in v_2 estimated using the SZ(8/64) algorithm for different values of the random phase error parameter, ϵ.

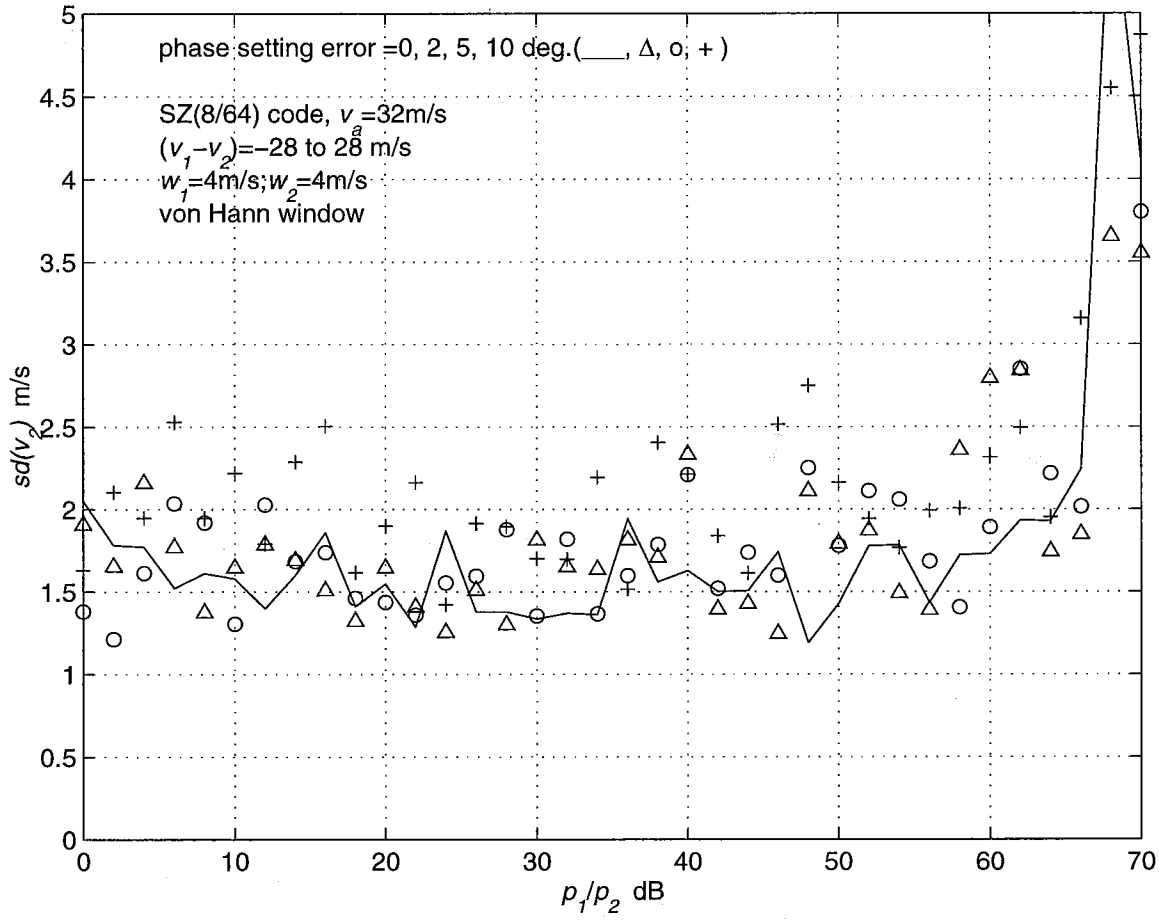

Fig. 4.4. The effect of a uniformly distributd random phase setting error in the phase shifter on the $sd(\hat{v}_2)$ for different phase setting error parameter values.

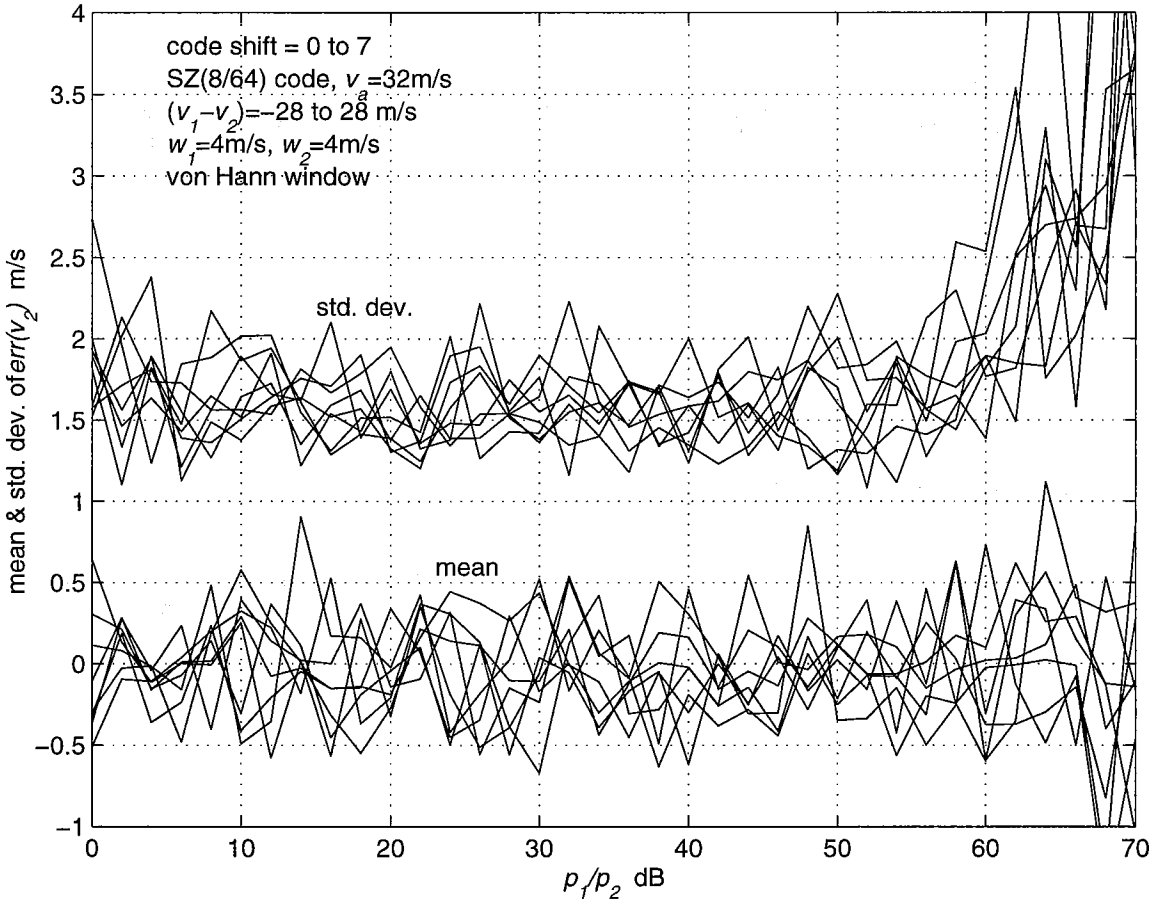

Fig. 4.5. The effect of the code shift on the $sd(\hat{v}_2)$ and the mean $\hat{v}_2$.

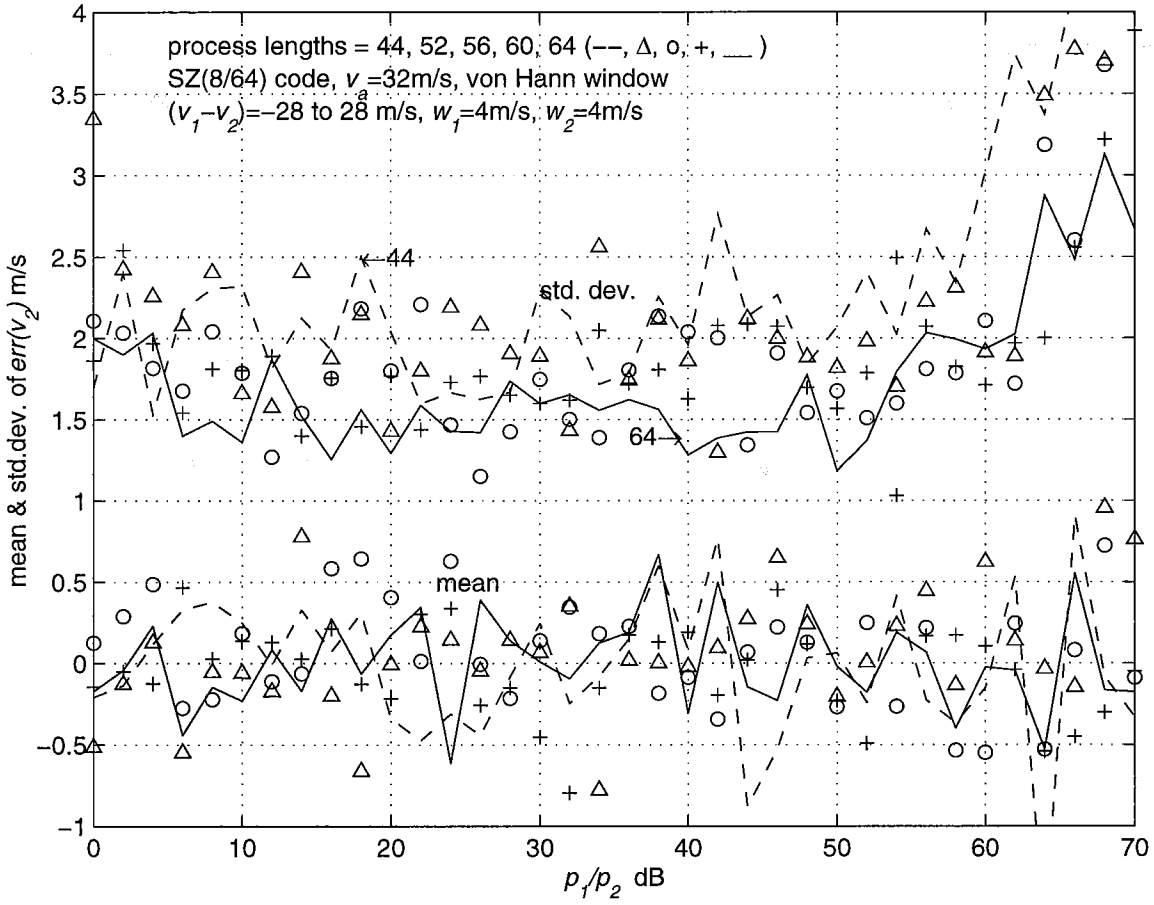

Fig. 4.6. The variation of the mean and the standard deviation of the error in v_2 estimate with changes in the processing sample length for SZ(8/64) coded signal.

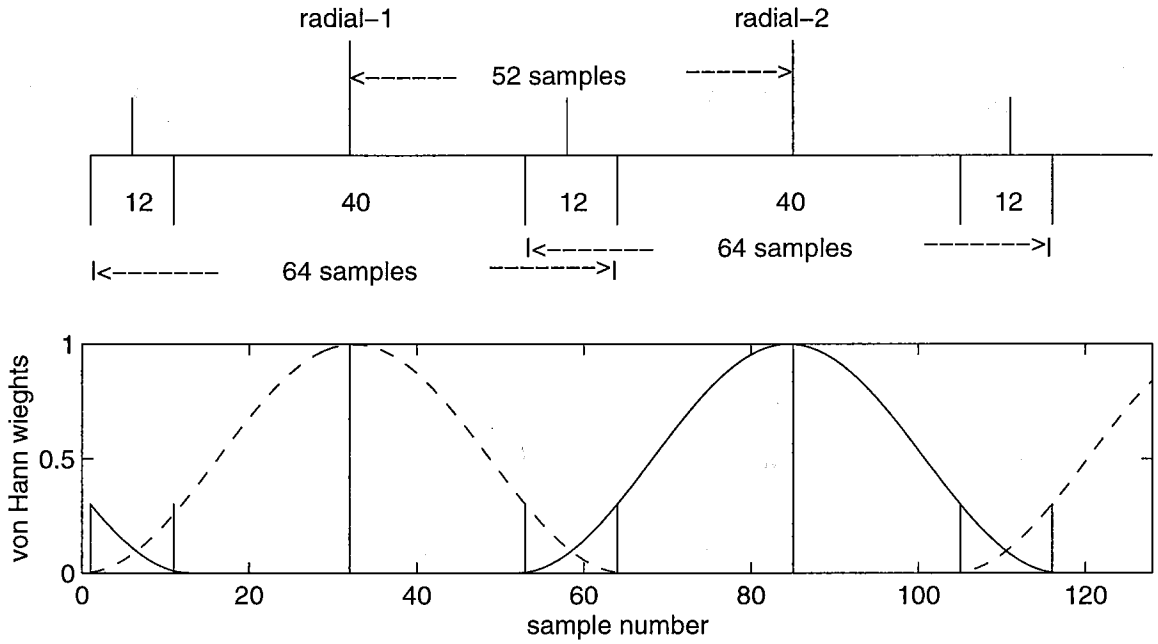

Fig. 4.7. A proposed sample overlap scheme for obtaining 64 length sample sequences without changing the WSR-88D scan parameters.

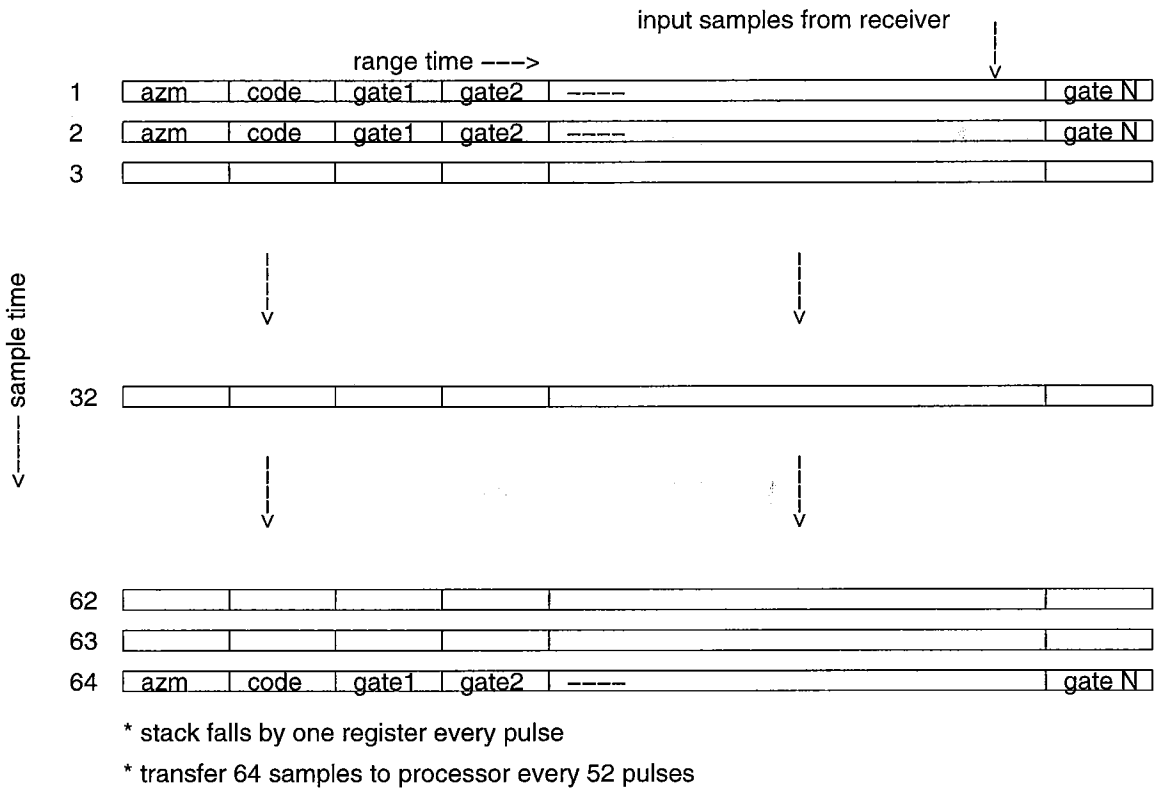

Fig. 4.8. A proposed data storage and flow schematic for obtaining 64 length sample sequences.

5. GENERALIZED SZ CODES

All the results presented so far are for the SZ(8/64) coding scheme. It is indicated in Section 2 that SZ(8/64) may not be the optimum code when the practical effects of the window, noise, and phase shifter errors are included. In this section, we examine the important properties of SZ codes with alternative values of *n/M* and compare the overall performance of the codes, which will aid in the selection of a best code for implementation on the WSR-88D radar.

It may also be noted that the SZ(*n/M*) code is not unique in terms of its properties. For example, we can synthesize several codes that behave the same way as the SZ(8/64) code with respect to the velocity recovery. However, there are some commonalities among the codes which may not be easily recognizable in the switching code but can be identified from the modulation code. The modulation code, ϕ_k (see Table 2.1a), has a periodicity of 8, and the phase change steps are $\pi/8$, $3\pi/8$, $5\pi/8$, $7\pi/8$, $-7\pi/8$, $-5\pi/8$, $-3\pi/8$, $-\pi/8$. The tips of the vectors $exp(j\phi_k)$ form a polygon with 4 sides that is traced twice, once each in the clockwise and the counter clockwise directions, in a period of 8 (see Fig. 5.1a). Several other codes can be put together by reordering these phase changes, but all of them do not have the velocity recovery property of the SZ(8/64) code. Each modulation code is different and has a corresponding switching code. The useful codes are the ones that produce a symmetric side band structure about the d.c. line, when the code is subjected to the notch filtering and cohering processes. The side band structure can be different, but the symmetry is critical for the estimation of the velocity. Thus, it would be more appropriate to say that the SZ(8/64) is a member of a group of SZ(8/64) codes, and in this code group, we include only the codes that have the velocity recovery property. A general expression for the switching phase sequence of the SZ code group is

$$\psi_k^{(q)} = -\sum_{m=0}^{k} \{(n\pi/M) \sum_{p=0}^{2q}(m+p)^2 + \text{const.}\} \; ; \quad q= 0,1,2,..., \quad k=0,1,2,...M-1. \tag{5.1}$$

The corresponding expression for the modulation code group is

$$\phi_k^{(q)} = (n\pi/M) \sum_{p=0}^{2q} (k+p)^2 + \text{const.} \; ; \quad q= 0,1,2,..., \quad k=0,1,2,...M-1. \tag{5.2}$$

The constant is arbitrary and is included for generality, but it may be set to zero. The constant does not affect the performance of the code; however, the appearance of the switching code changes with the constant when mapped onto the $[0, 2\pi)$ space. For example, Fig. 5.1 shows the polar plots of the SZ(8/64) group of codes along with the corresponding switching codes with the constant set to zero. With the addition of a constant to the modulation codes, the polygon representing the modulation code rotates but does not change its shape. However, the pattern of the switching codes would change due to the summation in (5.1). Like the SZ(8/64) code, the properties of all these codes are independent of a shift in the code. We get one code for each permissible value of q, for any given n and M. For example, the SZ(8/64) code is obtained by setting q=0. A group consists of all the codes with a given *n/M*. (Different q values may lead to

the same code, and the number of distinct codes in each group is determined by M and n.) It may be noted that for q values greater than a certain limit, the codes repeat. Some of these codes are encountered in the treatment of multiple trip echo overlay and are discussed in section 5.6.

5.1. SZ(12/64) coding scheme.

The SZ(12/64) coding scheme is similar to the SZ(8/64) coding scheme except for a change in the switching code. Some modifications are needed in the location of the PNF when the ground clutter filtering is used because of the change in the PNF width, n_w. Further, the de-convolution procedure cannot be used for the width estimation; hence, this code can be used for the reflectivity and the velocity recovery only. The magnitude domain convolution procedure gives the correct width only if M/n is an integer.

The switching and the modulation phase code sequences for the SZ(12/64) code are listed in Table 5.1. The SZ(12/64) switching code cycles through all the 32 phase states of a 5-bit phase shifter, with phase shifts in multiples of 11.25°. The spectrum of the modulation code has 16 non-zero coefficients with a separation of $M/16$ coefficients. The maximum notch width that can be used in the decoding algorithm is n_w=0.625. Thus, the region of recovery of v_2 in the $\{p_1/p_2;w_1\}$ space is limited by the residual power ratio, R_p, for that notch width.

The code spectrum after the notch filtering and cohering has 15 non-zero coefficients, of which one at d.c. is the largest, and the rest have a symmetry about the d.c. line. Of the 14 side bands, only four are significant, and the rest are small (each of these coefficients contain < 2 percent of the total power; the total power in the 8 small coefficients is < 9 percent). The side bands with significant amplitudes are spaced 12 coefficients apart for M=64. Thus, when a signal is modulated by the code and subjected to the notch filtering and cohering processes, the resulting spectrum has less overlapped power compared to the SZ(8/64) code and, hence, would result in a lower variance for the recovered velocity, v_2. There is a further reduction in $var(\hat{v}_2)$ because of the smaller notch width used.

Although many of the side bands in the spectrum after the notch filtering and cohering processes have small amplitudes compared to the main signal spectrum, and the overlapped power is small compared to that in the case of the SZ(8/64) code, the separation between them is only M/16 coefficients, and there is a multiple overlap of the side bands. This prevents the magnitude domain deconvolution from reconstructing the original signal spectrum within a reasonable error. Therefore, recovering the spectrum width, w_2, is difficult in this case.

If the ground clutter filter is applied, then a shift in the PNF center location is required whenever the 1st trip signal is stronger, and v_1 is within the interval $(w_{cf}/2-n_w v_a)< v_1 <(n_w v_a-w_{cf}/2)$, which is smaller than the interval for the SZ(8/64) code. This is to ensure that there are sufficient numbers of non-zero coefficients left in the spectrum after the two notch filters are applied. This problem does not arise if the 2nd trip signal is stronger; therefore, no shift in the PNF is required. It is centered on the velocity of the stronger signal. However, there is an increase in the residual noise power from the overlaid stronger signal because of the GCF, as in the case of the SZ(8/64) coding scheme.

The window, the phase error in the phase shifter, and the system noise effects are similar to those discussed in Section 3.

5.2. SZ(16/64) coding scheme.

The SZ(16/64) code further improves the var(v_2) at the expense of a reduced velocity recovery region in $\{p_1/p_2;w_1\}$ space. The switching and the modulation phase code sequences for the SZ(16/64) code are listed in Table 5.2. The SZ(16/64) switching code cycles through all the 8 phase states of a 3-bit phase shifter, with phase shifts in multiples of 45°. The spectrum of the code has only 4 non-zero coefficients with a separation of $M/4$ coefficients. The maximum notch width that can be used in the decoding algorithm is n_w=0.5; hence, it has a smaller region of recovery.

The code spectrum after the notch filtering and cohering processes has 3 non-zero coefficients, i.e, the d.c. line which is the largest, and two symmetrically located side bands spaced M/2 coefficients from the d.c. line. Thus, when a signal modulated by the code is subjected to the notch filtering and cohering processes, the resulting spectrum has much less overlap compared to the other two codes; hence, it has the lowest $var(\hat{v}_2)$.

For a n_w=0.5, the interval v_1 for which the GCF and the PNF overlap is less than v_a; hence, it is not practical to shift the PNF center location whenever v_1 is outside this interval because it will adversely affect the filtering of the stronger 1st trip signal. It is less damaging to lose coherency in the weaker 2nd trip signal, because of the less than the minimum number of coefficients in the spectrum after PNF, than to risk an increased residual power by shifting the PNF center location. This situation occurs when the 1st trip is stronger, and the ground clutter filter is applied. If the second trip is stronger, the effect is similar to that for the other two codes. The window, the phase shifter error, and the system noise effects are also similar to those discussed in Section 3.

5.3. Overall performance and comparison of the three SZ coding schemes.

For comparing the performance of the three SZ coding schemes, it is best to use the criterion of their potential to recover the mean velocity of the weaker of the two overlaid signals, because it is the most important and difficult parameter to recover. Since all three schemes use notch filtering and cohering processes to recover the velocity of the weaker signal, a comparison of the spectra of the weaker and stronger signals after notch filtering and cohering, brings out the relative merits of the schemes. Fig. 5.2 shows an example of a simulated signal modulated by the three codes and then subjected to the notch filtering and cohering process. The notch widths are appropriately chosen for each code. The signal power loss is proportional to the notch width and, hence, is the largest for SZ(8/64) code. The overlap in the cohered spectrum clearly is the smallest in the case of the SZ(16/64) code; thus, it has the lowest standard error in the velocity estimate (compare Figs. 5.4, 5.3, and 3.16; the SZ(8/64) has the largest standard error, and the SZ(12/64) code performs somewhere in between). Figs. 5.3 and 5.4 show the standard deviation of the weaker signal velocity estimate for the SZ(12/64) and SZ(16/64) coding schemes. Similar plots for the SZ(8/64) code and for the autocovariance algorithm in the absence of any overlaid signal are given earlier (see Fig. 3.16). In generating these figures, simulation results are fitted to a 2nd degree polynomial to obtain smooth curves.

A plot of the stronger echo spectrum after the notch filtering and cohering steps is shown in Fig. 5.5, where the signal is coherent, and the notch is centered on the mean velocity. The

residual power after the notch filtering and cohering steps is noise-like in all three cases but has different power levels. The residual power is more than twice in the case of SZ(16/64), compared to that for SZ(8/64) code. This difference in power is a function of the spectrum width of the signal. Thus, the noise due to the residual power is a function of w_1, which puts a limit on the p_1/p_2 ratio, whereas the noise due to the overlap in the spectrum (see Fig. 5.2) is a function of the width w_2 which controls the $sd(\hat{v}_2)$ in the region of recovery.

The random phase error in the phase shifter with ϵ=0.5° limits the R_p to a much lower value for all three codes, thus reducing the difference between the recovery regions for the three codes. Therefore, for comparing the overall performance of the three coding schemes, a series of plots depicting the $sd(\hat{v}_2)$ in $\{p_1/p_2;w_1\}$ space for a few selected w_2 values are given. Again, we make the assumption that the 1st trip is stronger, and only the 1st and 2nd trips echoes are present in the signal. In order for the comparisons to be realistic, we have chosen the parameters closest to those of the WSR-88D. The following parameters are used to generate the plots from simulations:

(a) Radar frequency is 3 GHz.
(b) Short PRT is 0.7812 millisec. (gives v_a=32 m s^{-1}; r_a=117 km).
(c) p_1/p_2 values are varied from 0 to 50 dB in steps of 2 dB.
(d) w_1 is varied from 0.5 to 8 m s^{-1} in steps of 0.5 m s^{-1}.
(e) w_2 is kept constant for each plot.
(f) The random phase error in the phase shifter is uniformly distributed over ±0.5°.
(g) The SNR of the weaker 2nd trip signal is >30 dB.
(h) The von Hann window is used in processing the time series.
(i) Number of samples used in all cases is 64.
(j) Number of simulations used for computing $sd(\hat{v}_2)$ is 40.
(k) No ground clutter is present in the signal.

The performance of the three algorithms in the presence of the ground clutter may have differences because of the way in which the PNF center is adjusted to minimize the effect. But this performance is not used for comparison because (a) the difference in the performance is likely to be small, and (b) the ground clutter is present in less than 20 percent of the total area under consideration. (In $2r_a$=234 km, the ground clutter is typically present over 0 to 20 km, and affects velocity recovery in the r_a to r_a+20 km also.)

Figs. 5.6 through 5.8 show the $sd(\hat{v}_2)$ in $\{p_1/p_2;w_1\}$ space for three selected values of w_2. The coding scheme used in each case is indicated in the figure. Larger widths are chosen (4, 6, and 8 m s^{-1}) because the difference among the schemes is more prominent for these values. Although the random phase coding technique is not discussed in this part of the report, the results are included in the figures for comparison. An examination of the three figures shows that the velocity recovery region is bounded by the $R_p(n_w)$ curve for larger w_1 values and an upper boundary that is nearly independent of w_1 and is due to the random phase error in the phase shifter. Further, the $sd(\hat{v}_2)$ in the region of recovery is the lowest in the case of the SZ(16/64) code and the largest for the random phase algorithm. The recovery region is nearly independent of w_2, but the $sd(\hat{v}_2)$ increases for larger w_2. At w_2=8 m s^{-1}, the SZ(16/64) coding scheme is the only one that still recovers the weaker signal velocity with a reasonable standard error. The choice of the coding scheme depends on several factors. First and most important is the recovery

of the weaker signal velocity. The other two spectral parameters are to be considered only if the SZ coding scheme is used in the stand alone mode without the long PRT scan. It may be noted here that the SZ(12/64) coding scheme does not recover the spectrum width of the weaker signal; hence, it cannot be used if all three parameters are required to be estimated using the short PRT data alone. All three coding schemes recover the stronger signal parameters; there is an increase in the estimate variance if p_1/p_2 is within about ±5 dB, but it is within the tolerable limit for each parameter.

All the results presented in this report use M=64 samples in the processing of the time series. The variance of the estimates is a strong function of the number of samples, and hence, if the number of samples is larger, the choice clearly will shift towards a SZ code with a lower (n/64) value. A lower value of n allows larger notch width to be used in rejecting the stronger signal, provided the variance of the recovered weaker signal velocity is tolerable.

Besides the performance of the coding schemes with respect to the recovery of the velocity of the weaker signal, several other aspects of the schemes need to be compared in selecting the best code. A summary of the comparison among the three schemes, SZ(8/64), SZ(12/64), and SZ(16/64), is given below. Some of the points listed below pertaining to the width estimation are applicable only for the SZ-1 algorithm. If the SZ-2 algorithm is implemented, these points are to be ignored in comparing the coding schemes (see section 5.4 for SZ-1 and SZ-2 algorithms).

Summary of comparison among the three coding schemes:

	SZ(8/64)	**SZ(12/64)**	**SZ(16/64)**
1. recoverable parameters:			
a) p_1 and p_2	yes	yes	yes
b) v_1 and v_2	yes	yes	yes
c) w_1 and w_2	yes	w_1 only	yes
2. PNF notch width, n_w	0.75	0.625	0.5
3. $sd(\hat{v}_2)$ in the recovery region ($sd(\hat{v}_2) < 2$ m s^{-1}):			
w_2=4 m s^{-1}	1.64 m s^{-1}	1.40 m s^{-1}	1.28 m s^{-1}
w_2=6 m s^{-1}	1.87 m s^{-1}	1.81 m s^{-1}	1.71 m s^{-1}
w_2=8 m s^{-1}	*	1.97 m s^{-1}	1.89 m s^{-1}
4. sensitivity to random phase error:	medium	highest	least
5. sensitivity to phase setting error:	low	low	low

Note: * the region of $sd(\hat{v}_2) < 2$ m s^{-1} is zero.

5.4. Decoding algorithms.

In the following two sub-sections, two algorithms are given: one working in the stand-alone mode, and the other for use in conjunction with the long PRT scan data. Both are developed for SZ(n/64) coded transmission in the short PRT mode. The algorithms may need minor modifications for use with SZ codes optimized for code lengths other than multiples of 64.

5.4.1. SZ-1 algorithm. (*stand alone mode; **does not** use long PRT data*)

<<<----------**START** of algorithm

1. Input raw time series E_{1k} ; k=1,2, ... M.
- The phase switching sequence ψ_k ; SZ(n/M) code.

2. Cohere the 1st trip signal.
- $E_1 = E_{1k} \exp\{-j\psi_k\}$.
- 1st trip is coherent; 2nd trip is phase coded by a sequence $\phi_k = n\pi k^2/M$; k=0,1,2,.... M-1.

3. Multiply by von Hann window weights, h_k .
- $E_1 = E_1\ h_k$.

4. Filter the ground clutter.
- E_1 = GCF(E_1).

5. Cohere the second trip.
- $E_2 = E_1 \exp\{-j\phi_k\}$.

6. Autocovariance process E_1 and E_2 to get $\hat{p}_1,\hat{v}_1,\hat{w}_1,\hat{w}_1'$ and $\hat{p}_2,\hat{v}_2,\hat{w}_2,\hat{w}_2'$ (for the computation of $\hat{w}_1',\hat{w}_2'$ use Eq. 6.27 of Doviak and Zrnic, 1993, and for the computation of $\hat{w}_1,\hat{w}_2$ use Eq. 6.32 of Doviak and Zrnic, 1993).

7. Compute $\hat{w}_1'/\hat{w}_2'$ ratio.
- if $\hat{w}_1'/\hat{w}_2' > 1$, trip=2, second trip is stronger - process E_2.
- if $\hat{w}_1'/\hat{w}_2' < 1$, trip=1, first trip is stronger - process E_1.

8. If trip=2, interchange E_1 & E_2, and all the parameters in step number 6.
- with this interchange, E_1 is the time series with stronger signal coherent.
- we need to recover $\hat{p}_2,\hat{v}_2$ and $\hat{w}_2$ of the weaker signal.

[Note: The processing steps 9 to 17 are the same for the two cases in step 7 with E_1 replaced by E_2. This is accomplished by step 8, and the trip numbers are restored in the step 18.]

9. Compute spectrum of E_1.
- S_1' = DFT [E_1].

10. Notch ($n_w M$) coefficients centered on $\hat{v}_1$ to get S_1 from S_1'.
Note: (a) n_w is not to exceed the maximum permissible value, (1-2n/M).
(b) for SZ(8/64) & SZ(12/64) optimum PNF center location to be computed if trip=1 (i.e. 1st trip stronger) and GCF is applied.

11. Compute mean power p from the remaining coefficients.
Multiply p by $1/(1-n_w)$ to get mean power p_2.

12. Compute power ratio $pr = 10 \log_{10}(\hat{p}_1/\hat{p}_2)$ dB.

13. If pr< 25 dB, correct error in p_1 estimate.
- $\hat{p}_1' = \hat{p}_1 - \hat{p}_2$.
- compute corrected power ratio $\hat{pr} = \hat{p}_1'/\hat{p}_1$.

14. Cohere the weaker signal in S_1.
- e_1 = IDFT [S_1]
- if trip = 1, $e_2 = e_1 \exp\{-j\phi_k\}$.
- if trip = 2, $e_2 = e_1 \exp\{ j\phi_k\}$.

15. Compute autocorrelation $R(1)$ for e_2, and compute mean velocity, $\hat{v}_2$.

16. Magnitude deconvolution. (for SZ(8/64) and SZ(16/64) only)
- compute magnitude spectrum, $s_2' = |\ \mathrm{DFT}(e_2)\ |$.
- multiply by the deconvolution matrix, $s_2 = D\ s_2'$.
[The deconvolution matrix, D, is a part of the program. D is pre-computed and supplied to the algorithm, or stored as a part of the program.]

17. Compute autocorrelation $R(1)$ for s_2, and compute width, $\hat{w}_2$.

18. If trip = 2, interchange parameters ($\hat{p}_1,\hat{v}_1,\hat{w}_1$) and ($\hat{p}_2,\hat{v}_2,\hat{w}_2$).

19. Output the 1st and 2nd trip parameters and go to the next data set.

<<<----------**END** of algorithm

5.4.2. SZ-2 algorithm. (*recovers velocities* $\hat{v}_1$ and $\hat{v}_2$ only).

This algorithm assumes that the long PRT scan data is autocovariance processed to estimate mean power and width of both 1st and the 2nd trip signals. The SZ-2 algorithm recovers only velocities using the short PRT time series data. The SZ-2 algorithm is computationally much less demanding than the SZ-1 algorithm.

<<<----------**START** of algorithm

1. Inputs:
- Raw time series E_{1k}; k=1,2, ... M.
- The phase switching sequence ψ_k; SZ(n/M) code.

2. Cohere the 1st trip signal.
- $E_1 = E_{1k} \exp\{-j\psi_k\}$.
- 1st trip is coherent; 2nd trip is phase coded by a sequence $\phi_k = n\pi k^2/M$; k=0,1,2,.... M-1.

3. Multiply by von Hann window weights, h_k .
- $E_1 = E_1 \; h_k$

4. Filter the ground clutter.
- E_1 = GCF(E_1).

5. Cohere the second trip.
- $E_2 = E_1 \exp\{-j\phi_k\}$.

6. Autocovariance process E_1 and E_2 to get $\hat{v}_1,\hat{w}_1'$ and $\hat{v}_2,\hat{w}_2'$.
(For the computation of $\hat{w}_1',\hat{w}_2'$, use Eq. 6.27 of Doviak and Zrnic, 1993)

7. Compute $\hat{w}_1/\hat{w}_2$ ratio.
- if $\hat{w}_1/\hat{w}_2 > 1$, trip=2, second trip is stronger - process E_2.
- if $\hat{w}_1/\hat{w}_2 < 1$, trip=1, first trip is stronger - process E_1.

8. If $\hat{w}_1/\hat{w}_2 > 1$, interchange E_1 & E_2, and all the parameters on line number 6.
- with this interchange, E_1 is the time series with stronger signal coherent.
- we need to recover velocity v_2 of the weaker signal.

[Note: The processing steps 9 to 12 are same for the two cases in step 7 with E_1 replaced by E_2. This is accomplished by step 8, and the trip numbers are restored in step 13.]

9. Compute spectrum of E_1.
- $S_1' = \text{DFT}\ [\ E_1\ ]$.

10. Notch ($n_w M$) coefficients centered on $\hat{v}_1$ to get S_1 from S_1'.
Note: (a) n_w is not to exceed the maximum permissible value, (1-2n/M).
(b) for SZ(8/64) & SZ(12/64) optimum PNF center location to be computed if trip=1 (i.e., 1st trip stronger) and GCF is applied.

11. Cohere the weaker signal in S_1.
- $e_1 = \text{IDFT}\ [\ S_1\ ]$.
- if trip = 1, $e_2 = e_1 \exp\{-j\phi_k\}$.
- if trip = 2, $e_2 = e_1 \exp\{\ j\phi_k\}$.

12. Compute autocorrelation $R(1)$ for e_2, and compute mean velocity $\hat{v}_2$.

13. If trip = 2, interchange parameters $\hat{v}_1$ and $\hat{v}_2$.

14. Output 1st and 2nd trip velocities, $\hat{v}_1$, $\hat{v}_2$, and go to next data set.
($\hat{p}_1,\hat{p}_2,\hat{w}_1,\hat{w}_2$ are obtained from the long PRT data.)

<<<----------**END** of algorithm

5.5. Algorithm implementation on the WSR-88D.

The two algorithms presented in Sections 5.4.1 and 5.4.2 are for the estimation of spectral parameters from a phase coded time series. For practical implementation on the radar, it is necessary to include several other aspects, such as the need to adjust the process notch filter position based on the velocity and ground clutter information. A decision on whether to apply the GCF or not, based on a ground clutter map, also needs to be incorporated. The ground clutter filter affects the 1st trip signal parameters, and it is required to correct the error to the extent possible. To minimize the effect of GCF on the estimated 2nd trip signal parameters, the position of the PNF has to be adjusted. Appropriate logic has to be built in to the decoding program to accomplish this.

From all the discussions in this report, it appears imperative that we retain the long PRT scan for the lowest two elevations, and it is best to retain the batch mode with an increased number of samples in the Doppler mode (65 samples). It is also suggested that the long PRT scan data processing is modified for the width estimation, in addition to the reflectivity. Further, if there is no overlaid echo, only steps 1, 2, 4, and 6 in the algorithm need to be applied. Just as in the case of ground clutter filtering, it is possible to devise a map to demarcate areas where the full algorithm is to be applied based on the long PRT reflectivity data.

A suggested schematic of the algorithm for implementation including all the above mentioned points is given in Fig. 5.9. To implement this scheme on the WSR-88D, a new processor is needed but requires minimal changes in the scan parameters of the radar in the batch mode alone. The SZ(16/64) code is proposed to be used for all the phase coded transmissions, and to obtain the required minimum of 65 samples, the scan parameters in the batch mode need to be modified (i.e., a minimum of 65 pulses to be transmitted in the short PRT). No change is required in the lowest two elevation scans. The sample overlap scheme is suggested for obtaining the 64 samples in the Doppler mode (Fig. 4.7, Fig. 4.8).

5.6. Multiple trip echo overlay.

Although the report considers only the 1st and 2nd trip echo overlay, the algorithm is applicable for any two trip echo overlays with some modifications. These modifications can be incorporated into the algorithm if the long PRT reflectivity data is used to decide the trip numbers of the overlaid signals. In the worst case, there can be as many as 4 trip echoes overlaid in the lowest two elevation scans if the long to short PRT ratio is about 4. In the multiple trip overlay case, it is necessary to identify and tag the region where velocity is not recoverable, or the recovered velocity is likely to be erroneous. Here, we consider various cases and suggest possible methods for recovering the velocities and tagging the unrecoverable regions. The discussion is based on the assumption that velocities are to be recovered over 0 to $2r_a$ only in the presence of multiple trip overlay up to 4 trips.

Before considering the different possible situations, we first examine the codes required to cohere the 3rd and 4th trips, and the corresponding properties of the modulation codes which are crucial for the recovery of the weaker signal velocity. If ψ_k, k=1, 2, 3... is the switching phase code sequence, and the 1st trip is cohered, the 2nd and higher order trip echo signals get modulated in phase sequences given by

$$
\begin{aligned}
&1^{st}\text{ trip} && \phi_{1,k} = 0\ , && \text{(coherent)}\\
&2^{nd}\text{ trip:} && \phi_{2,k} = \psi_{k-1} - \psi_k && = n\pi k^2/M,\\
&3^{rd}\text{ trip:} && \phi_{3,k} = \psi_{k-2} - \psi_k && = n\pi\{k^2+(k-1)^2\}/M,\\
&4^{th}\text{ trip:} && \phi_{4,k} = \psi_{k-3} - \psi_k && = n\pi\{k^2+(k-1)^2+(k-2)^2\}/M,\\
&m^{th}\text{ trip:} && \phi_{m,k} = \psi_{k-m+1} - \psi_k && = n\pi\{\sum_{p=0}^{m-2}(k-p)^2\}/M, \quad \text{etc.}
\end{aligned}
\qquad (5.3)
$$

Comparing these expressions to (5.2), it is clear that even numbered trip signals are modulated by the SZ codes belonging to the SZ(n/M) group, while the odd numbered trip signals are modulated by codes which do not belong to the group. In fact, every alternate odd numbered trip signals (i.e., 3, 7, 11,..etc.) belong to a group which behave as the SZ($2n/M$) code, and the signals with trip numbers 5, 13,... etc. are modulated with codes belonging to the SZ($4n/M$) group, and so on. The following table gives the arrangement of the code groups as a function of trip numbers.

Trip numbers and code groups when 1st trip is cohered.

trip number	modulation code group (**SZ(8/64)** switching code)	modulation code group (**SZ(16/64)** switching code)
1	coherent	coherent
2	*8/64*	16/64
3	*16/64*	32/64
4	*8/64*	16/64
5	32/64	coherent
6	*8/64*	16/64
7	16/64	32/64
8	*8/64*	16/64
9	coherent	coherent

Similar tables can be generated for any *n/M*. If other than the 1st trip is cohered, the modulation code groups for each trip can be obtained by simply shifting the trip numbers cyclically (over 1 to 8; 9th is the same as the 1st). For example, if the 3rd trip is cohered, the modulation code groups are obtained by shifting the trip numbers 3 to 8 up, such that trip 3 is at the top of the table, and shifting 1 & 2 to the bottom, in the place of 7 & 8. The right hand column remains the same for the SZ(8/64) code. Since our interest is in the trip numbers 4 and less, we can restrict our attention to the codes of only two sets, the SZ(*n/M*) and SZ(2*n/M*) sets. From the table (given above), it is obvious that there can be situations where we encounter the SZ(16/64) group of codes while the switching code is SZ(8/64). In such cases, appropriate changes in the PNF width (i.e., $\{n_w\}_{max}=(1-2n/M)$) need to be made in the decoding algorithm. Another important point to note is that for the SZ(16/64) switching code, the 3rd trip modulation code is SZ(32/64) which has $\{n_w\}_{max}=0$; thus, under certain circumstances, it may not be possible to recover the 1st trip velocity. (I.e., situations like the 1st and 3rd trip signals overlaid with 3rd trip signal stronger.) To cohere the m^{th} trip signal, we need to multiply the time series by the complex conjugate of the appropriately shifted switching code, or if the time series has the 1st trip coherent (i.e., the 1st trips signal needs to be cohered to filter the ground clutter), then the complex conjugate of the appropriate modulation code has to be used.

Now, we shall classify the overlaid signals into groups with 2, 3, or 4 trip signals overlaid and address each group of situations separately. All these situations are relevant only in the lowest two elevation scans of the WSR-88D because of the large range. We reiterate the assumption that only v_1 and v_2 are required to be estimated.

(a). Two trip overlay:

Possible combinations are (1 & 2), (1 & 3), (1 & 4), (2 & 3), (2 & 4), and (3 & 4).

(1 & 2) - Use the algorithm SZ-1 or SZ-2 (they are designed for this case).

(1 & 3) - If the 1st trip signal is stronger, recover only v_1 using SZ-1 algorithm. If the 3rd trip signal is stronger, use the code $\phi_{3,k}$ in place of $\phi_{2,k}$ in the SZ-1 or SZ-2 algorithms. Note that the code $\phi_{3,k}$ belongs to a different group, and the PNF width needs to be adjusted accordingly. For example, if the SZ(8/64) switching code is used in the transmission, $\phi_{3,k}$ would belong to the SZ(16/64) group, and we have to use n_w=0.5. If the switching code is SZ(16/64), then v_1 is not recoverable in this case.

(1 & 4) - Replace the code $\phi_{2,k}$ with $\phi_{4,k}$ in the SZ-1 or SZ-2 algorithm.

(2 & 3) - This case is the same as the (1 & 2) case with $\phi_{1,k}$ and $\phi_{2,k}$ replaced by $\phi_{2,k}$ and $\phi_{3,k}$, respectively. Note that we still have to use $\phi_{1,k}$ for cohering the 1st trip if the GCF is to be applied (i.e., the ground clutter is present).

(2 & 4) - This case is similar to the (1 & 3) case. If the 2nd trip signal is stronger, recover v_2 using the SZ-1 or SZ-2 algorithms. If the 4th trip signal is stronger, the v_2 can be recovered if the SZ(8/64) code is used in the transmitter switching. With SZ(16/64) code transmission, v_2 is not recoverable.

(b). Three and four trip overlay:

Possible combinations are: (1, 2, & 3), (1, 2, & 4), (2, 3, & 4), and (1, 2, 3, & 4). In each case, the decoding logic depends on the relative power levels of the signals. In some cases, one or both velocities can be recovered, and in some other cases, none can be recovered. The logic required to route the computation has to be worked out individually for each case and can be complex. One example is given below.

(1, 2, & 3) - If $p_1>(p_2+p_3)$, recover v_1 using SZ-1 or SZ-2;
and if $p_2>p_3$, notch filtering and cohering steps can recover v_2;
else tag v_2 as "not recoverable."
If $p_2>(p_1+p_3)$, recover v_2 using SZ-1 or SZ-2;
and if $p_1>p_3$, notch filtering and cohering steps can recover v_1;
else tag v_1 as "not recoverable."

The cases of 3 or 4 trip overlay are generally small; hence, for simpler implementation on the WSR-88D, it would be appropriate to recover only the velocities, v_1 or v_2, only for the two cases, $p_1>(p_2+p_3+p_4)$ and $p_2>(p_1+p_3+p_4)$. In all other cases of 3 and 4 trip overlay, tag both velocities as "not recoverable," although in many cases, one or both velocities may be recoverable with additional computation.

Finally, it is important to set some criteria on the relative power levels in classifying the overlaid signals. For example, if the relative powers p_1 to p_4 are 0, 10, 45, and 30 dB, the

case can be treated as trips (1 & 2) overlaid, (1, 2, & 4) overlaid, or (1, 2, 3, & 4) overlaid, depending on the criteria that we define for classfication. One criteria could be the SNR of the signal, and the other criterion can be the power ratio. Thus, if the $SNR_i < 0$ dB, p_i is neglected and, if the ratio of the strongest to the weaker signal is greater than 40 dB, we can neglect the weaker signal. This is based on the logic that the largest p_1/p_2 ratio for which v_2 can be recovered is about 40 dB. With this criteria, the above mentioned example can be considered as trips (1, 2, & 4) overlaid.

Table.5.1a. Modulation phase code sequence for *n/M*=12/64 in degrees.

k	ϕ_k	k	ϕ_k	k	ϕ_k	k	ϕ_k
0	0.00	16	0.00	32	0.00	48	0.00
1	33.75	17	33.75	33	33.75	49	33.75
2	135.00	18	135.00	34	135.00	50	135.00
3	-56.25	19	-56.25	35	-56.25	51	-56.25
4	180.00	20	180.00	36	180.00	52	180.00
5	123.75	21	123.75	37	123.75	53	123.75
6	135.00	22	135.00	38	135.00	54	135.00
7	-146.25	23	-146.25	39	-146.25	55	-146.25
8	0.00	24	0.00	40	0.00	56	0.00
9	-146.25	25	-146.25	41	-146.25	57	-146.25
10	135.00	26	135.00	42	135.00	58	135.00
11	123.75	27	123.75	43	123.75	59	123.75
12	180.00	28	180.00	44	180.00	60	180.00
13	-56.25	29	-56.25	45	-56.25	61	-56.25
14	135.00	30	135.00	46	135.00	62	135.00
15	33.75	31	33.75	47	33.75	63	33.75

Table.5.1b. Switching phase code sequence for *n/M*=12/64 in degrees.

k	ψ_k	k	ψ_k	k	ψ_k	k	ψ_k
0	0.00	16	90.00	32	180.00	48	-90.00
1	33.75	17	123.75	33	-146.25	49	-56.25
2	168.75	18	-101.25	34	-11.25	50	78.75
3	112.50	19	-157.50	35	-67.50	51	22.50
4	-67.50	20	22.50	36	112.50	52	-157.50
5	56.25	21	146.25	37	-123.75	53	-33.75
6	-168.75	22	-78.75	38	11.25	54	101.25
7	45.00	23	135.00	39	-135.00	55	-45.00
8	45.00	24	135.00	40	-135.00	56	-45.00
9	-101.25	25	-11.25	41	78.75	57	168.75
10	33.75	26	123.75	42	-146.25	58	-56.25
11	157.50	27	-112.50	43	-22.50	59	67.50
12	-22.50	28	67.50	44	157.50	60	-112.50
13	-78.75	29	11.25	45	101.25	61	-168.75
14	56.25	30	146.25	46	-123.75	62	-33.75
15	90.00	31	180.00	47	-90.00	63	0.00

Table.5.2a. Modulation phase code sequence for n/M=16/64 in degrees.

k	ϕ_k	k	ϕ_k	k	ϕ_k	k	ϕ_k
0	0.00	16	0.00	32	0.00	48	0.00
1	45.00	17	45.00	33	45.00	49	45.00
2	180.00	18	180.00	34	180.00	50	180.00
3	45.00	19	45.00	35	45.00	51	45.00
4	0.00	20	0.00	36	0.00	52	0.00
5	45.00	21	45.00	37	45.00	53	45.00
6	180.00	22	180.00	38	180.00	54	180.00
7	45.00	23	45.00	39	45.00	55	45.00
8	0.00	24	0.00	40	0.00	56	0.00
9	45.00	25	45.00	41	45.00	57	45.00
10	180.00	26	180.00	42	180.00	58	180.00
11	45.00	27	45.00	43	45.00	59	45.00
12	0.00	28	0.00	44	0.00	60	0.00
13	45.00	29	45.00	45	45.00	61	45.00
14	180.00	30	180.00	46	180.00	62	180.00
15	45.00	31	45.00	47	45.00	63	45.00

Table.5.2b. Switching phase code sequence for n/M=16/64 in degrees.

k	ψ_k	k	ψ_k	k	ψ_k	k	ψ_k
0	0.00	16	0.00	32	0.00	48	0.00
1	45.00	17	45.00	33	45.00	49	45.00
2	-135.00	18	-135.00	34	-135.00	50	-135.00
3	-90.00	19	-90.00	35	-90.00	51	-90.00
4	-90.00	20	-90.00	36	-90.00	52	-90.00
5	-45.00	21	-45.00	37	-45.00	53	-45.00
6	135.00	22	135.00	38	135.00	54	135.00
7	180.00	23	180.00	39	180.00	55	180.00
8	180.00	24	180.00	40	180.00	56	180.00
9	-135.00	25	-135.00	41	-135.00	57	-135.00
10	45.00	26	45.00	42	45.00	58	45.00
11	90.00	27	90.00	43	90.00	59	90.00
12	90.00	28	90.00	44	90.00	60	90.00
13	135.00	29	135.00	45	135.00	61	135.00
14	-45.00	30	-45.00	46	-45.00	62	-45.00
15	0.00	31	0.00	47	0.00	63	0.00

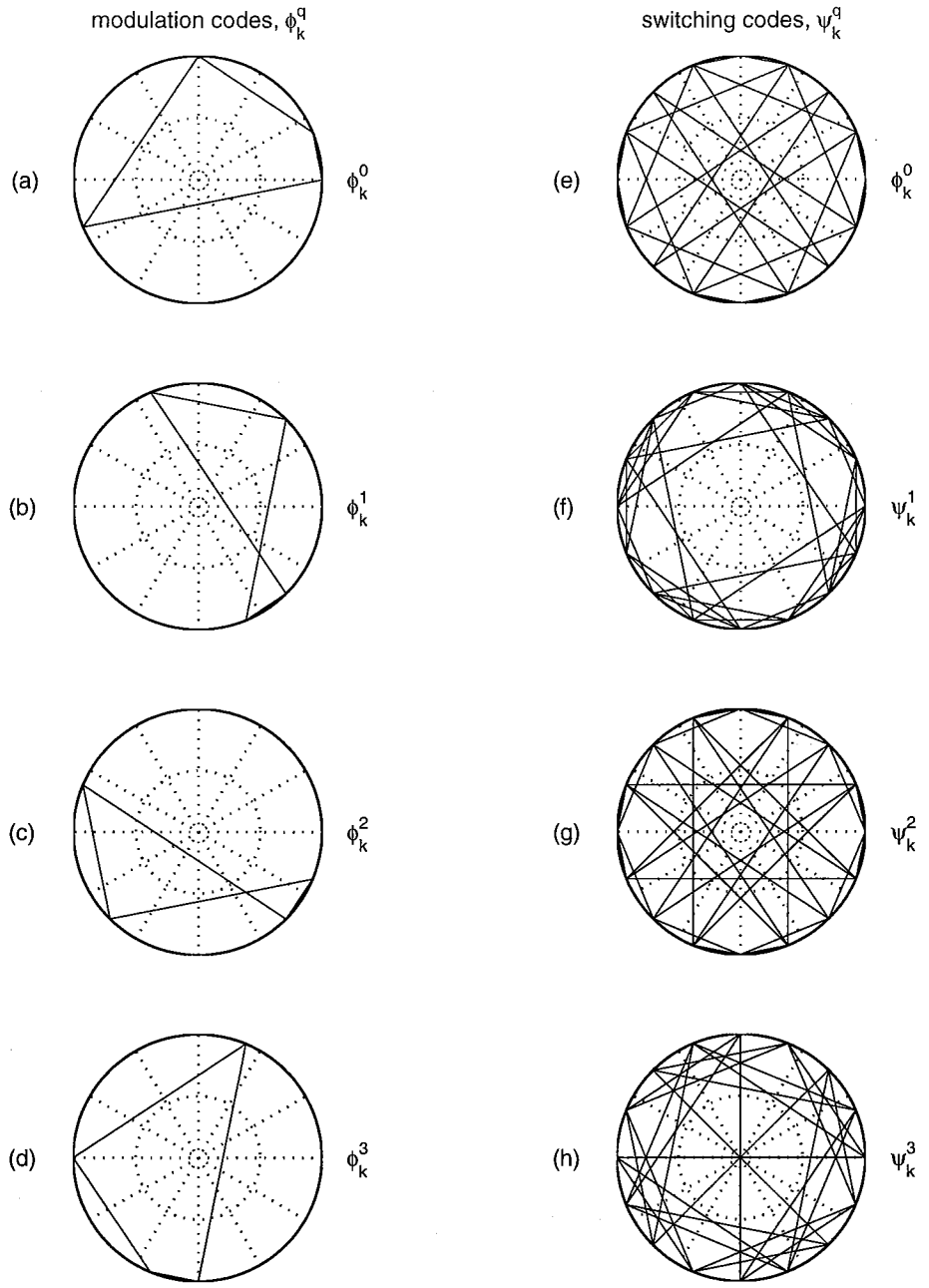

Fig. 5.1. The SZ(8/64) modulation and switching code group phase diagrams.

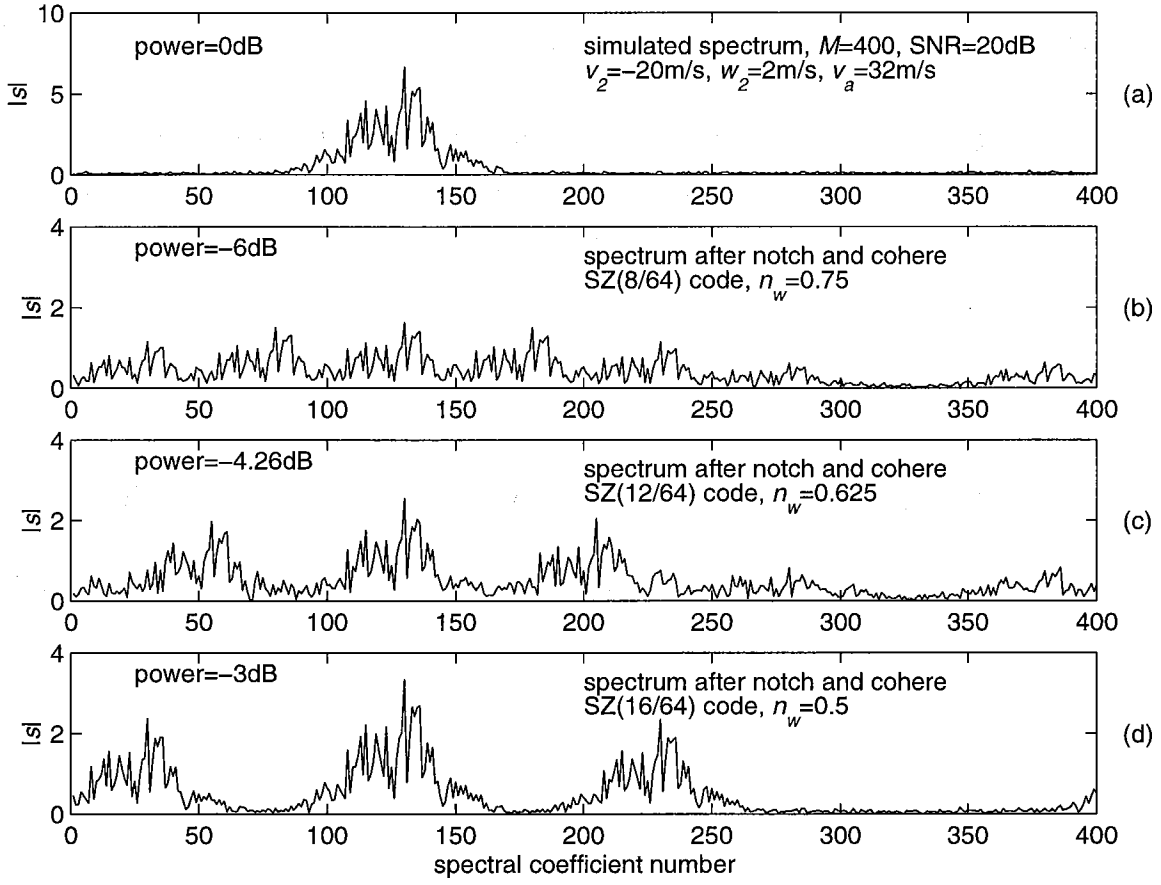

Fig. 5.2. Weaker signal spectrum after the notch and cohere process: (a) the signal spectrum, (b) using the SZ(8/64) code, n_w=0.75, (c) using the SZ(12/64) code, n_w=0.625, (d) using the SZ(16/64) code, n_w=0.5.

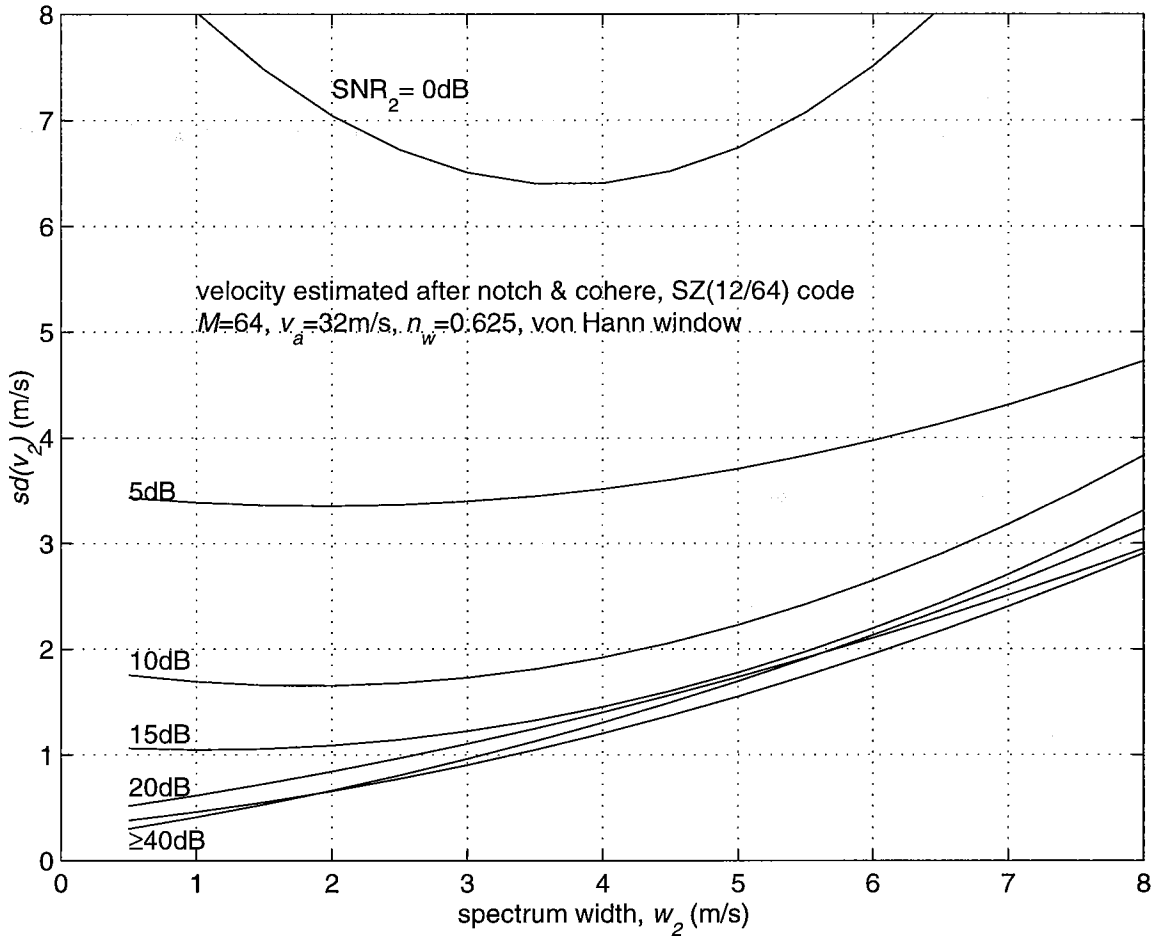

Fig. 5.3. $sd(\hat{v}_2)$ versus the spectrum width, w_2, with the von Hann window for the SZ(12/64) algorithm. 100 simulations are used for each w_2 and SNR_2 to compute $sd(\hat{v}_2)$, and a 2nd degree polynomial is fitted to get a smooth curve.

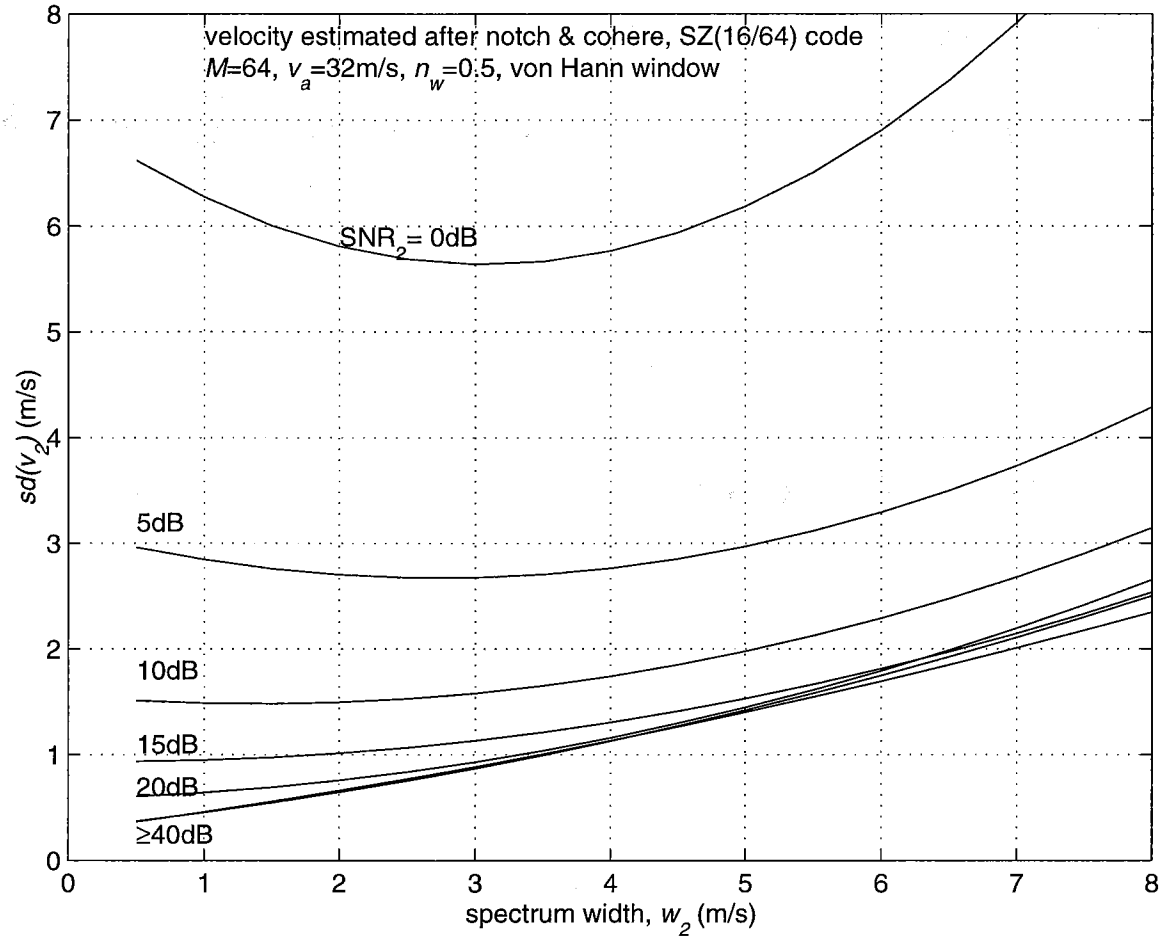

Fig. 5.4. $sd(\hat{v}_2)$ versus spectrum width, w_2, with the von Hann window for the SZ(16/64) algorithm. 100 simulations are used for each w_2 and SNR_2 to compute $sd(\hat{v}_2)$, and a 2nd degree polynomial is fitted to get a smooth curve.

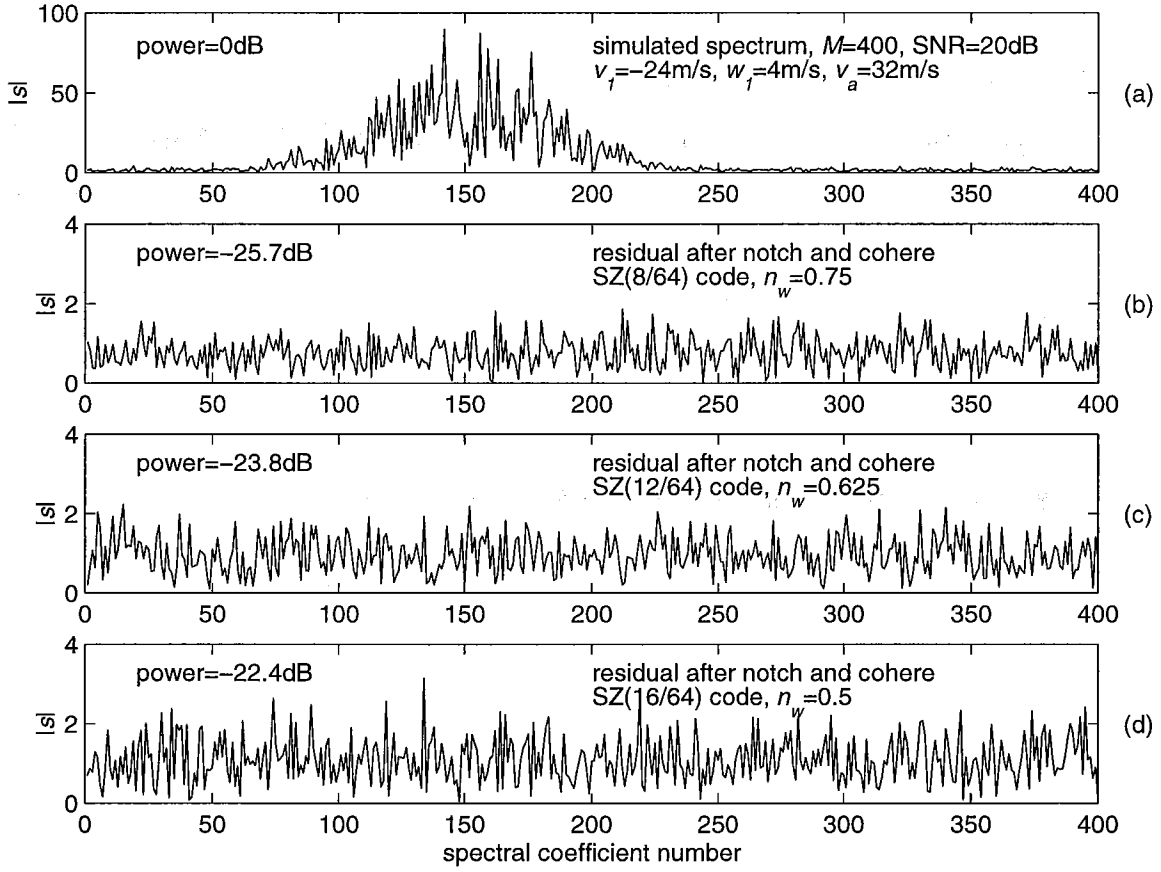

Fig. 5.5. Stronger signal spectrum after the notch and cohere process: (a) the signal spectrum, (b) using the SZ(8/64) code, n_w=0.75, (c) using the SZ(12/64) code, n_w=0.625, (d) using the SZ(16/64) code, n_w=0.5.

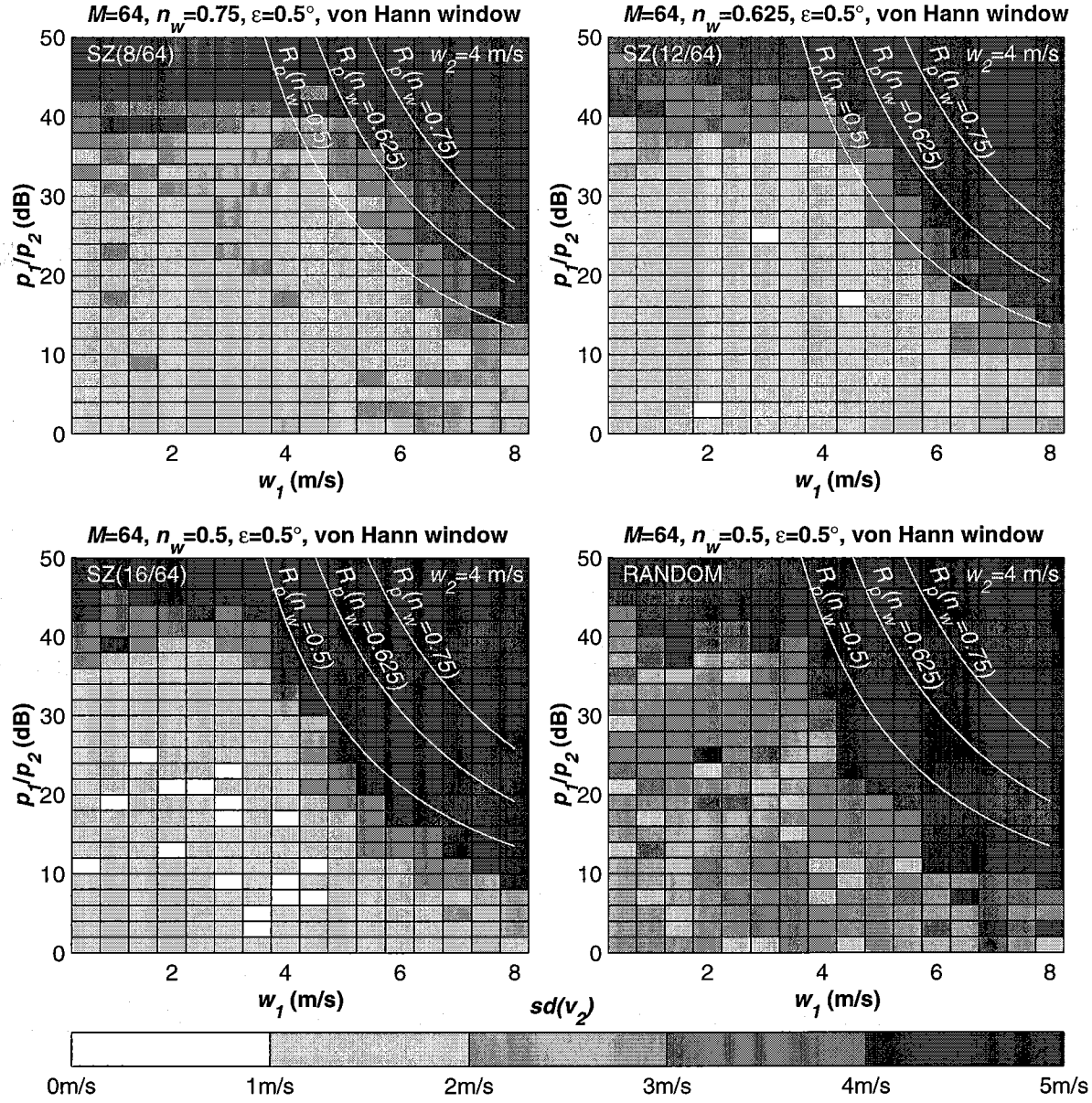

Fig. 5.6. Plots of $sd(\hat{v}_2)$ as a function of p_1/p_2 and w_1, for the SZ(8/64), SZ(12/64), SZ(16/64), and the random phase coding schemes -- a comparison. (M=64, w_2=4 m/s; von Hann window; random phase error parameter, ϵ=0.5°; v_a=32 m/s).

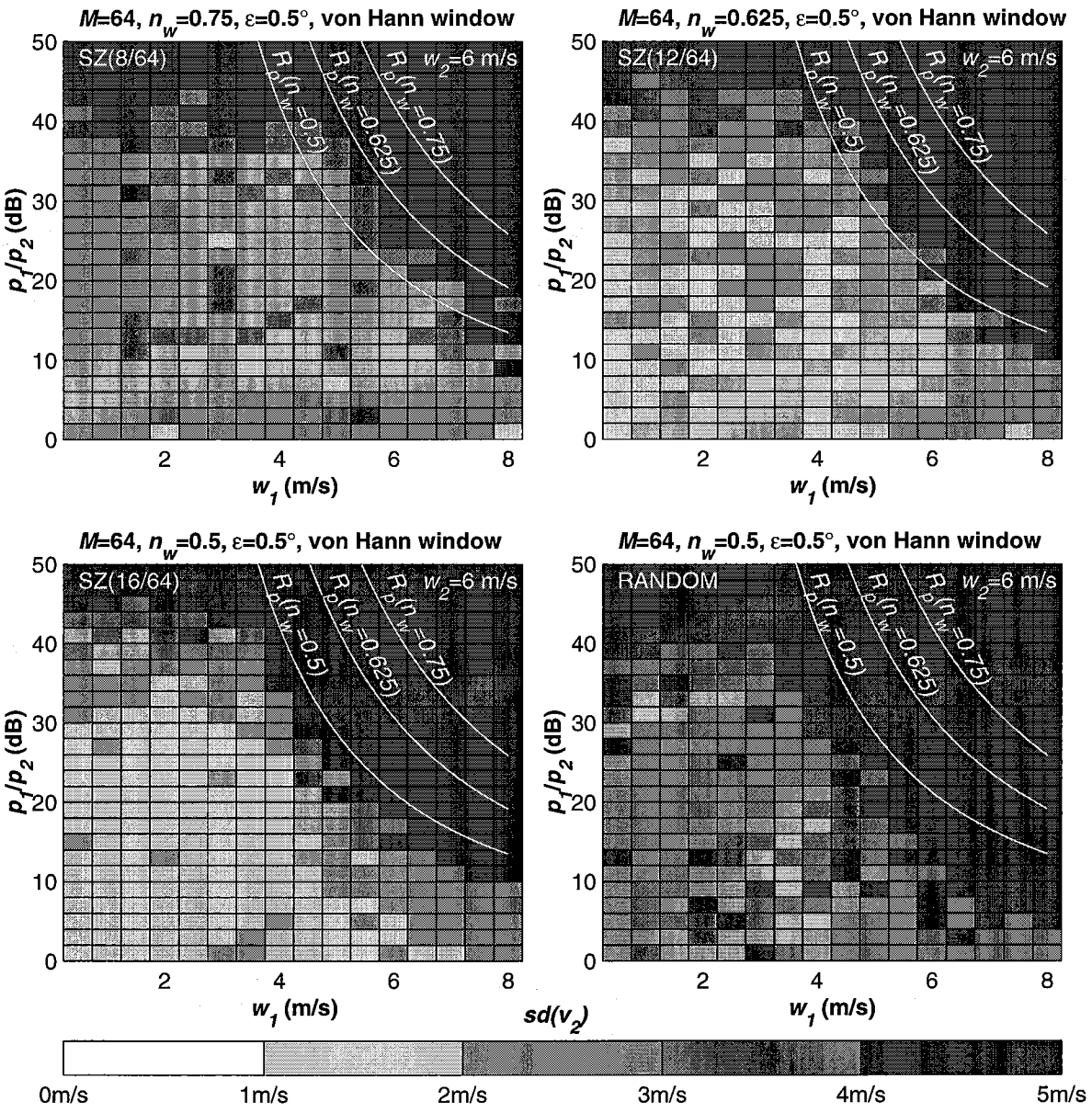

Fig. 5.7. Plots of $sd(\hat{v}_2)$ as a function of p_1/p_2 and w_1, for the SZ(8/64), SZ(12/64), SZ(16/64), and the random phase coding schemes -- a comparison. (M=64, w_2=6 m/s; von Hann window; random phase error parameter, ϵ=0.5°; v_a=32 m/s).

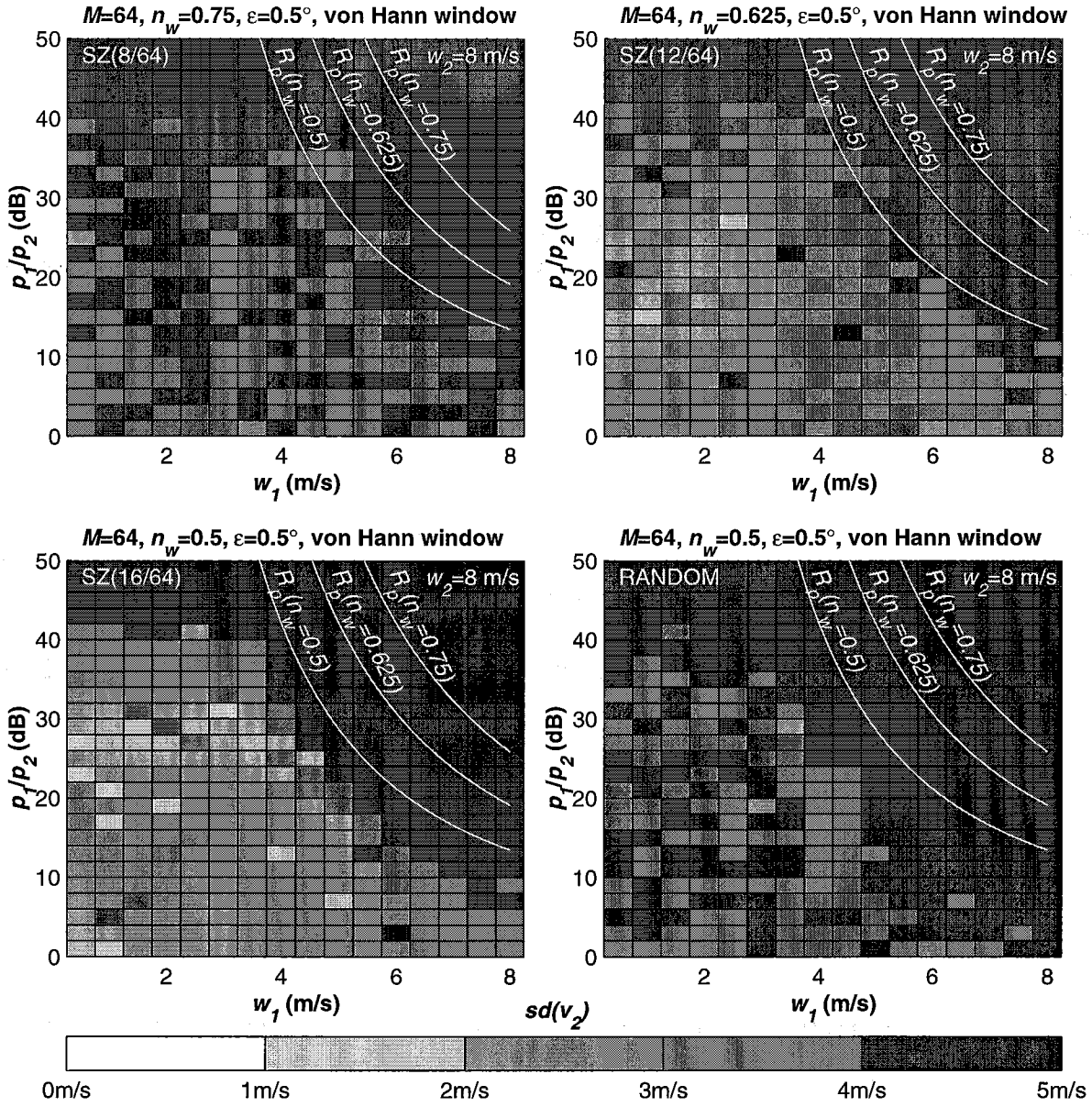

Fig. 5.8. Plots of $sd(\hat{v}_2)$ as a function of p_1/p_2 and w_1, for the SZ(8/64), SZ(12/64), SZ(16/64), and the random phase coding schemes -- a comparison. (M=64, w_2=8 m/s; von Hann window; random phase error parameter, ϵ=0.5°; v_a=32 m/s).

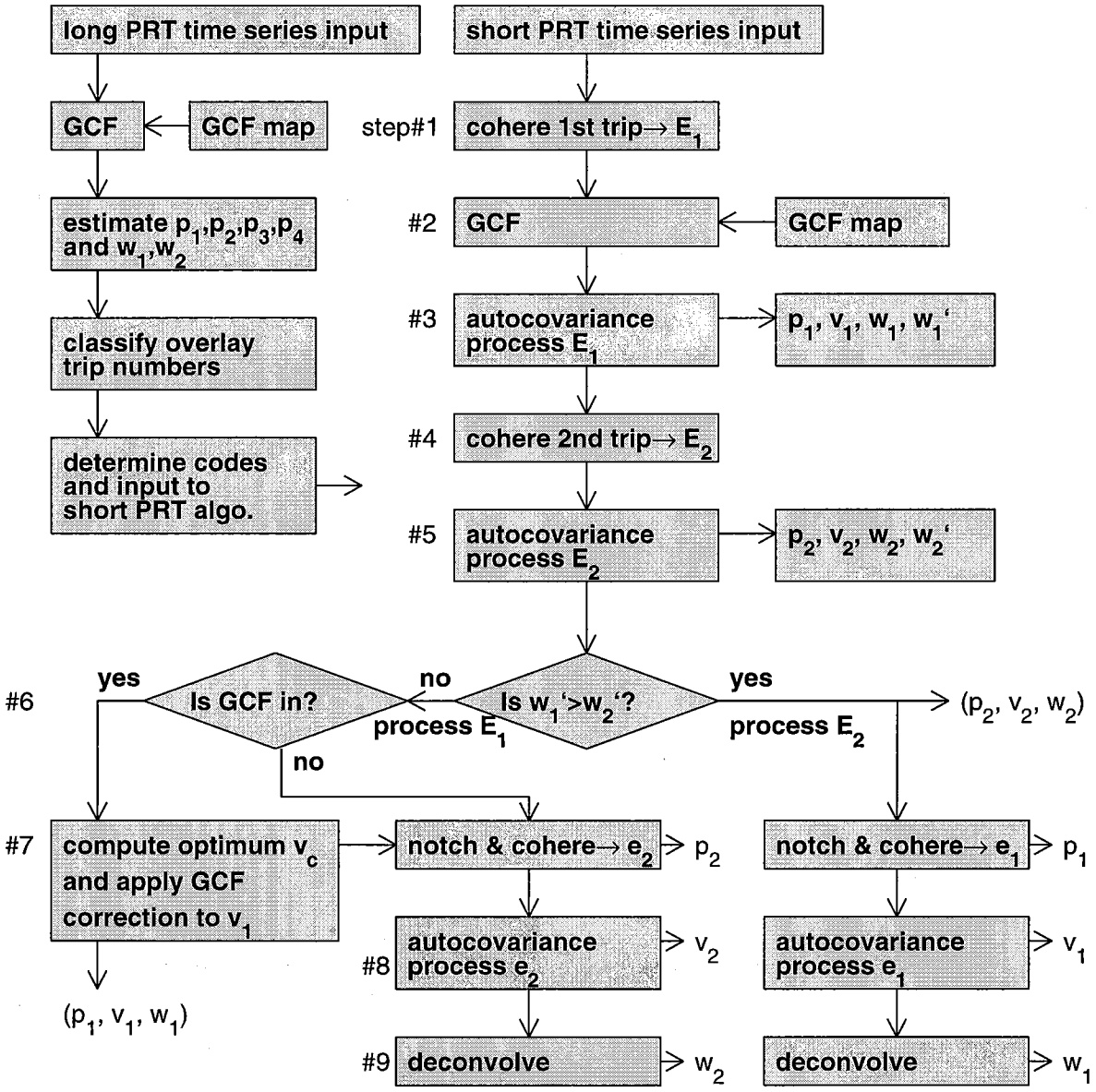

Fig. 5.9. Overall schematic of the algorithm implementation on the WSR-88D.

6. SOME EXAMPLES USING SYNTHETIC DATA

6.1. Synthetic overlaid data.

So far, we have discussed the performance of the SZ coding schemes in recovering the spectral parameters of the overlaid weather signals. Extensive simulation results presented give us a quantitative idea of the capabilities and limitations of the SZ coding scheme. In this section we present some synthetic weather PPI displays to illustrate the recovery of the velocities in the overlaid 1st and 2nd trip echo regions. This gives only a qualitative feel for the usefulness of the SZ coding scheme in removing the "blue haze" (overlaid regions where velocity is flagged) in the WSR-88D velocity display.

The following procedure is used in generating the displays. First, patterns of the reflectivity, velocity, and the spectrum width are generated which mimic the storm pictures seen on the radar PPI displays. The total range selected is from 0 to $2r_a$. We call these patterns input patterns. Care is taken to select a storm pattern which has all the different situations of overlaid strong and weak signals with different combinations of velocities and widths. Next, the spectral parameters of each resolution cell are used to generate a time series using the simulation program. The two time series, E_1 & E_2, for the resolution cells at r and $(r_a + r)$ are combined with SZ phase coding to generate the overlaid time series, E_{sz}. A second time series, E_n, is generated with no coding as obtained in the WSR-88D, and a third one, E_r, with random phase coding. The three SZ codes, viz., SZ(8/64), SZ(12/64), and SZ(16/64), are used in the SZ coded time series.

The time series, E_1 & E_2, are processed by the autocovariance algorithm to estimate the spectral parameters and are used for generating the radar PPI displays of the three parameters which represent an ideal situation of no overlaid echoes. This display is our reference for judging how good our recovered velocities are, using the different coding schemes. In the following discussions, we shall refer to these displays as **reference displays**. The time series, E_n, is processed by a separate autocovariance algorithm which mimics the WSR-88D processing; i.e., it tags the regions where the overlaid power ratio is within -5 dB$\leq p_1/p_2 \leq$5 dB in the velocity display. For the overlaid power ratio outside the ±5 dB interval, the recovered velocity is assigned to the range cell with the stronger signal. This generates a velocity display that is similar to the WSR-88D velocity display with "blue haze" for the overlaid region where the velocity is not recoverable.

The time series, E_{sz}, is processed using the appropriate SZ decoding algorithm to recover all three spectral parameters of both 1st and 2nd trip echoes. Similarly, the random phase algorithm is used for processing E_r. The recovered velocity displays are compared with the WSR-88D velocity display to get a qualitative feel of the improvement that can be obtained using SZ coding. A comparison with the reference displays gives a feel for the goodness of the recovered parameters vis-a-vis the autocovariance algorithm in the absence of overlay and coding. Note that the quantization of the parameters for color coding mask many of the finer differences in the recovered parameters. Furthermore, the input patterns of the reflectivity, velocity, and spectrum width may not cover all the possible combinations of overlay situations. That is the reason for saying that the displays give us a qualitative feel of the performance of the algorithms.

In generating the time series, all the practical effects of the window, noise, and the phase error are included. The following are the parameters used in the simulations:

radar frequency	:	3 GHz
PRT	:	0.7812 millisec.
receiver noise level	:	-113 dBm
number of samples	:	64
unambiguous range	:	117.18 km
unambiguous velocity	:	32 m s^{-1}
window	:	von Hann
phase error, ϵ	:	±0.5° (uniform distribution)
number of gates	:	234
gate spacing	:	1 km
azimuth spacing	:	1°
number of radials	:	360
reflectivity	:	35 dBZ (uniform)
velocity	:	-32 to +32 m s^{-1}
spectrum width	:	1 to 4 m s^{-1}

To obtain signal power for a given reflectivity, the following reference is used:
-7 dBZ reflectivity at 50 km range corresponds to SNR=0 dB; i.e., signal power=-113 dBm (Doviak and Zrnic, 1993, Table 3.1).

6.2. Comparison of PPI displays with and without the SZ coding.

A series of color pictures are given in Figs. 6.1 through 6.3. The first picture (Fig. 6.1) shows the radar PPI display of the velocity over 0 to $2r_a$ range. This is a **reference** display generated assuming no overlay. The reflectivity is assumed to be uniform +35 dBZ, and the spectrum width is increasing radially from 1 to 4 m s^{-1}. The velocity pattern is obtained from a uniform wind with a direction change as a function of range (or height). These are used as input parameters for the simulation program to generate time series of length 64 for each resolution cell, and the time series is used to estimate the velocity shown in Fig. 6.1, assuming no overlay. Although the input velocity pattern is a smooth function, the uncertainty in the velocity estimate makes the display noisy as in an actual radar display. For these input parameters, the overlaid power ratio, p_1/p_2, spans from 6 dB at $2r_a$ to 41 dB at (r_a+1) km. Fig. 6.2 is the simulated WSR-88D velocity display with ±5 dB threshold on the p_1/p_2 ratio to tag the overlaid regions with the "blue haze." If the overlaid power ratio is >5dB or <-5dB, only the stronger signal is assumed to be present, and the velocity is assigned to the stronger of the two echoes although it has a small bias due to the overlaid signal. For the weather pattern considered, the overlaid power ratio is such that only the 1st trip velocity is recoverable, and there are some cases where both v_1 and v_2 are tagged. Fig. 6.3 is the velocity recovered using the SZ(8/64) coding scheme. Comparing this with the reference display in Fig. 6.1, it is clear that the velocities of both trips are recovered, and the velocity pattern is also faithfully reproduced except for a slightly larger variance.

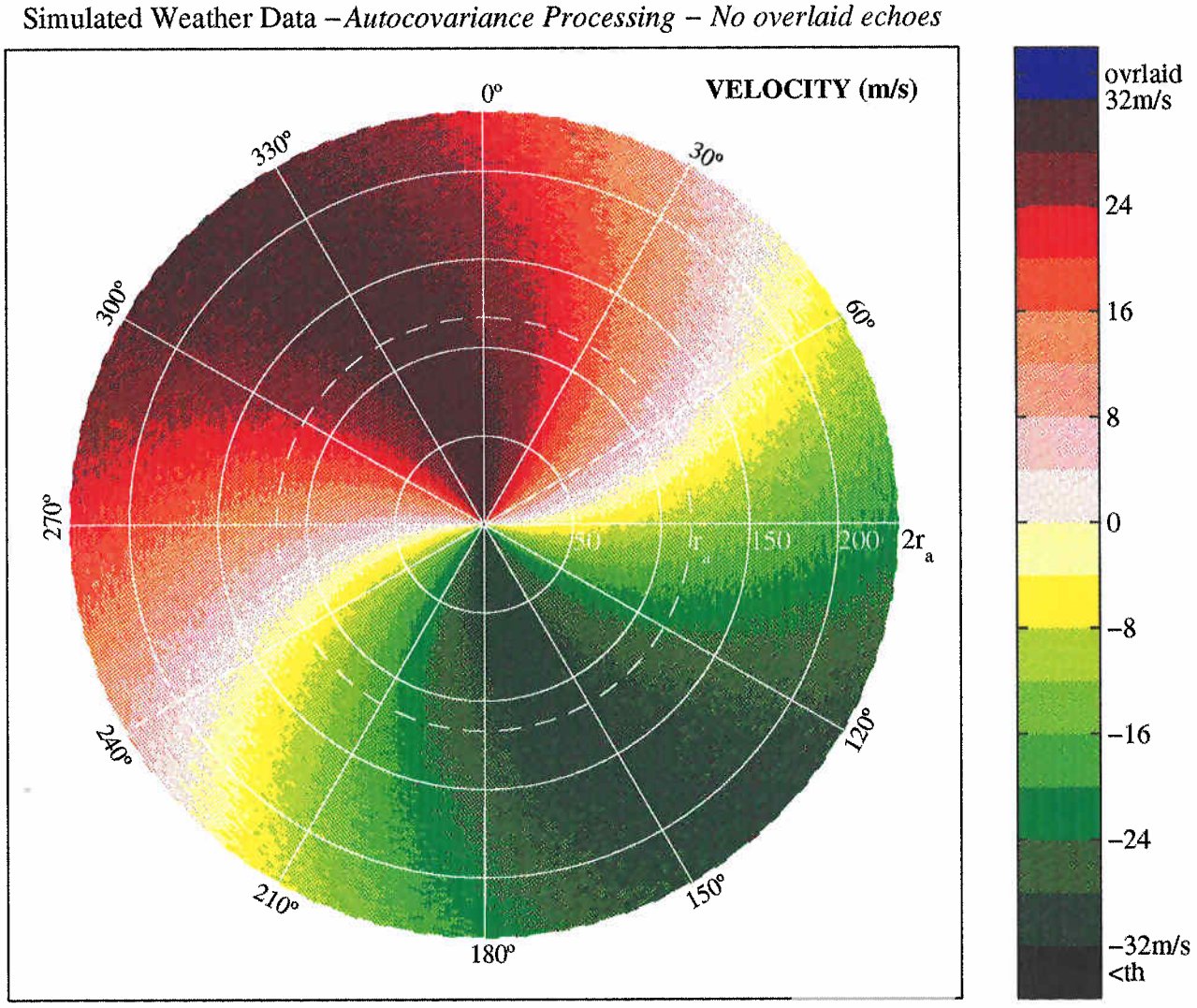

Fig. 6.1. PPI display of simulated velocity field of uniform wind with direction change as a function of range (or height), over 0 to $2r_a$ assuming no overlay. The autocovariance algorithm is used to get the velocity estimate from the simulated time series using 64 samples. The reflectivity is assumed to be -35dBZ over the entire PPI and the spectrum width is increasing along the radial from 1 to 4 m s^{-1}.

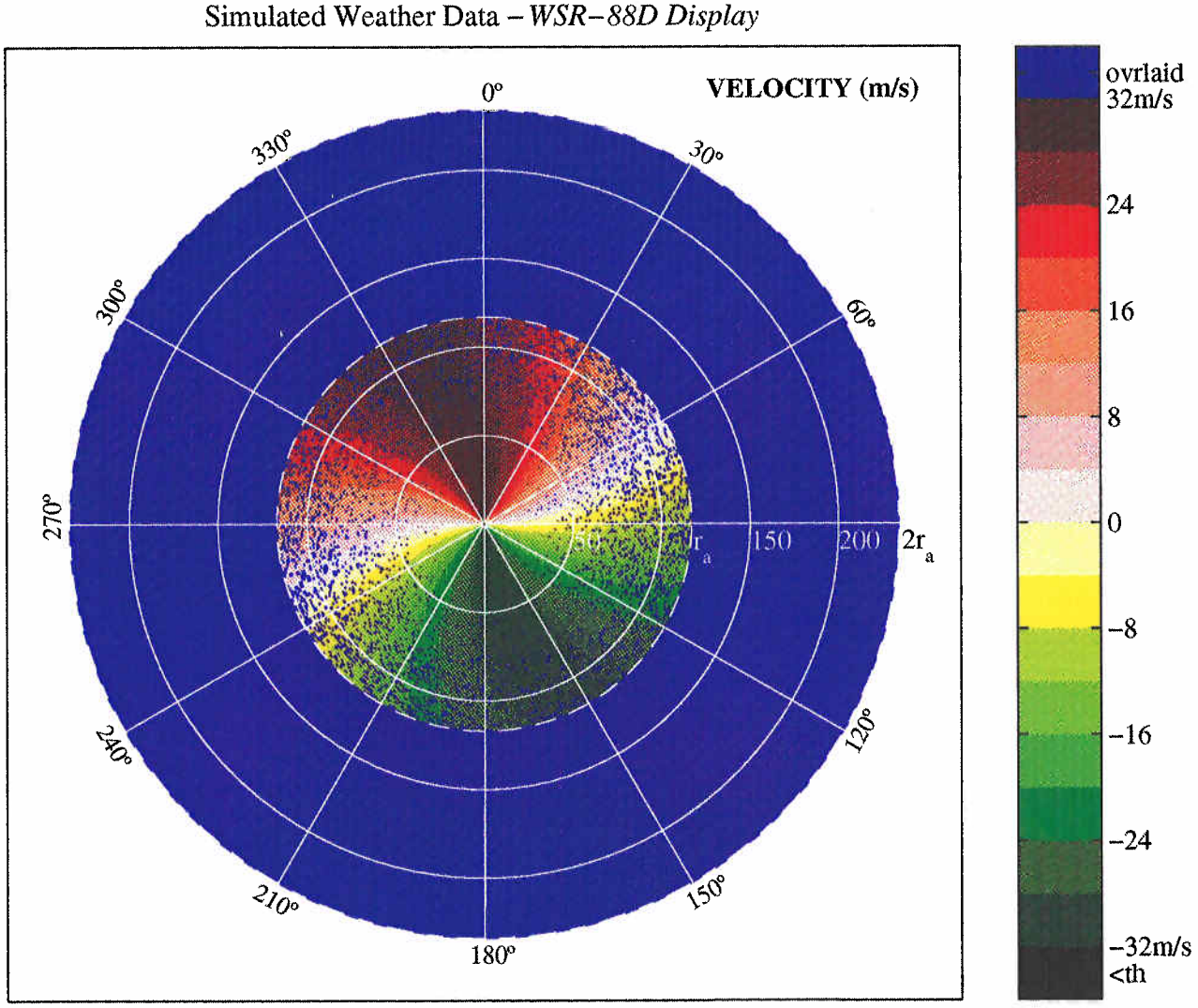

Fig. 6.2. Simulated WSR-88D velocity display for the same input parameters as in Fig. 6.1 with a ±5 dB threshold on the p_1/p_2 ratio.

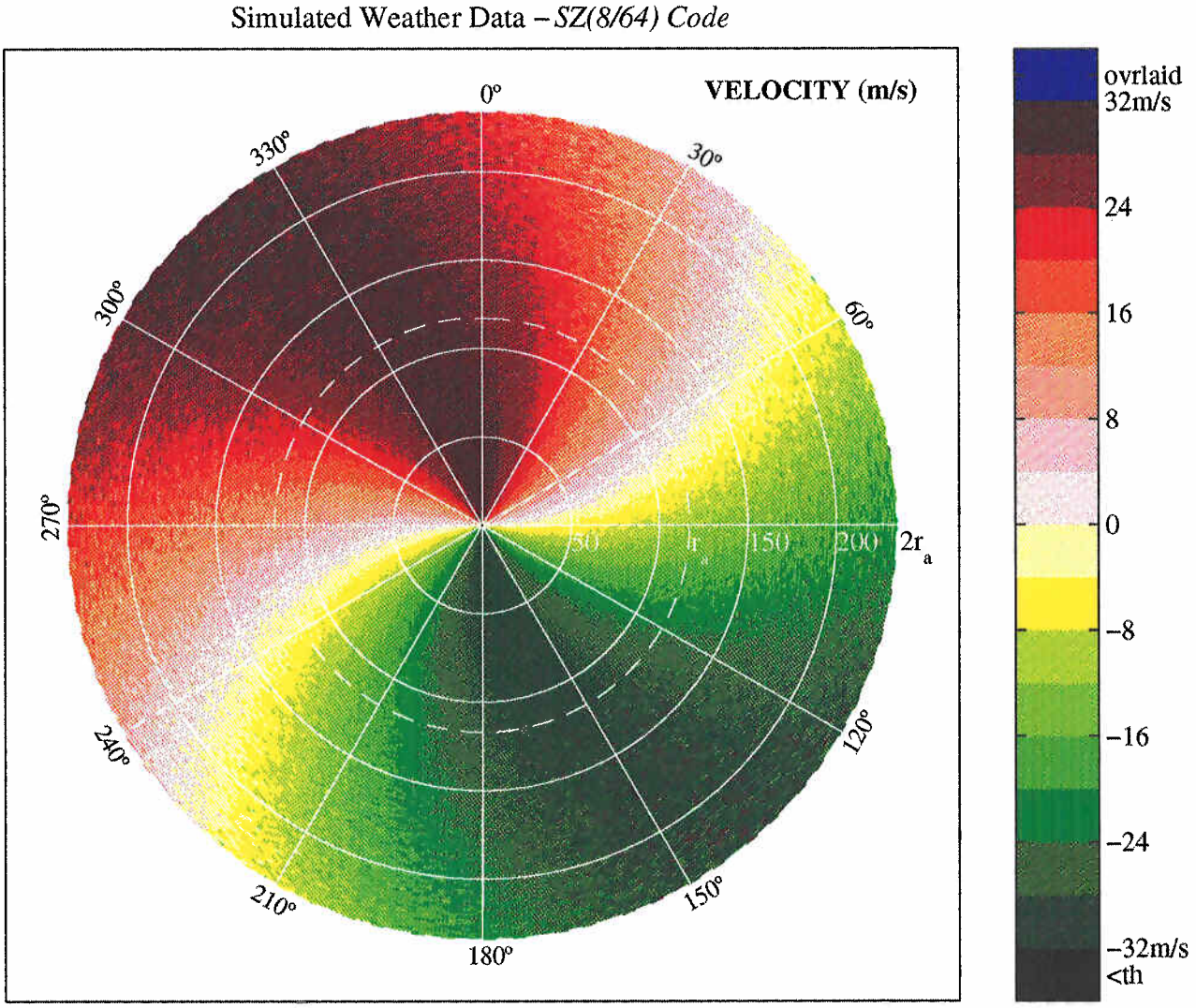

Fig. 6.3. Simulated velocity display using the SZ(8/64) phase coding scheme for the same input parameters as in Fig. 6.1.

7. SUMMARY AND CONCLUDING REMARKS

In this report (Part 2), the results of a detailed simulaton study of the SZ phase coding scheme for the range ambiguity resolution in the WSR-88D is presented. Several different phase codes belonging to the the family of SZ phase codes are investigated to evaluate their potential to recover the spectral parameters of the weaker of the two overlaid weather signals. The performance of the random phase coding scheme is also given for comparison.

Several practical effects that are always present in a radar signal such as the noise, window effect, phase error, etc. are also included in the simulation to get realistic performance characteristics of the coding schemes. Many aspects of the implementation of the SZ phase coding scheme in the WSR-88D are also considered, and the compatibility of the phase coding scheme with the current scan strategy of the radar is also discussed.

The simulation studies indicate that the proposed SZ(*n/M*) phase coding scheme performs better than all the previous phase coding schemes reported in the literature, and is the best candidate for implementation on the WSR-88D to mitigate the range ambiguity problem. The uniform PRT used in the phase coding scheme allows effective filtering of the ground clutter. A decoding algorithm has been developed to estimate all the spectral parameters of the two overlaid weather signals. The algorithm uses processing in the spectral domain and, hence, needs a computationally powerful RDA for the implementation.

The proposed phase coding scheme is compatible with the current WSR-88D scan parameters in the two lowest elevation scans. A sample overlap scheme has been proposed to obtain the required 64 samples (I.e., for efficient use of FFT) without changing the present WSR-88D scan parameters. With the phase coding techinque, there may not be a need for the option of choosing PRTs to minimize the overlaid regions.

In the intermediate elevation scans, the batch mode can be replaced by the SZ phase coded transmission, since the maximum range requirement is often limited to about 250 km (only 1st and 2nd trip signals will be present if r_a is chosen to be 125 km) in these elevations. However, for these elevations, the staggered/variable PRT scheme may be an alternative because the ground clutter filtering is not a major issue at these elevations. The SZ coding scheme needs to be compared with the variable/staggered PRT scheme.

8 REFERENCES

1. Chu, D. C., **1972**: Polyphase codes with good periodic correlation properties. *IEEE Trans. on Information Theory*, vol. **IT-18**, 531-532.

2. Cornelius, R., R.Gagnon, and F.Pratte, **1995:** WSR-88D Clutter processing and AP clutter mitigation., *Interagency MOU between OSF and FSL, Final report submitted by FSL-ATD engineering team.* 182 pages.

3. Doviak, R.J., and D.Sirmans, **1973**: Doppler radar with polarization diversity., *J. Atmos. Sci.*, **30**, 737-738.

4. Doviak, R.J. and D.S.Zrnic, **1993**: *Doppler Radar and Weather Observations.* , Academic Press, New York, 562pp.

5. Laird, B.G., **1981**: On ambiguity resolution by random phase processing. , *20th Conference on Radar Meteorology., AMS*, 327-331.

6. Sachidananda, M., and D.S.Zrnic, **1986**: Recovery of spectral moments from overlaid echoes in a Doppler weather radar. *IEEE Trans. on Geoscience and remote sensing.* , vol. **GE-24,** No.5, 751-764.

7. Sachidananda, M., D.S.Zrnic, and R.J.Doviak, **1997**: Signal design and processing techniques for WSR-88D ambiguity resolution, Part-1. *National Severe Storms Laboratory*, July 1997. 100 pages.

8. Sirmans, D., **1992**: Clutter filtering in the WSR-88D, NWS/OSF, Norman,OK.

9. Siggia, A., **1983**: Processing phase coded radar signals with adaptive digital filters., *21st Conference on Radar Meteorology., AMS*, 167-172.

10. Zahrai, A. and D.S.Zrnic, **1993**: The 10cm Wave length polarimetric weather radar at NOAA's National Severe Storms Laboratory., *Journal of Atmospheric and Oceanic Technology,* **10**, No.5, 649-662.

11. Zrnic, D.S., **1975**: Simulation of weather like Doppler spectra and signals., *Journal of Applied Meteorology.*, vol.**14**, No.4, 619-620.

12. Zrnic, D.S., **1979**: Random phase radar. , *NSSL memorandum,* April 1979.

13. Zrnic, D.S., and P.Mahapatra, **1985**: Two methods of ambiguity resolution in pulsed Doppler weather radars. *IEEE Trans. on Aerospace and Electronic Systems.* , vol. **AES-21,** No.4, 470-483.

14. Zrnic, D.S. and Said Hamidi, **1981:** Considerations for the design of ground clutter cancelers for weather radar. *Interim report# DOT/FAA/RD-81/72, Syayems Research & Development Service, Washington, D.C.*

9. LIST OF NSSL REPORTS FOCUSSED ON POSSIBLE UPGRADES TO THE WSR-88D RADARS

Doviak, R.J. and D.S.Zrnic, **1998:** NOAA/NSSL's WSR-88D Radar for Research and Enhancement of Operations: Polarimetric Upgrades to Improve Rainfall Measurements. 110 pp.

Sachidananda, M., **1997:** Signal Design and Processing Techniques for WSR-88D Ambiguity Resolution, Part I. 100 pp.

Sirmans, D., D.S.Zrnic, and M.Sachidananda, **1986:** Doppler radar dual polarization considerations for NEXRAD, Part I. 109 pp.

Sirmans, D., D.S.Zrnic, and N.Balakrishnan, **1986:** Doppler radar dual polarization considerations for NEXRAD, Part II. 70 pp.